Chemical Vapor Deposition Methods for the Controlled Preparation of Supported Catalytic Materials

Philippe Serp and Philippe Kalck*

Laboratoire de Catalyse Chimie Fine et Polymères, Ecole Nationale Supérieure d'Ingénieurs en Arts Chimiques Et Technologiques, 118 Route de Narbone Toulouse 31077, France

Roselyne Feurer

CIRIMAT-UMR-CNRS/INPT/UPS, Ecole Nationale Supérieure d'Ingénieurs en Arts Chimiques Et Technologiques, 118 Route de Narbone Toulouse 31077, France

Received April 10, 2002

Contents

I. Introduction

The controlled preparation of heterogeneous catalysts is a gentle art, and various procedures are at the disposal of chemists to elaborate efficiently supported catalysts.[1] However, perfectly designed catalysts still remain a challenge: indeed, an heterogeneous catalyst consists of a solid support and an active phase each presenting their own physical and chemical properties, which can evolve during the preparation. Many studies have been devoted to liquid-phase methods to prepare supported catalysts,

10.1021/cr9903508 CCC: $39.75
Published on Web 08/03/2002

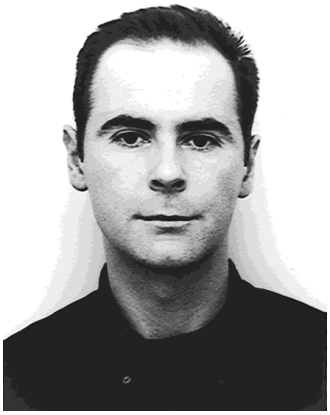

Philippe Serp was born in Montauban, France, in 1966. After receiving his Ph.D. from the Université Paul Sabatier de Toulouse in 1994 where he worked on CVD catalysts with Professor Philippe Kalck, he moved to Universidade de Porto (Portugal) to carry out postdoctoral research with Professor José-Luis Figueiredo on catalytic CVD to prepare carbon fibers. Since 1998, he has been Associate Professor in the Laboratoire de Catalyse, Chimie Fine et Polymères of ENSIACET. His current research interests include CVD and catalytic CVD preparation of nanostructured materials as nanoparticles or nanotubes, and the understanding of homogeneous carbonylation catalytic reactions.

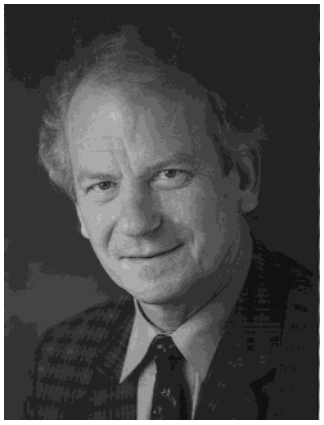

Philippe Kalck was born near Besançon, France, in 1944. He studied in Toulouse, and received his Diplôme d'Ingénieur Chimiste from the Ecole Nationale Supérieure de Chimie de Toulouse (ENSCT) in 1967. He remained in Toulouse for his doctoral research under the supervision of Professor René Poilblanc, completing his Doctorat d'Etat in 1975. Up until 1980, he combined research at the Laboratoire de Chimie de Coordination (CNRS) with teaching at the ENSCT. At that point, he was appointed Professor at the Institut National Polytechnique de Toulouse (of which the ENSCT forms part), and started a research group devoted to the catalysis of carbonylation reactions that has now become the Laboratoire de Catalyse, Chimie Fine et Polymères in the Ecole Nationale Supérieure des Ingénieurs en Arts Chimiques et Technologiques. He is particularly attached to promoting links between industry and academia, and spent two years on secondment to Rhône-Poulenc Chimie between 1986 and 1988. His research interests include the design of highly selective catalysts and the molecular understanding of catalytic processes, fields in which he has published over 145 papers and supervised 45 Ph.D. students.

and so, according to our own experience and to their promising development, we have focused our attention on gas-phase procedures, i.e., chemical vapor deposition (CVD) and related techniques.

One review directly concerns the preparation of supported catalysts by CVD and related techniques and covers the literature until 1995.[2] Three other papers treat partially the subject,[3−5] and several chapters in the book *Advanced Catalysts and Nanostructured Materials* published in 1996 are relevant

Roselyne Feurer is Associate Professor of solid-state chemistry in the Chemistry and Chemical Engineering School (ENSIACET), in Toulouse. She received her "Diplôme d'Ingénieur Chimiste" degree from this school, a M.Sc. from the University of Bordeaux, and a Ph.D. from the National Polytechnic Institute, Toulouse, in 1983. Her current research interests in CIRIMAT focus on the investigation of the fluidized bed MOCVD process for the preparation of noble metals supported catalysts.

to this topic.[6] Our bibliography covers the period 1990−2001 and includes most of the former literature.

Investigations on the reactions between transition metal carbonyl complexes and solid surfaces to produce surface organometallic complexes and subsequent catalysts have been initiated in the early 80s.[7−10] Then, similar studies on surface organometallic chemistry have been extended to other coordination compounds, some of them volatile.[11−15] These detailed studies, including very recent sophisticated investigations, are analyzed in the first part of this review. Such an approach allows a good knowledge of the first step of the CVD process.

The second part is devoted to the catalysts reported in the literature that have been prepared by a gas-phase method. Among the various methods called CVD in the literature, we have introduced a classification to make a clear distinction between the one-step and the two- or more generally multistep processes. When possible, we have reported the relationship between the structure and the catalytic activity of these materials, and compared their performance to that of catalysts prepared by liquid-phase impregnation.

In a third part, we have taken into consideration the surface modifications of the support either to adjust the morphology, i.e., the pore opening size, or to control its acid base properties. The preparation of TiO_2 deposits on various silica or alumina supports is considered separately, since supported TiO_2 can present its own catalytic activity, or become a new support. Finally, preparations of catalytic membranes are also described. In this part of the review, the deposits do not involve nanoparticles, but can go from submonolayers, to thin films, including overlayers. This field is certainly the more recent one, the first review on the subject having appeared in 1996,[16] and extended studies are missing, so that a complete rationalization is still difficult.

The present review shows that the study of the surface reactions between a catalyst precursor and

a support is a key point in the design of a supported catalyst. Our analysis has been focused on catalytic materials, but we had in our hands numerous papers from different fields in which this approach has been followed, for instance, for the elaboration of microelectronic devices or for metallurgical coatings by CVD. Thus, this review can provide valuable information for researchers coming from different disciplines.

We believed that, as the CVD method allows the production of deposits in a controlled manner and on a large scale, it could be applied to the preparation of supported catalysts. Such a unified view has prompted us to review the literature with the point of view of the physicochemical processes that occur at a gas−solid interface in the course of the elaboration.

II. Studies on the Mechanisms of Adsorption and Reaction of Transition Metal Compounds on a Surface

Historically, Mond has demonstrated in 1890[17] that $[Ni(CO)_4]$ is a very convenient precursor for the preparation of pure nickel films by CVD at low temperature. Later on, it has been shown that these films are active hydrogenation catalysts.[18] The progressive availability of various transition metal carbonyls has led to many studies on the preparation of supported catalysts from these precursors. Indeed, all homoleptic carbonyl complexes decompose at relatively low temperatures (<773 K) yielding zerovalent supported metals. Moreover, as the CO ligand is very sensitive to the electronic variations in the coordination sphere of a given metal, many studies from the 70s to the present day have been devoted to infrared measurements to follow the progressive transformation of a carbonyl complex when it is adsorbed on a surface.

The tremendous progress in the analytical techniques that occurred in the mid-80s allowed further investigations of the chemical and physical properties of surfaces down to the nanoscale level.[19] Such investigative tools, as well as the great strides made in the synthesis of coordination compounds, have opened the new field of surface chemistry, and more particularly of surface organometallic chemistry. Studies on the early steps of film growth by organometallic chemical vapor deposition (OMCVD), and on the deposition of nanomaterials have appeared. Indeed, the OMCVD technique has moved toward systems in which the ratio between the substrate area and the gas-phase volume becomes larger (porous and/or finely divided supports, ultrathin films, small particles) so that the surface reactions become a crucial parameter. Thus, the interactions between the metallic species and the surface take such a great importance that it is necessary to have a deep knowledge of the surface itself.

For this reason, after a brief description of the main supports used in catalysis (metal oxides, activated carbons, zeolites), the first part of this review will deal with the interactions that have been clearly established between an organometallic complex and a surface. Although our present objective is to focus on the gas-phase deposition methods, we will, when necessary, take into account the surface chemistry of organometallic complexes dissolved in an inert solvent to impregnate a support. A comprehensive table that covers the supports used, the precursors, the experimental conditions, and the characterization of the final material is given below (Table 1).

A. Description of the Supports

The supports usually used in catalysis, i.e., metal oxides, activated carbons, or zeolites are characterized by large specific areas and by the presence of anchoring sites on their surface. Among the most studied metal oxides, we find silica, alumina under different allotropic forms, magnesia, and titania. The specific area and the porosity vary greatly from one support to the other. According to IUPAC, three types of pores can be distinguished for a given support according to their size: micropores, less than 2 nm; mesopores, ranging from 2 to 50 nm; and macropores, greater than 50 nm. The types, as well as the concentration, of the anchoring groups have been investigated by thermogravimetric analysis, infrared spectroscopy, nuclear magnetic resonance spectrometry, or more occasionally, extended X-ray adsorption fine structure. The acid−base properties of the surfaces have also been characterized by infrared spectral studies of adsorbed molecules.[20]

1. Silica

Micro-, meso- and macroporous silica can be prepared selectively. Thus, very high specific areas can be reached, until 800 $m^2\ g^{-1}$, but it is possible to obtain silica with low specific areas. The bulk of this solid consists of SiO_4 tetrahedra sharing their oxygen atoms. There exist several forms of amorphous and crystallized silica, among them α-quartz has been used as model support, most often the 0001 plane.[21,22] It can be mentioned that spherical and flat nonporous supports can be also used, especially for specific studies.[19] The fully hydrated surface of silica contains hydroxyl groups terminating the bulk with a concentration ranging from 4 to 6.5 OH nm^{-2}.[19,23] They are isolated or bonded to vicinal OH groups through hydrogen bonds, and constitute a monolayer. This hydrophilic surface is covered by several layers of physisorbed water. Such a surface, with pK_a value of 4 to 7, depending on the methods of measurements, shows a weakly acidic behavior.

Physisorbed water can be rather easily removed by heating at 473 K, whereas silanol group elimination requires higher thermal treatments (Figure 1). Although there are some discrepancies between the temperature values published in the literature (presumably due to the pressure at which the experiments have been performed), the first step of dehydroxylation leads to isolated and geminal hydroxyl groups. Above 1073 K, only isolated OH groups still subsist, ca. 1 OH nm^{-2}, with the simultaneous formation of siloxane hydrophobic groups which preclude rehydration. Above 1100 K, complete dehydroxylation can be reached giving rise to more or less

Table 1. Selected Studies of Reactions of Transition Metal Compounds with the Surface of a Support

precursor	support	conditions	main identified species	ref
$[Mo(CO)_6]$	Al_2O_3 thin film *FH*[a]	295 K, 6.6×10^{-5} Pa	$[Mo(CO)_6]$ weakly adsorbed	46
	γ- Al_2O_3 pellets *FH*	295 K, time dependence	$[Mo(CO)_6]_{ads}$ + $[Mo(CO)_5]$Surf[b]	45
	γ- Al_2O_3 pellets *PD*	295 K, outgassing	$[Mo(CO)_6]_{ads} \rightarrow [Mo(CO)_5]_{ads} \rightarrow [Mo(CO)_3]_{ads}$	45
	γ- Al_2O_3 wafer *FH*	373 K and heating	$[Mo(CO)_3]_{ads} \rightarrow [Mo(CO)_{3-n}]_{ads}$	49
	γ- Al_2O_3 wafer *PD*	373 K	$[Mo(CO)_3]_{ads}$ more stable	49
	Al_2O_3 film *FH*	80−175 K, UHV	$[Mo(CO)_5]_{ads}$ and $[Mo(CO)_3]_{ads}$	50
	Al_2O_3 film *FH*	205−450 K, UHV	$[MoO_2(CO)_n]$ + $(oxalates)_{ads}$	50
	γ-Al_2O_3 *PD*	373 K	$[Mo(CO)_5]_{ads}$	58
	γ-Al_2O_3 *PD*	773 K	Mo^{6+}, Mo^0	58
	γ-Al_2O_3 *PD*	573 K	Mo^{4+} and Mo^0 or Mo^{2+}	59
	γ-Al_2O_3 *HD*	573 K	Mo^0	59
	SiO_2 *FH*	>283 K, vacuum	$[Mo(CO)_6]_{ads}$, no stable subcarbonyl species	47
	SiO_2 *PD*	326 K → 373 K, N_2	partially decarbonylated Mo species	64
	TiO_2 single crystal[c]	150 K	$[Mo(CO)_6]_{ads}$	70
	TiO_2 single crystal	400−700 K	no subcarbonyls, Mo^0 + C(graphitic or carbidic)	70
	NaY zeolite (673 K, vacuum)	295 K	$[Mo(CO)_6]_{ads} \rightarrow [Mo(CO)_5]_{ads}$	73
	NaY zeolite (673 K, vacuum)	370 K	$[Mo(CO)_3]_{ads}$	73
	NaY zeolite (673 K, vacuum)	373 K → 473 K	$[Mo(CO)_3]_{ads}$	78
	NaY zeolite (623 K, vacuum)	298 K	$[Mo(CO)_6]_{ads}$, 2 per cage	80
	NaY zeolite (623 K, vacuum)	623 K	Mo^0	80
	NaY zeolite (dehydrated)	673 K, vacuum	Mo^0	86
	HY zeolite (623 K)	673 K	Mo^{5+}	83
$[Mo(\eta^3\text{-}C_3H_5)_4]$	HY zeolite	673 K	Mo^{5+}	165
$[Cr(CO)_6]$	γ-Al_2O_3 *FH*	283 K	$[Cr(CO)_6]_{ads}$	47
	γ-Al_2O_3 *FH*	>283 K, vacuum	decarbonylation, no stable subcarbonyl species	47
	γ-Al_2O_3 *PD*	328 K	$[Cr(CO)_6]_{ads}$, $[CrCO)_5]_{ads}$ − $[Cr(CO)_4]_{ads}$	55
	γ-Al_2O_3 *PD*	473 K	complete decarbonylation	55
	γ-Al_2O_3 *HD*	298 K	$[Cr(CO)_6]_{ads}$	60
	γ-Al_2O_3 *HD*	298 K, outgassing	desorption of $[Cr(CO)_6]_{ads}$ + $[Cr(CO)_5]_{ads}$	60
	SiO_2 *PD*[c]	473 K, atm. pressure	Cr^{n+}, evolution of H_2, CH_4, CO, and CO_2	67
	SiO_2 *PD*	298 K	$[Cr(CO)_6]_{ads}$	68
	SiO_2 *PD*	423 K, static vacuum	complete decarbonylation	68
	NaX zeolite (673 K)	298 K	$[Cr(CO)_6]$ encapsulated	76
	NaX zeolite (673 K)	373 K, outgassing	$[Cr(CO)_4]_{ads}$ and $[Cr(CO)_3]_{ads}$	76
	NaX zeolite (673 K)	423 K	$[Cr(CO)_3]_{ads}$	76
$[Cr(neopentyl)_4]$	SiO_2 *PD* (473 K)	298 K	-SiO−Cr(neopentyl)$_2$	151
	SiO_2 *PD* (473 K)	333 K	Cr^{4+}	151
	SiO_2 *PD* (773 K)	298 K	-SiO−Cr(neopentyl)$_3$	151
$[Cr(acac)_3]$	SiO_2 *PD*	473−553 K	-SiO−Cr(acac)$_2$	160
	SiO_2 *PD*	673 K, H_2O	Cr^{3+}	160
	SiO_2 *PD*	673 K, O_2	Cr^{6+}	160
$[Cr(\eta^5\text{-}C_5H_5)_2]$	SiO_2 *HD*	298 K	-SiO−Cr(η^5-C_5H_5)	161
$[Cr(CO)_3(\eta^6\text{-}C_6H_6)]$	γ-Al_2O_3 *HD*	298 K	$[Cr(CO)_3(\eta^6\text{-}C_6H_6)]_{ads}$	162
	γ-Al_2O_3 *HD*	333 K, outgassing	subcarbonyl species	162
	SiO_2 *HD*	298 K	$[Cr(CO)_3(\eta^6\text{-}C_6H_6)]_{ads}$	163
	SiO_2 *HD*	358 K	desorption of $[Cr(CO)_3(\eta^6\text{-}C_6H_6)]_{ads}$	163
$[W(CO)_6]$	γ-Al_2O_3 *PD*	473 K	$[W(CO)_3]_{ads}$	54, 57
	γ-Al_2O_3 *PD*	723 K	complete decarbonylation	54, 57
	NaY zeolite (623 K)	>473 K	W^0	89
	HY zeolite (623 K)	>473 K	W^{5+}	89
$[Fe(CO)_5]$	SiO_2 *PD*	298 K	$[Fe(CO)_5]$ weakly adsorbed	91
	SiO_2 *PD*	298 K, outgassing	easy desorption of $[Fe(CO)_5]$	91
	MgO *HD*	298 K	$[(CO)_4Fe(CO_2)]^{2-}Mg^{2+}$	95
	MgO *HD*	>350 K	Fe^0	95
	C (graphite)	298−300 K	$[Fe(CO)_5]$ physisorbed	97
	C (graphite)	>378 K	decarbonylation, Fe^0	97
	HY zeolite (623 K, vacuum)	298 K	$[Fe(CO)_5]$ physisorbed	98
	HY zeolite (623 K, vacuum)	333 K, outgassing	$[Fe(CO)_4]$-zeolite	98
	HY zeolite (623 K, vacuum)	523 K, outgassing	Fe^{2+}	98
	Na zeolite (720 K, vacuum)	450 K	Fe^0	103
	γ-Al_2O_3 *PD*	<423 K	zerovalent subcarbonyl	102
	γ-Al_2O_3 *PD*	>573 K	Fe^{2+}	102

Table 1 (Continued)

precursor	support	conditions	main identified species	ref
$[Fe_3(CO)_{12}]$	γ-Al_2O_3 *PD*	313 K, vacuum	$[HFe_3(CO)_{10}](OAl\equiv)$	96
	SiO_2 *PD*	317 K, vacuum	$[Fe_3(CO)_{12}]$ weakly adsorbed	96
	HY (623 K, vacuum)	333 K, outgassing	$[Fe_3(CO)_{12}]_{ads}$	98
	HY (623 K, vacuum)	523 K, outgassing	Fe^{2+}	98
$[Co_2(CO)_8]$	SiO_2 *HD*	298 K	$[Co(CO)_8]_{ads}$	105, 106
	SiO_2 *HD*	outgassing	$[Co_4(CO)_{12}]_{ads}$	105, 106
	MgO *HD*	298 K	higher nuclearity clusters neutral and anionic	105, 106
	γ-Al_2O_3 *PD*	sublimation, vacuum	$[Co_2(CO)_8]$, $[Co_4(CO)_{12}]$ and $[Co(CO)_4]^-$ adsorbed	107
	γ-Al_2O_3 *PD*	313 K	$[Co_4(CO)_{12}]_{ads}$	108−111
	γ-Al_2O_3 *PD*	520 K, outgassing	various oxides	108−111
	γ-Al_2O_3 *PD*	293 K, O_2	$[Co^{II}]_4$ moieties	108−111
	γ-Al_2O_3 *PD*	773 K, O_2	$[Co_3O_4]_n$ spinel-like particles	108−111
$[Re_2(CO)_{10}]$	MgO film (111) *HD*	320 K	$[Re(CO)_4(OMg\equiv)]_2$	118
	MgO film (111) *HD*	>400 K	$Re(CO)_3(OMg\equiv)_3$	118
	MgO film (111) *HD*	>600 K	Re metal cluster	118
$[RhCl(CO)_2]_2$	SiO_2 wafers, *FH*, *PD* or *HD*	298 K	$[RhCl(CO)_2]_2$ weakly adsorbed	122, 123
	γ-Al_2O_3 wafers, *PD*	298 K	$[Rh^I(CO)_2]$, $[Rh^I(CO)]$ + remaining Cl	123
	γ-Al_2O_3 (100), −OH free	108 K	multilayer adsorption	127
	γ-Al_2O_3 (100), −OH free	231 K	outer multilayer desorption	127
	γ-Al_2O_3 (100), −OH free	270−573 K	only one monolayer left	127
	γ-Al_2O_3 (100), −OH free	>623 K	Rh^0 and Cl (atomic ratio Cl/Rh=3)	127
	TiO_2 [110]	300 K	$[Rh^I(CO)_2]$ coordinate to 2 O_{surf} + remaining Cl	128−137
	TiO_2 [110]	500 K	Rh^0 particles (+ Cl until 800 K)	128−137
	NaY, HY *FH*	353 K	$[Rh^I(CO)_2]$	138
$[Rh(\eta^3\text{-}C_3H_5)_3]$	SiO_2[d] *PD*	298 K	$[Rh\ (\eta^3\text{-}C_3H_5)_2]$ grafted	142
	SiO_2[d] *PD*	623 K	Rh^0 particles	142
	TiO_2 *PD*	293 K, H_2	grafted Rh−H species	144, 145
$[Cu(hfacac)_2]$	SiO_2 *FH*, *PD* or *HD*	143 K	physisorption	154
	SiO_2 *FH*, *PD* or *HD*	298 K	$[Cu(hfacac)_2]$ H bonded (−OH groups) + interaction with siloxane bridges	154
	SiO_2 *FH*, *PD* or *HD*	673 K	hfacacH evolution + ill defined products and/or desorption	154

[a] *FH*: fully hydroxylated; *PD*: partially dehydroxylated; *HD*: highly dehydroxylated. [b] Surf: −OH of the support. [c] The same studies has been performed for $[Mo(CO)_6]$, $[Cr(CO)_6]$, and $[W(CO)_6]$. [d] A similar study has been performed on Al_2O_3, TiO_2, and MgO. The order of reactivity for the grafting is $TiO_2 > SiO_2 \gg Al_2O_3 > MgO$.

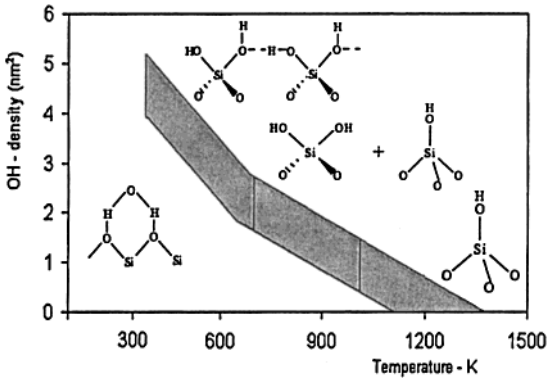

Figure 1. OH group density as a function of temperature pretreatment (adapted from ref 19).

strained Si−O−Si frameworks which present a weak Lewis acidity.

Preparation, physical and chemical characterization, as well as surface modification of silica have been described in detail by Vansant et al.[23]

2. Alumina

The structural chemistry of alumina is richer and somewhat more complicated than that of silica because, according to the elaboration temperature and the porosity, the crystalline forms are different. Generally, the specific areas of these supports are comparable to those of silica. Among the various allotropic forms, η-Al_2O_3 and in a lesser extent γ-Al_2O_3, whose lattices are close to a spinel structure, are the most commonly used supports in catalysis. The η-alumina presents a more acidic character. Knözinger and co-workers[24] have demonstrated (by infrared spectroscopy) five types of OH groups depending on the environment of the aluminum atoms in the defect spinel structure (Figure 2). A recent review dealing with the historical attempts to resolve the controversial structure of γ-alumina and including recent computational results has been published by Sohlberg and co-workers.[25]

The total concentration of the OH groups on alumina ranges from 10 to 15 OH nm^{-2} for a fully hydroxylated support (i.e., roughly three times the concentration on a silica). Half of these OH groups can be removed by heating at 650 K, and one-third more at 800 K. But even in the range 1173−1273 K, OH groups still remain on the surface.

Varying the temperature treatments can modify the acid−base properties of these supports. Indeed, at room temperature η- and γ-Al_2O_3 present a weak Brönsted acidity (OH groups) as well as Lewis basic

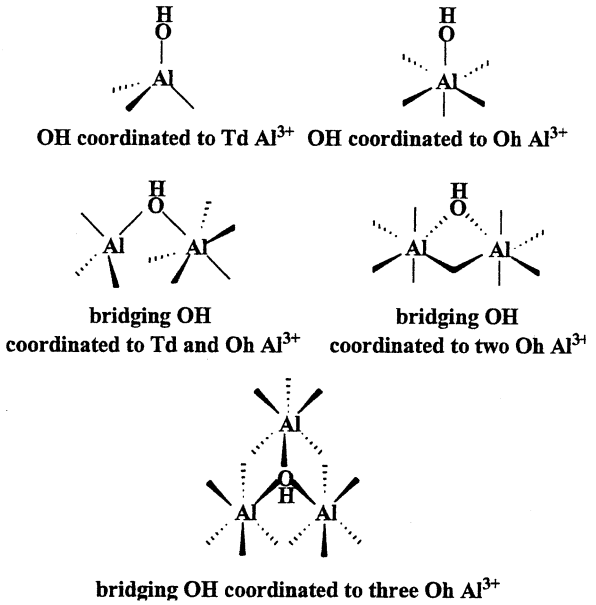

Figure 2. Different types of OH groups on the alumina surface (adapted from ref 24).

sites due to the presence of OH or O^{2-}, and Al^{3+}.[26] When physisorbed water is eliminated at 473 K, the Brönsted acidity is increased by elimination of the hydrogen interactions of water with the hydroxyl groups. Further heating until 900 K decreases this acidity (removal of OH groups) and causes the simultaneous presence of Lewis acidic (Al^{3+}) and basic (O^{2-}) sites. It is worth noting that heating alumina also induces significant modifications in the structure, which thus change the acid−base properties.

3. Titania

Generally, the specific areas of titania are somewhat lower than those of the two previous supports. Two allotropic forms are encountered: anatase at low temperatures and rutile at high temperatures. The most common commercial support contains 80% anatase and 20% rutile with a specific area of 50 m^2 g^{-1}. A fully hydroxylated titania can reach 10 OH nm^{-2}; dehydroxylation at 473 K induces a dramatic decrease in OH population (2 OH nm^{-2}). A complete dehydroxylation requires temperature of 1000 K. Moreover, the techniques of preparation of single crystals often used as models for adsorption studies need high temperatures, so that partially hydroxylated model surfaces are obtained. Due to the ionic character of this support, both Brönsted acidic and basic OH groups have been evidenced. This support is much more acidic than alumina but largely less basic than magnesia. However, the problem of the precise interpretation of the different hydroxyl groups of anatase has not been solved, as concluded in a recent review about surface chemistry of TiO_2.[27]

4. Magnesia

Magnesium oxide presents the simplest structure, i.e., rock-salt, and has been largely used as model support (100 face). It can also be prepared as large surface area powders (>100 m^2 g^{-1}) with hydroxyl concentrations around 10 OH nm^{-2}. Dehydroxylation by heating leads to an OH concentration of 4 OH nm^{-2} at 850 K and 1 OH nm^{-2} remains even at 1073 K. Among the different oxide supports, MgO is the most basic and presents two types of sites: Mg−O−Mg and -OH groups, these latter groups being very weakly acidic in character.

Other oxides have been used, but less extensively studied, for instance, CaO, ZrO_2, La_2O_3, and CeO_2, and will not be presented here.

5. Zeolites

Zeolites are built from SiO_4 and AlO_4 edge-sharing tetrahedra, and involve cations to neutralize the negative charge due to the presence of aluminum. The cations can be exchanged either by protons or transition metals, and their properties are thus modified. The arrangement of the various tetrahedra leads to a great variety of frameworks, which define channels and cages. Such low-density microporous materials show different thermal stability, depending on structural and compositional factors. A great number of zeolites can be synthesized by varying the SiO_2/Al_2O_3 ratio. The first generation of synthetic zeolites presents low silica-to-alumina ratios (<10): typical zeolites are A, X, Y, mordenite... The second generation, among which ZSM-5 is the most well-known, contains SiO_2/Al_2O_3 building blocks ratios >20.

This class of supports presents high specific surface areas (300 to 1000 m^2 g^{-1}) with a controlled porosity, which stems from the presence of channels (0.4 to 0.7 nm) and supercages, the size of which being in the 1.14−1.4 nm range. Thus, they offer the possibility of restricting the particle size distribution of the metal particles and, at the same time, of imposing a steric influence on catalytic reactions. Their pores contain physisorbed water, which can be easily and reversibly removed by heating, without affecting the structure of the material. The concentration of OH groups in internal and external surface is usually around 2 mmol g^{-1}.

Among the great variety of zeolites, few of them are used in catalysis as supports, each of them having its own specificity, so that no more general description will be attempted in this review.

6. New Mesoporous Molecular Sieves Supports

Since 1992, the family of materials generically called M-41S has attracted the attention of many scientists working in the field of catalysis.[28,29] Their synthesis, characterization, and catalytic properties have been recently reviewed.[30,31] They present a uniform mesoporous structure (silicate or aluminate) ordered in a hexagonal (MCM-41), cubic (MCM-48), or laminar (MCM-50) array. Their pore size may be tuned from ca. 2 to 10 nm by using different synthetic strategies. The surface area of these materials is usually higher than 700 m^2 g^{-1}.

In the case of aluminosilicates, the Si/Al ratio governs the specific surface area, the pore volume, and the acidic properties of these materials. As in the case of zeolites, cation exchange can be performed to tune the acid−base properties. The high surface

area of MCM-41 together with the presence of silanol groups able to be functionalized have been of great use to support organometallic compounds, achieving high dispersion of the metallic phase.

Very recently, different groups of researchers have independently synthesized samples of a new class of hybrid porous material that incorporate organic components within a silica framework.[32−34]

7. Carbons

The increasing importance of carbon materials in catalytic processes has been recently analyzed.[35] Carbon supports are generally graphitic materials, which can vary from highly oriented pyrolytic graphite (HOPG as model support) to quasi amorphous activated carbons. This latter kind of support, whose activation results from various oxidizing treatments, is by far the most used. They present a large surface area, near to 1000 $m^2\ g^{-1}$ essentially due to the presence of micropores. Although the chemistry of the carbon surfaces still needs a better understanding, in addition to the "graphene" sheets which provide aromatic CH groups, several acidic and basic groups have been evidenced.[36,37] Carboxylic acid, anhydride, lactone, lactol, and hydroxyl groups have been characterized as weak acidic sites. About the basic properties, although less understood, quinone, cyclic ketone, and ether groups are reported, as well as the π electrons of the aromatic rings.

The concentrations and the nature of these surface functional groups can be modified by suitable thermal or chemical post-treatments.[38] Temperature programmed desorption (TPD) measurements allow one to follow the CO and CO_2 gas evolution arising from the decomposition of the surface groups and to show that all of them have disappeared at 1300 K. From this CO/CO_2 evolution, the concentration of these groups can be estimated to 2−3.5 mmol g^{-1}. A schematic representation of these functions is shown in Figure 3.

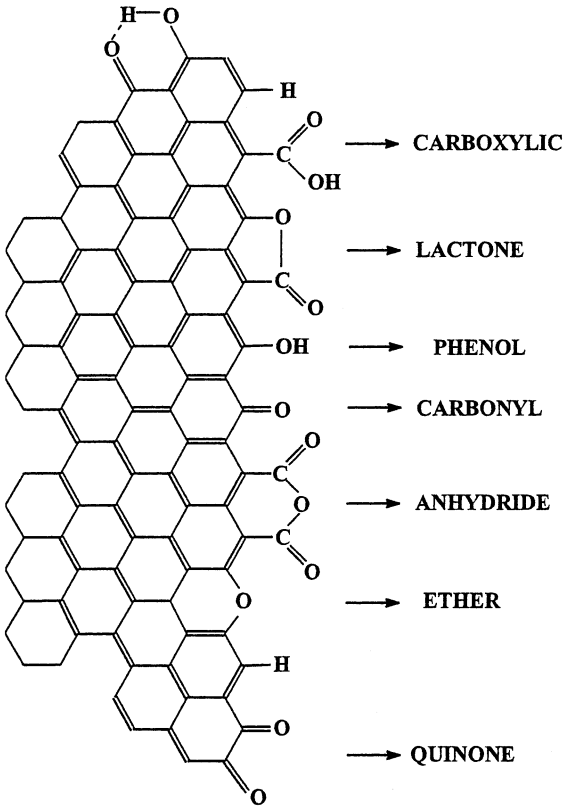

Figure 3. Surface containing oxygen groups on activated carbon (adapted from ref 38).

Finally, it is worth mentioning that new forms of carbon such as fullerenes or carbon nanotubes have also been used recently as supports for heterogeneous catalysts.[39]

8. Conclusion

It can be seen that the surface of any support contains various kinds of grafting sites. It is interesting to refer to the seminal view of Basset and Choplin[40] who consider these sites as rigid ligands as in molecular coordination chemistry. These surface ligands can bound to the metal, donating one electron (X ligand), or two (L ligand). Table 2 summarizes the various types of ligands, assuming the 18-electron rule is obeyed for the metal center.

Table 2. Types of Surface Ligands and Counting of Electrons[a]

Type of surface ligand	Number of electrons given by this ligand to M	Examples
Z	0	Al^{3+}, Mg^{2+}, Ti^{4+}, ...
X	1	−O−M
L	2	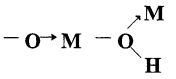
X_2	2	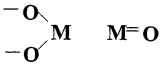
XL	3	
$2X_2$	4	

[a] Adapted from ref 40.

B. Interactions between a Zerovalent Organometallic Complex and the Support

1. Zerovalent Carbonyl Metal Complexes of Molybdenum, Chromium, and Tungsten

Although these interactions have been largely described,[41−44] we will focus our attention on the possible correlations, that we can deduce from the literature, between the gas-phase adsorption studies, the decarbonylation steps, and the nature of the final deposits, when available.

a. Alumina Support. Due to the high catalytic activity of deposits prepared from $[Cr(CO)_6]$, $[Mo(CO)_6]$, or $[W(CO)_6]$ (mainly in polymerization or metathesis reactions) as well as to the importance of these precursors for the elaboration of coatings for metallurgic applications, a great number of studies

have been carried out on these three carbonyl complexes, especially by infrared and temperature programmed desorption (TPD). The early steps of adsorption and reactions on the surface of alumina have been studied in detail.

First of all, it appears clearly that the hydroxylation level of the surface influences the nature of the adsorbed species and of the resulting deposit. When vapors of $[Mo(CO)_6]$ come in contact with a fully hydroxylated γ-alumina, physisorbed $[Mo(CO)_6]$ species have been detected in the early stages. Indeed, the infrared spectra are consistent with a perturbation of the O_h symmetry, presumably due to an interaction between the oxygen atom of a surface OH group and the carbon atom of one CO ligand.[45] A study by inelastic electron tunneling spectroscopy[46] has allowed the proposal of an additional interaction between the oxygen atom of a CO ligand and an aluminum atom. The OC···OH surface interaction provides the labilization of the CO ligand in *cis*-position, so that the loss of one CO gives $Mo(CO)_5(L)$ where the sixth ligand is now an oxygen atom from a surface OH group.[45] Further CO loss occurs slowly to provide ill-defined $Mo(CO)_x$ species, also called lower subcarbonyl species. If, still at room temperature, the system is placed for hours under reduced pressure, these subcarbonyl species are the only one present on the surface.

For chromium and tungsten, the physisorbed $[M(CO)_6]$ species are the only one observed at room temperature, and, as in the case of $[Mo(CO)_6]$ on silica, no subcarbonyls have been observed.[47]

Heating at 373 K produces $Mo(CO)_3$ fragments grafted onto the surface[48] by two different types of sites, which have not been clearly identified. A progressive decarbonylation occurs with further heating, and at 473 K complete decarbonylation occurs. EPR spectra have shown that molybdenum has been oxidized, mostly to Mo^{5+}. This oxidation is accompanied by a stoichiometric release of H_2 (from the hydroxyl protons), as shown by TPD experiments.[49] A more recent paper related to the synthesis of model catalysts under UHV from $[Mo(CO)_6]$ on planar hydroxylated alumina films grown on molybdenum substrates has allowed the study of low loading catalysts.[50] Under these conditions, $[Mo(CO)_6]$ adsorbs at 80 K and desorbs almost completely at 200 K, with only 2% of a monolayer reacting with the surface. The decarbonylation of the adsorbed carbonyl occurs between 80 and 175 K, and adsorbed $Mo(CO)_5$ and $Mo(CO)_3$ species are identified. On the basis of IR and XPS analysis, oxalate and $Mo^{IV}O_2(CO)_x$ species are proposed to be formed when heating upon 205 K. TPD experiments have shown that the Mo^{4+} species is thermally stable up to 450 K, whereas the oxalate species decomposes at 300 K to form a bidentate carbonate species. Then, above 560 K, this latter carbonate species reacts to evolve CO, and molybdenum carbide is formed. It has been observed that, on partially dehydroxylated (50%) alumina films, the extent of decarbonylation and thus the oxalate coverage is decreased by 50%.

On a partially hydroxylated support (573−773 K, under vacuum) $[Mo(CO)_6]$ is adsorbed in a first step at room temperature. However, as acidic sites have appeared during the dehydroxylation process, the system evolves rapidly and an interaction between a CO ligand and two types of Lewis acidic sites takes place. As previously noted for the fully hydroxylated alumina, $Mo(CO)_5$ is slowly obtained at room temperature, and an additional interaction between a CO ligand and an Al^{3+} surface ion is proposed.[45] Nevertheless, CPMAS solid state ^{13}C NMR measurements have shown that the $Mo(CO)_5$ surface species can rotate around the surface−molybdenum bond, so that this $CO\cdots Al^{3+}$ interaction is certainly weak. Evidence is also provided that this $Mo(CO)_5$ species presents some restricted mobility.[51] Similarly, $W(CO)_5$ and $Cr(CO)_5$ surface species have been suggested in several papers.[52,53] Recent thorough infrared studies carried out by Pakkanen and his group have allowed the assignment of the interactions of $W(CO)_5$ with three types of sites: tetrahedral-, octahedral-, and defective surface Al^{3+}.[54] For $Cr(CO)_5$, only one ν_{CO} band has been detected, together with a ν_{CO} band which has been assigned to $Cr(CO)_4$.[55] For molybdenum, further decarbonylation, obtained by heating at 373 K under a stream of helium or overnight pumping, provides $Mo(CO)_3$ bound to the surface which is stable until 473 K. A convincing scheme shows an octahedral environment for this species in which three coordination positions are occupied by three oxygen atoms from the support, and an oxygen atom of one CO ligand interacting with a surface Al^{3+} (Figure 4). However, some controversy exists in the literature concerning the existence of dimeric $Mo_2(CO)_6$ species.[45,51] The corresponding $W(CO)_3$ species[56,57] is quoted but not $Cr(CO)_3$.[52,55] The $W(CO)_3$ moieties appears to be relatively stable, since it is observed, from $[W(CO)_6]$, by TPD under a helium flow at 408 K. The decarbonylation reaction is reversible,[56] and $W(CO)_3$ species decomposed above 623 K.[57] It is worth noting that these $M(CO)_3$ species are to be considered as molybdenum(0), or tungsten(0) tricarbonyl complexes as the three other coordination positions are occupied by three oxygen donating ligands from the surface. TPD observations have shown that, when the temperature is increased, a redox reaction that depends on the OH concentration occurs between the metal center and the hydroxyl surface groups giving rise to H_2 and CO as well as some CO_2 and CH_4 evolution.[56,58] The oxidation state of Mo or W varies largely, as evaluated from the H_2 evolution in TPD, and has been shown by XPS to be Mo^{4+}, Mo^{2+}, in addition to Mo^0.[59] Chromium has been less studied, but a similar oxidation reaction pathway occurring above 373 K has been proposed.[52]

The interactions between $[Cr(CO)_6]$, $[Mo(CO)_6]$, or $[W(CO)_6]$ and a highly dehydroxylated alumina (heated at 1073 K under dynamic vacuum for 20 min) have been studied by Zecchina et al. by infrared spectroscopy.[60] In addition to a $[M(CO)_6]$ species physically adsorbed, three species of C_{4v} symmetry have been clearly identified: they are assigned to $[M(CO)_6]$ in interaction with defective aluminum sites, tetrahedral sites, and octahedral sites in the decreasing order of interaction. The ν_{CO} band for the O-bound CO to the surface is found near 1800 cm^{-1}

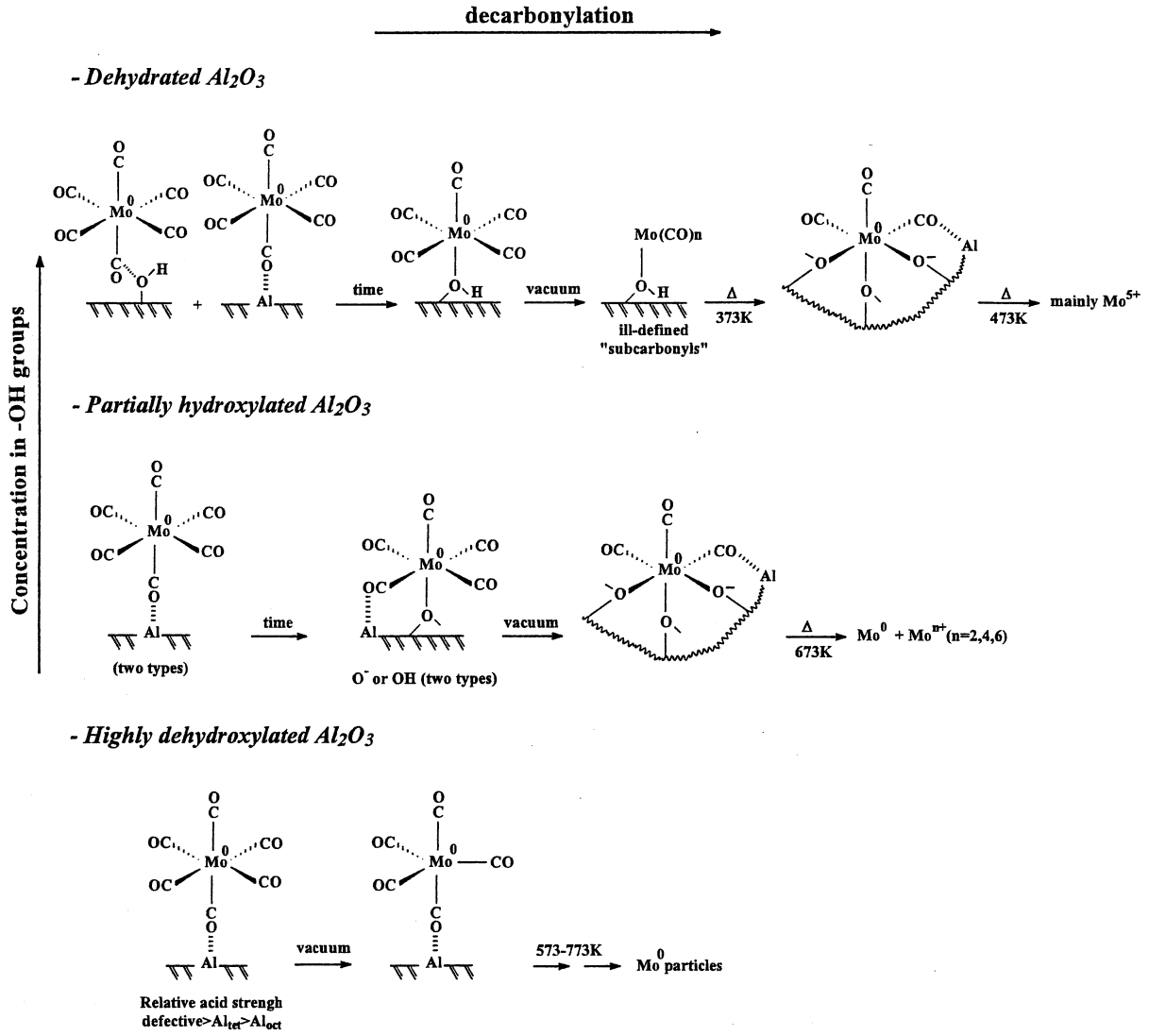

Figure 4. Surface organometallic chemistry of $[Mo(CO)_6]$ on alumina.

and the stronger the interaction, the lower this CO stretching frequency. Prolonged outgassing at room temperature gives rise to some desorption and to the loss of a CO ligand to afford a $M(CO)_5$ species, more likely monomeric than dimeric, attached by O bonding to a Lewis acid Al^{3+} site. From the infrared analysis, a bipyramidal geometry has been assigned to $Mo(CO)_5$ and $Cr(CO)_5$, the situation being more confused for $[W(CO)_6]$. Further outgassing under heating allows more CO ligands to be evolved but no assignment has been done for the remaining species; then, as almost no hydroxyl group remains on the surface, complete decomposition affords molybdenum(0) on alumina.[58,59,61,62] The same situation should prevail for chromium and tungsten. Figure 4 displays the various molybdenum species observed on an alumina support, depending on the degree of dehydroxylation.

Very recently, DFT calculations have been performed to modelize the interactions between $[M(CO)_6]$ ($M = Cr, Mo, W$) and alumina.[63] The acidic and basic surface sites of alumina have been first modelized as tetrahedral or octahedral clusters. Two kinds of interactions are possible: (i) a weak interaction between an Al^{3+} Lewis acid site and a CO ligand of the complex, and (ii) a stronger interaction between AlO^- basic site and a vacant site created when the complex loses one of the CO ligand; in this case, a metal−oxygen bond is formed. For Lewis basic sites models, the strength of the M−O bond increases in the order: $[Cr(CO)_6] \leq [Mo(CO)_6] \leq [W(CO)_6]$, whereas the nature of the metal has no effect on the interaction with a Lewis acid site. The stronger interaction between $[W(CO)_6]$ and alumina could explain the peculiar behavior of alumina-supported tungsten catalyst. Briefly, the hydroxylation degree of alumina controls the temperature of complete decarbonylation of the $[M(CO)_6]$ species but also the oxidation state of the final deposit.

b. Silica, Titania, and Magnesia. On a fully hydroxylated silica, and under mild conditions (298−318 K), the physically adsorbed $[M(CO)_6]$ species have been clearly identified by infrared spectroscopy with a weak interaction between the oxygen atom of a carbonyl ligand and the surface. Whereas the experimental conditions differ markedly from one paper to the other one, no subcarbonyl species have been observed[47] except by Pakkanen et al. who adsorb

$[Mo(CO)_6]$ in the 326−373 K temperature range on high surface area silica in a fluidized bed reactor.[64] Nevertheless, the subcarbonyl molybdenum species have not been definitely characterized. On partially dehydroxylated support, the same situation prevails. The adsorption at room temperature of $[Cr(CO)_6]$ on SiO_2 (treated under vacuum at 773 and 1073 K) has been studied by Hunter et al.[65] Beside the unperturbed physically adsorbed molecule, three different interactions, through O-bond, with Lewis acid sites have been observed. The strength of these interactions depends on the Lewis acidity of the electron deficient silicon sites resulting from the thermal treatment. The same authors[66] have demonstrated that, on silica−alumina supports (13% alumina) the adsorption process is quite similar to the one observed on partially dehydroxylated alumina.

Complete decarbonylation of $[M(CO)_6]$ requires temperatures around 473 K (atmospheric pressure)[67,68] and produces metal oxides with simultaneous loss of H_2, CH_4, and CO_2 with heating until 873 K.

Thus, it appears that the interactions between metal hexacarbonyls and silica are weaker than those observed for alumina and that they concern mainly physically adsorbed species. The absence of strong Lewis acid cationic sites presumably explains the poor stabilization, not only of the hexacarbonyls themselves but also of the subcarbonyl species. This phenomenon is probably connected to the total decarbonylation temperature, which is lower for partially dehydroxylated silica than for the corresponding alumina. Stronger interactions have been obtained when $[Cr(CO)_6]$ or $[Mo(CO)_6]$ are adsorbed on preexisting Cr/SiO_2 or Mo/SiO_2 which are due to the presence of cationic chromium or molybdenum surface sites; in this case physisorbed and chemisorbed species are simultaneously observed.[68,69]

Titania has been mainly used as model support in single crystalline form (110 plane). The adsorption at 150 K of $[Mo(CO)_6]$ on OH free sample has been studied by FT-RAIRS and XPS.[70] The only phenomenon is physisorption of multilayers that desorbs at 220 K without formation of subcarbonyl species. Addition of OH groups on the TiO_2 surface prior to $[Mo(CO)_6]$ adsorption, under the same conditions, does not modify this behavior. Chemical vapor deposition from $[Mo(CO)_6]$ on (110) dehydroxylated TiO_2, in UHV chamber, has been reported by the same author at 400 K. No subcarbonyl is observed and the deposits consist of metallic molybdenum and significant amounts of graphitic carbon.

A different behavior is reported in the case of magnesia, a highly basic suppport.[71] Adsorption of $[M(CO)_6]$ (M = Cr, Mo, or W) on highly dehydroxylated MgO, at room temperature, results in the formation of chemisorbed species, in addition to small amounts of physisorbed species. An adsorption mechanism of the metal carbonyls is proposed, by analogy with homogeneous phase reaction between $[M(CO)_6]$ and Li^+R^-, leading to the formation of $[(CO)_5M\text{-}(COO)]^{2-}Mg^{2+}$ species. By outgassing in the 293−350 K range, a stepwise decarbonylation occurs. After infrared studies, the authors propose the formation of clusters of different nuclearity. At 523 K, they report a complete decarbonylation and the formation of metallic particles.

c. Zeolites. Most of the studies of adsorption and decomposition of metal carbonyls have been carried out with Na and HY zeolites. Prior to the adsorption, the supports are dehydrated by outgassing at around 650 K. Many workers have investigated the interaction of $[Mo(CO)_6]$ with these supports. Room temperature adsorption of $[Mo(CO)_6]$ vapors on HY or NaY zeolites results in the formation of two adsorbed species presenting a slightly distorted octahedral symmetry.[72,73] In the case of $[Cr(CO)_6]$ on HY support, Zecchina et al. have observed physisorbed $[Cr(CO)_6]$ and hydrogen bonded $M-CO\cdots H_{surface}$ species.[74] On NaX[74] or NaY[75] zeolites, $[Cr(CO)_6]$ can be encapsulated at room temperature into the zeolite and interacts strongly with the surface, probably through the extraframework cations. An infrared study shows that progressive heating and evacuating induces the formation of $Cr(CO)_4$ and then $Cr(CO)_3$ encapsulated species. This latter surface−$Cr(CO)_3$ species remains stable until 423 K under vacuum.[76]

In an extensive structural and spectroscopic study of $[M(CO)_6]$ on MY, Özkar et al. propose an interaction between extraframework cations of the zeolite and CO ligands.[77] Saturation adsorption at room temperature give around two $[Mo(CO)_6]$ per HY or NaY supercage.[77−81] Stepwise decarbonylation occurs by heating under vacuum and the temperatures of CO evolution depend on the electronegativity of the cation or of the proton and on the Si/Al ratio.[78,79] Different interpretations have been proposed in the early studies,[81−83] based on the formation of different mono- or dimeric subcarbonyl species. It appears now that the more stable species consists of $Mo(CO)_3$ formed at 373 K.[73,77,82,84,85] Indeed, EXAFS structural data indicate a monomeric *fac*-$Mo(CO)_3(O\text{-zeolite})_3$ structure,[77,84] characterized by a shortening of the Mo−C bond compared to that observed in $[Mo(CO)_6]$ and by a high oxygen sensitivity producing Mo^{6+} species.[85] A complete decarbonylation has been observed by all the authors at around 500 K under vacuum. In these conditions, the decomposition leads to zerovalent molybdenum species.[77,83,86,87] On NaY supports, EXAFS, XPS, and ^{129}Xe NMR spectrocopy have shown that, after decomposition at 473 K in vacuo, Mo_2 species are uniformly dispersed in the zeolite supercages.[87] If the decomposition is performed under molecular oxygen, molybdenum(VI) oxide dimeric species (Mo−Mo distance: 0.321 nm) were produced.[88] However, in the case of HY support, molybdenum becomes oxidized by zeolite protons,[72,82,83] and the presence of Mo^{5+} species have been proposed from EPR studies.[72] Similar results have been reported in the case of the decomposition of $[W(CO)_6]$ on Y zeolites.[89] From XPS results, $[Mo(CO)_6]$ decomposition on HNaY leads to Mo^0 and Mo^{2+} species,[90] and to Mo^{6+} species after air oxidation at 523 K.

2. Other Zerovalent Metal Carbonyl Complexes

Besides these numerous studies on chromium, molybdenum, and tungsten carbonyls and their interactions with various supports which justify the

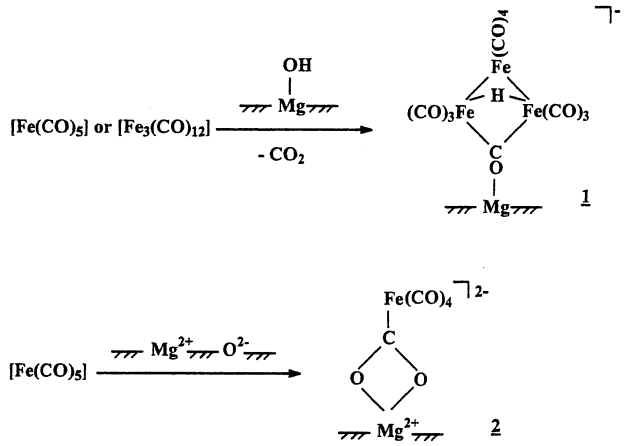

Figure 5. Surface organometallic chemistry of $[Fe(CO)_5]$ on magnesia.

separate analysis of each support, some work has been carried out on the reactivity of $[Fe(CO)_5]$, $[Fe_2(CO)_9]$, $[Fe_3(CO)_{12}]$, $[Re_2(CO)_{10}]$, and $[Co_2(CO)_8]$, with surfaces of silica, alumina, magnesia, zinc oxide, and zeolites.

a. Iron Precursors. Concerning the three iron complexes, their interactions with the supports have been examined, mainly by infrared spectroscopy. Partially dehydroxylated silica has been shown to lead to physisorption,[91−93] so that, for instance, $[Fe(CO)_5]$ can be easily removed from the support, due to the weak interactions that exist between the iron complex and the silanol groups. Photochemical irradiation of this physisorbed $[Fe(CO)_5]$ produces mainly $[Fe_3(CO)_{12}]$ presumably through an $Fe(CO)_4$-(SiO_2) intermediate species.[93]

A thorough study on the nature of the species formed at 298 K by reacting $[Fe(CO)_5]$ and $[Fe_3(CO)_{12}]$ with the surface has shown that, for alumina, magnesia, and zinc oxide a heterogenized $[HFe_3(CO)_{11}]^-$ species is obtained.[91] Indeed, a surface hydroxyl group reacts with the iron carbonyl to provide the hydride complex with simultaneous elimination of one equivalent of CO_2. This complex has been shown to be grafted to the support through a direct bond between the bridging carbonyl group and an acidic center of the surface (Al^{3+}, Mg^{2+}...).[91,92] Once more, the presence of surface OH groups determines the reactivity and thus the nature of the chemisorbed species: whereas fully hydroxylated and hydrated magnesia gives rise to grafted $[HFe_3(CO)_{11}]^-$,[94] a total dehydroxylation of magnesia allows one to obtain the anchoring through an $[(CO)_4Fe(CO_2)]^{2-}Mg^{2+}$ interaction,[95] as summarized in Figure 5.

EXAFS studies carried out on the chemisorption at 313 K of $[Fe_3(CO)_{12}]$ on γ-Al_2O_3 activated at 573 K in dry air revealed the presence of $[HFe_3(CO)_{10}$-$(OAl\equiv)]$, where the bridging CO of **1** has been replaced by an oxygen atom directly bound to a surface aluminum atom.[96] The small differences in the experimental conditions could explain that, in this case, a loss of two CO ligands has been observed.

With graphite as the support, $[Fe(CO)_5]$ is physisorbed as with silica.[97] Similarly, iron carbonyls are mainly physisorbed on various zeolites,[98−100] although it has been suggested that small amounts of a $[Fe(CO)_4$-zeolite] species can be produced at 298 K from $[Fe(CO)_5]$ on HY-zeolite.[98]

It is tempting to rationalize these results by considering that provided a polarized bond is present between the main metal of the support and the oxygen atom of a hydroxyl group, a chemisorbed iron carbonyl can be obtained. The first step is a nucleophilic attack of one CO ligand by an oxygen atom, like in the water gas shift reaction; then the hydroxycarbonyl species loses CO_2 to provide the hydrido species **1**, the Lewis acid site on the surface giving a strong interaction with the bridging CO ligand.

Starting from these adsorption measurements, several studies have been done on the decomposition of the surface carbonyl. Hence, fully or partially hydrated MgO supports have been studied by Basset and his group. In the first case, complete decarbonylation of $[Fe_3(CO)_{12}]$ occurs at 383 K, whereas a partially hydrated magnesia requires 403 K: CO, CO_2, and H_2 have been identified in the gas phase. For the fully hydrated magnesia, Fe^0 dispersed particles and Fe^{2+} sites have been identified by Mössbauer and ESR spectroscopies. Moreover, on partially hydrated magnesia, Fe^0 particles are not oxidized.[94] On completely dehydroxylated MgO supports, metallic iron is obtained upon decarbonylation of $[Fe(CO)_5]$ at around 350 K.[95] On γ-alumina (calcinated at 773 K), decomposition of $[Fe(CO)_5]$ or $[Fe_3(CO)_{12}]$ leads to zerovalent subcarbonyl species at temperatures below 423 K, and to oxidized iron Fe^{2+} at higher temperatures ($\approx$573 K). In this case, in addition to CO, CO_2 and H_2, methane was detected as a decomposition product.[101,102] On synthetic graphite supports, $[Fe(CO)_5]$ decomposition produces metallic iron at temperature as low as 378 K.[97] Similarly, low temperatures of decarbonylation (ca. 343 K) were reported by Derouane and co-workers during their NMR investigations on HY-zeolite, where highly dispersed pyrophoric iron particles are produced.[100] Infrared and thermogravimetric studies performed on adsorption and decomposition of $[Fe(CO)_5]$,[103] $[Fe_2(CO)_9]$, and $[Fe_3(CO)_{12}]$[98,104] have shown that, contrary to alkali metal containing zeolites, a HY-zeolite promotes the formation of Fe^{2+} species at ca. 550 K.

b. Cobalt Precursor. Many studies have been carried out by infrared spectroscopy on cobalt carbonyls to elucidate their interaction with different supports. For all the studied supports, in the absence of a partial CO pressure, the first reaction is mainly the transformation of $[Co_2(CO)_8]$ into the cluster $[Co_4(CO)_{12}]$. Whatever the degree of dehydroxylation of silica, there exists a weak interaction between the cluster and the surface through a direct interaction between a bridging carbonyl group and a hydrogen atom of an OH group.[105−112] Decarbonylation can be achieved more or less rapidly at 373 K in vacuo,[107] or eventually under nitrogen,[112] and a subcarbonyl species with a ν_{CO} band at ca. 2000 cm^{-1} has been detected. Cobalt should be in the zero oxidation state since CO uptake, at room temperature, is facile and provides $[Co_4(CO)_{12}]$ with small amounts of $[Co_2$-$(CO)_8]$.[107] Nevertheless, Pakkanen and his group[113]

have estimated possible charged or radical species by computational methods. The geometry of $Co(CO)_4$ and $Co(CO)_3$ interacting with SiO_2 via Si−Co, Si−O−Co, and Si−O−C−Co bonds have been optimized and the interaction energies were calculated. All bond distances between a cobalt atom and its nearest neighbors are shorter when the number of CO ligand decreased. The interaction energies of charged species ($[Co(CO)_4]^-$, $[Co(CO)_3]^-$, $[Co(CO)_4]^+$, $[Co(CO)_3]^+$) are much stronger than the interaction energies of radical species $^{\bullet}Co(CO)_4$ and $^{\bullet}Co(CO)_3$, and depend on the surface site ($\equiv SiO^- > \equiv Si^+ > \equiv SiO^{\bullet} > \equiv Si$). The strongest interaction has been found for the negatively charged $[Co(CO)_4]^-$ and $[Co(CO)_3]^-$ species bonded to the silica surface via Si−O−Co bonds.

Introduction of oxygen at 293 K favors the removal of CO ligands and provides a surface species that approximatively contains one CO ligand and an oxygen atom per cobalt.[112] Further heating at 473 K under vacuum results in a total decarbonylation and the formation of cobalt(II) species.[108]

With the more basic Al_2O_3[107−111,114] and MgO[105,106] supports, the situation is somewhat more complex. Indeed, as soon as $[Co_2(CO)_8]$ and/or $[Co_4(CO)_{12}]$ are gas-phase adsorbed or impregnated they react with the surface. In addition to the transformation of $[Co_2(CO)_8]$ into $[Co_4(CO)_{12}]$ and small amounts of $[Co_6(CO)_{16}]$, basic O^{2-} sites assist the disproportionation of the cobalt carbonyls to provide $[Co(CO)_4]^-$ and cobalt(II) species of the type $[Co(CO)_xB_y]^{2+}$ where B represents a Lewis base. Moreover, $[Co_2(CO)_8]$ can react on the surface with $[Co(CO)_4]^-$ to form $[Co_6(CO)_{16}]^{2-}$, which has been detected by infrared spectroscopy. Simultaneously, carbonate and bicarbonate species have been detected, which result mainly from CO_2 formed through oxidation of the cobalt carbonyls by the oxide surface, followed by adsorption of the resulting species. EXAFS studies carried out on the species adsorbed on Al_2O_3 have allowed Iwasawa and co-workers to propose the structure of the initially adsorbed complex $[Co_4(CO)_{12}]$.[108] Various thermal treatments induce decarbonylation reactions and the formation of several forms of cobalt oxides by reaction with the OH groups or additional oxygen. Worth noting is the $[Co^{II}]_4$ moiety produced after treatment in O_2 at 293 K,[109,110] and the small spinel-like particles $[Co_3O_4]_n$ obtained after treatment in O_2 at 773 K,[111] that have been both identified by EXAFS.

Concerning the sublimation of $[Co_2(CO)_8]$ and $[Co_4(CO)_{12}]$ on X, and Y zeolites (pretreated at 673 K) the situation is, to some extent, similar to alumina.[115] $[Co_4(CO)_{12}]$ and the anionic species $[Co(CO)_4]^-$ appear rapidly under vacuum with other unidentified carbonyl species revealed by additional CO bands. Heating above 423 K results in the complete and irreversible decarbonylation whatever the zeolites.

c. Rhenium Precursor. As rhenium catalysts play an important role in reforming, alkenes metathesis, and hydrogenation reactions, the interaction of $[Re_2(CO)_{10}]$ with various supports has been investigated by several groups. Sublimation of this dimeric carbonyl at 330−350 K onto highly dehydroxylated alumina (1073 K under vacuum) results in the O-bonding of an axial CO ligand with an aluminum surface atom either in a tetrahedral or an octahedral environment.[116] Due to the presence of strong Lewis acid centers which induce the loss of the initial symmetry of $[Re_2(CO)_{10}]$ to reach a C_{4v} symmetry with the appearance of a new ν_{CO} band near 1800 cm^{-1}, the authors propose a CO-aluminum bond instead of a CO weak interaction as previously noted for partially (400 K) dehydrated alumina.[117] The decomposition of this surface complex has not been reported.

In the same temperature range (320 K), $[Re_2(CO)_{10}]$ vapors react with a model MgO (111) surface to afford $[Re(CO)_4(OMg)_{surf}]_2$. Further heating above 400 K provides a tricarbonyl species in which the rhenium center is bound to three oxygen surface atoms. Total decarbonylation occurs at 700 K leading to metallic rhenium.[118] On MgO powders, the $[Re(CO)_3(OMg)_{surf3}]$ species is also present on highly dehydroxylated supports, whereas on fully hydroxylated MgO a shift in the ν_{CO} bands has been correlated to the formation of $[Re(CO)_3(HOMg)_{surf3}]$.[119] On a support treated at 673 K, a mixed species has been proposed with two types of oxygen rhenium bonds $[Re(CO)_3(HOMg)_{surf2}(OMg)_{surf}]$. Density functional calculations carried out on these species were used to modelize the surface phenomena and have shown that the rhenium−oxygen bonds of $[Re(CO)_3(OMg)_3]$ are as strong as those found in coordination chemistry.[120] The concept of surface sites acting as polydentate ligands is thus strengthened. Tricarbonyl rhenium species grafted on silica or alumina under UV irradiation, or on a NaHY zeolite have also been reported.[117,121]

3. Conclusion

For a given support, the level of dehydroxylation plays a central role on the anchoring mode of the zerovalent carbonyl complex. Usually, there are strong interactions with the most Lewis acidic sites obtained after high-temperature treatment: the absence of OH groups precludes the oxidation of the metal during the final stages of decomposition and allows the formation of metallic deposits. Many studies have shown that the decarbonylation occurs step by step giving rise to intermediate subcarbonyl species.

However, in some cases, it is necessary to have hydroxyl groups to anchor a certain carbonylmetal complex: that means that the first stage of the interaction is related to a nucleophilic reaction of the support on the complex.

C. Interactions between Rhodium(I) and (III) Precursors and a Support

Because of its activity in the NO reduction reaction resulting in a large use in automotive catalytic converters, rhodium has been the subject of numerous catalytic studies, including model systems. Two precursors have been particularly investigated for gas-phase deposition, $[Rh^{I}Cl(CO)_2]_2$ and $[Rh^{III}(\eta^3\text{-}C_3H_5)_3]$.

The $[RhCl(CO)_2]_2$ complex adsorbs on silica powder pressed into wafers (pretreated between 373 and 1073 K under vacuum) without decomposition and

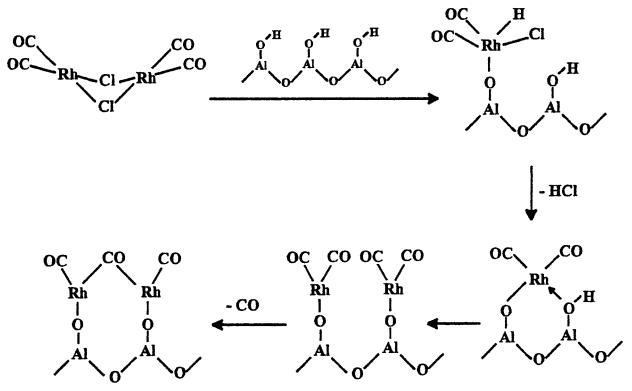

Figure 6. Postulated surface organometallic chemistry of $[RhCl(CO)_2]_2$ on alumina (adapted from ref 125).

can be extracted by solvent treatment.[122,123] When exposed to 600 Torr of CO at 800 K $[RhCl(CO)_2]_2/SiO_2$ reacts to give a $[RhCl(CO)_3]/SiO_2$ species.

Under the same conditions, the same authors have reported a different behavior on alumina support.[123] Two rhodium(I) carbonyl species, namely, $Rh^I(CO)_2$ and $Rh^I(CO)$, have been proposed from IR observations. Chemical analysis shows that all the chlorine is retained in the samples. Similar $Rh(CO)_2$ species have been obtained from zerovalent $[Rh_4(CO)_{12}]$ and $[Rh_6(CO)_{16}]$ cluster precursors on alumina[124] under UHV conditions; XPS measurements display a Rh $3d_{5/2}$ binding energy of 310.2 eV comparable to that for Rh^{3+} compounds.

Model studies concerning the $[RhCl(CO)_2]_2$ interaction with alumina surfaces have been carried out using inelastic electron-tunneling spectroscopy,[125] high-resolution electron energy loss spectroscopy,[126] or XPS-AES.[127] The first observation is that only one monolayer strongly adsorbs to the surface, while the outer physically adsorbed layers is desorbed upon warming below 273 K. At room temperature, different rhodium carbonyl species have been proposed including bridging carbonyls. A postulated adsorption mechanism is depicted in Figure 6. On the basis of the absence of Rh−Cl vibrations, the authors proposed an oxidative addition of an hydroxyl group followed by reductive elimination of HCl.

On a hydroxyl free substrate,[127] a TPD study of multilayer adsorbed $[RhCl(CO)_2]_2$ at 108 K shows the desorption of the outer multilayer at 231 K and, from 270 to 573 K, further CO evolution from thermal decomposition of the monolayer left on the surface. Above 623 K, AES data indicate about 3 Cl per Rh atom on the surface, and XPS measurements reveal zerovalent rhodium. Effective chlorine removal is achieved by temperature cycling between 108 and 623 K under 6.5×10^{-6} Pa of H_2O. After CO chemisorption, a mean particle size of 12 nm has been measured.

Several surface science techniques have been used by Evans and Hayden to follow the reactions occurring during the interaction of $[RhCl(CO)_2]_2$ with a TiO_2 (110) surface.[128−137] A general behavior similar to the one observed on Al_2O_3 model substrate has been observed. At 300 K, a rhodium(I) geminal dicarbonyl is formed by the dissociative adsorption of the precursor, and chlorine is coadsorbed on the TiO_2 (110) surface. The rhodium gem-dicarbonyls coordinate to two oxygen atoms of the surface adopting either a square planar or a tetrahedral geometry (Figure 7).[134] Very recently, the same authors have evidenced by scanning tunneling microscopy that, besides these rhodium(I) gem-dicarbonyl adlayers, some discrete particles are formed, preferentially at step edges of the support.[135,136] The $Rh^I(CO)_2$ species decompose at 500 K to produce metallic rhodium particles Rh^0_x, while chlorine remains on the surface even after heating until 800 K. Partial regeneration of the parent $Rh^I(CO)_2$ is observed by subsequent CO exposure. Reaction of H_2 with $Rh^I(CO)_2/TiO_2$ at 300 K produces an absorbed monocarbonyl intermediate, presumably Rh(H)CO together with a slight decrease of the amount of adsorbed chlorine. Further heating at 425 K under H_2 is accompanied by a reduction of the carbon and of the rhodium. The $Rh(CO)_2-TiO_2(110)$ is converted by exposure to NO at 300 K into highly dispersed $Rh(NO)^+$ species, that are thermally more stable than the geminal dicarbonyl species.[137] This $Rh(NO)^+$ species produced Rh^0-TiO_2 by heating at 600−650 K. The different reactions occurring on TiO_2 surface are depicted in Figure 7.

The rhodium(I) species containing two geminal-carbonyls has also been observed on NaY or HY dehydrated zeolites (773 K in vacuo) starting from

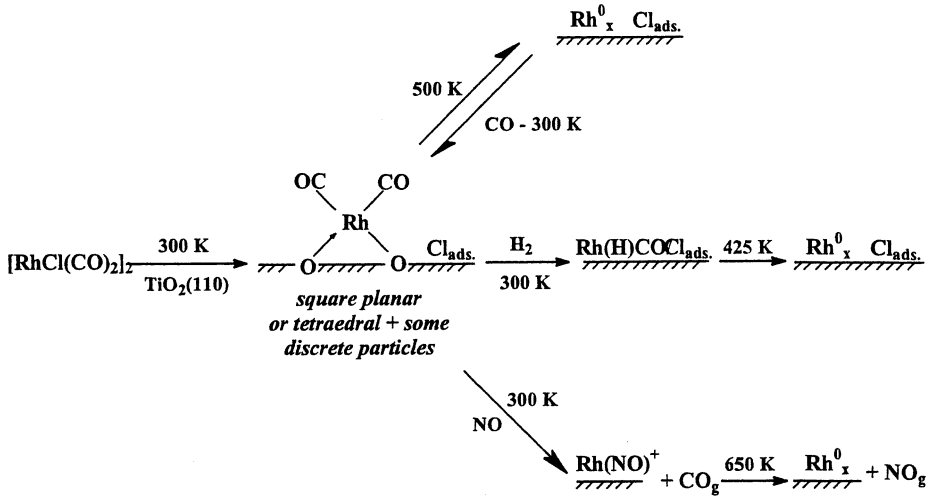

Figure 7. Surface organometallic chemistry of $[RhCl(CO)_2]_2$ on titania.

$[RhCl(CO)_2]_2$ or $[Rh_6(CO)_{16}]$ in the presence of dioxygen,[138] as well as on TiO_2 (110) starting from $[Rh(CO)_2(acac)]$.[139]

The $[Rh(\eta^3\text{-}C_3H_5)_3]$ precursor has been largely used to prepare supported rhodium on various substrates, and thus, its chemistry during the deposition and decomposition steps has been investigated. However, controversial conclusions have been reported, so that a clear description of this chemistry is not possible. Whatever is the nature of the support (silica, titania, alumina, or magnesia), the hydroxyl groups play a major role during the first step of interaction. Most of the authors propose a $\equiv M-O_{surf}\text{-}Rh(C_3H_5)_2$ rhodium(III) species, which is grafted to the surface through an oxygen−rhodium bond and which contains two allyl ligands.[140−143] On the contrary, Iwasawa has proposed the direct formation of a mono allyl rhodium(III) species on TiO_2 previously treated at 473 K.[144,145] Basset and co-workers have noted that the more acidic the support, the faster the grafting. The order of reactivity is $TiO_2 > SiO_2 \gg Al_2O_3 >$ MgO, the two first supports being activated between 298 and 523 K, and Al_2O_3 or MgO between 473 and 673 K. Due to the loss of physisorbed water an alumina activated in these latter conditions is more reactive than one activated in the 298−573 K temperature range. In a further step, the authors use dihydrogen as a reactive gas to promote the decomposition of the remaining allyl ligand(s). Immediate displacement of the allyl group is observed on titania support when dihydrogen is introduced at room temperature, and a band is detected at 2048 cm^{-1}.[144−147] This band has been assigned to a Rh−H vibration by Iwasawa et al.,[144,145] whereas Basset et al.[146,147] have assigned this band to a CO ligand arising from allylic alcohol formed by coupling of the allyl ligand with a surface OH group. Under similar conditions, Schwarz et al. have proposed the formation of rhodium-hydride species.[140,141] Finally, heating under dihydrogen in the temperature range 623−773 K affords metallic rhodium particles.[141,142,145]

D. Miscellaneous Metal Precursors

Several papers have appeared recently that deal with the first step(s) of anchoring of various elaborated precursors presenting, of course, a significant vapor pressure. Moreover, highly sophisticated analytical tools have been used to obtain very precise information, e.g., CP-MAS ^{13}C NMR, EXAFS, polarized total-reflection fluorescence extended X-ray absorption fine structure (PTRF-XAFS),[21,22] and sometimes theoretical calculations. In many cases, an approach of the grafting at the molecular level can be reached.

Thus, Basset and his group, have studied by IR, ^{13}C, and ^{119}Sn MAS NMR the reaction of tetraalkyl tin complexes with the surface of silica.[148] On partially dehydroxylated support (573−873 K) and below 373 K, the complexes are physisorbed via hydrogen-type bonding between the hydrogen of the terminal methyl group of the alkyl ligand and the oxygen of the surface silanol group. Above 373 K, a reaction occurs leading to the formation of essentially one type of surface complex $[\equiv Si-O-Sn(R)_3]$ and evolution of one mole of the corresponding alkane per mole of tin surface. Using the same analytical techniques as well as deuteriation experiments, they have shown that $[Zr(neopentyl)_4]$[149] or $[Ti(neopentyl)_4]$[150] react at 333 K with the surface of a partially dehydroxylated silica (773 K) to afford $[\equiv Si-O-Zr(neopentyl)_3]$ or $[\equiv Ti-O-Zr(neopentyl)_3]$ and loss of neopentane.[106] Similarly, $[Cr(neopentyl)_4]$ reacts with the surface of a partially dehydroxylated silica activated at 473 or 773 K containing a reduced number of surface OH groups. In the latter case, only one neopentane molecule is formed per chromium atom (0.92 measured) by reaction with an OH group providing the $[\equiv Si-O-Cr(neopentyl)_3]$ surface species. For the silica activated at 473 K, the species $[\equiv Si-O-Cr(neopentyl)_2]$ is mainly formed (1.87 neopentyl equivalents measured).[151] Further thermolysis under mild conditions (333 K) liberates one more alkyl ligand, eliminated as neopentane, to give a Cr^{IV} species which is formulated either as an $[(\equiv SiO)_2Cr{=}CH(^tBu)]$ alkylidene species or a $[(\equiv SiO)_2CrCH_2C(CH_3)_2CH_2]$ metallacyclobutane species. The presence of the alkylidene species seems more consistent with the deuteriation experiments,[151] and kinetic studies.[152] Vanadium(IV) species have been similarly generated.[152] The direct introduction by sublimation of an alkylidene complex, e.g., $[Ta(=CH^tBu)(neopentyl)_3]$, on a silica activated at 773 K, affords a surface species where the alkylidene moiety remains coordinated to the metal, whereas an alkyl group is removed as neopentane. From isotopic labeling experiments, the authors propose that an OH surface group is primarily added on the metal−carbene bond and that a α-hydrogen elimination occurs on one of the alkyl ligands to regenerate the alkylidene ligand.[153] The same mechanism is proposed for the second loss of an alkyl group, giving rise to $[(\equiv SiO)_2Ta(=CH^tBu)(neopentyl)]$.[153]

Due to their high volatility the β-diketonato complexes have been largely studied. Moreover, by trapping a hydrogen atom the ligand can be more or less easily eliminated as a volatile β-diketone molecule. Interaction of $[Cu(hfacac)_2]$, in which hfacac is a hexafluoroacetylacetonato ligand, with high surface area silica has been investigated by infrared in the frame of CVD deposit studies.[154] The supports have been more or less dehydroxylated with activation temperatures of 298, 673, and 1123 K. In any case, the authors observed a physisorption at 143 K. At 298 K, on silica treated at 1123 K an interaction with siloxane groups has been noticed, whereas on supports activated at 298 and 673 K, chemisorption is proposed to occur by the interaction between the copper atom and a silanol group.

The complex $[Cu(dpm)_2]$, in which the acetylacetonato ligand contains four *tert*-butyl substituents, i.e., 2,2,6,6-tetramethyl-3,5-heptanedionato, reacts at 323 K with the surface silanol groups of a silica treated at 733 K. Infrared measurements show that the OH groups disappear with the simultaneous appearance of CH_2 stretching frequencies due to ligand hydrogenation.[155] XPS[156] and EXAFS[157] measurements indicate that the oxidation state and the

oxygen distribution around the metal remain unchanged after chemisorption. Similar observations have been made with [Ca(dpm)$_2$].[156−158] Further reaction with water vapor at 673 K restores the silanol groups, allows the ligands to be removed, and produces copper(I) deposits. The same copper complex has been used by Iwasawa and co-workers to deposit submonolayers of copper oxide on α-quartz (0001).[159] EXAFS reveals that the copper atoms are dispersed on the 3-fold sites of the quartz surface.

The chemisorption of [Cr(acac)$_3$] on porous high surface area silica has been shown to occurs at 473−553 K and involves one silanol group, giving rise to the loss of one equivalent of acetylacetone and to the formation of a chromium−oxygen bond between the complex and the surface. The isolated OH groups present a higher activity than the strongly H-bonded OH groups as shown by varying the pretreatment of silica. The two other acac ligands can be removed at 673 K in air to produce Cr^{6+} species, or in the presence of water vapor to maintain the +III oxidation state of chromium.[160]

Chromocene has been used as chromium precursor and its grafting has been studied because it produces an active polymerization catalyst.[161] On highly dehydroxylated silica (973 K), sublimation of [Cr(η^5-C_5H_5)$_2$] at room temperature gives, in a first step, a reaction with the silanol groups of the surface. One equivalent of cyclopentadiene is evolved and the surface species [≡Si−O−CrCp] is formed, as shown by infrared spectroscopy. The authors show that further addition of chromocene can occur; it is weakly bonded through one cyclopentadienyl ligand to the first chromium atom and can be relatively easily removed under vacuum (this dinuclear species is supposed to be inactive in ethene polymerization).

The reaction of benzene tricarbonyl chromium, another catalyst precursor for ethene polymerization, with alumina, silica−alumina, or silica surfaces has also been studied,[162−164] and the resulting species are presented in Figure 8. Depending on the temperature pretreatment of the alumina support, two kinds of interactions have been indicated. On alumina pretreated at 773 K, the main adsorption involves H interactions between a hydroxyl group and a benzene ligand (Figure 8a). If the number of OH surface groups is decreased (T = 1073 K) then a direct bond is formed between an oxygen atom of a carbonyl ligand and an Al^{3+} surface cation (Figure 8b). Further treatments under mild conditions (333 K for instance, outgassing...) induce the loss of benzene and of carbonyl ligands to produce subcarbonyl species. On silica support,[163] pretreatment and coverage ratios play a major role on the adsorption process at 298 K. Silanol groups interact with one of the CO ligands when vicinal silanol groups are available (hydroxylated surface), and additionally via H-bonding with the benzene ligand for highly dehydroxylated surface (Figure 8c,d). Furthermore, for high temperatures treatments of the support (1073 K), electron-deficient silicon atoms are created, and constitute Lewis acid sites able to interact with a CO ligand via an oxygen atom. On the contrary to alumina supports, raising the temperature of the impregnated sample to 358 K results in desorption rather than decomposition of the precursor. Finally, on silica−alumina support, (pretreated at 773 K), [Cr(CO)$_3$(C_6H_6)] is first adsorbed (298 K) via ≡Si−OH···benzene ligand interaction and is rapidly transformed giving a [≡Al^{3+}-OCCr(CO)$_2$(C_6H_6)] species (Figure 8e,f).[164] In this case, ligand loss occurs upon evacuation at 298 K or on thermal treatment (353 K), producing subcarbonyl species.

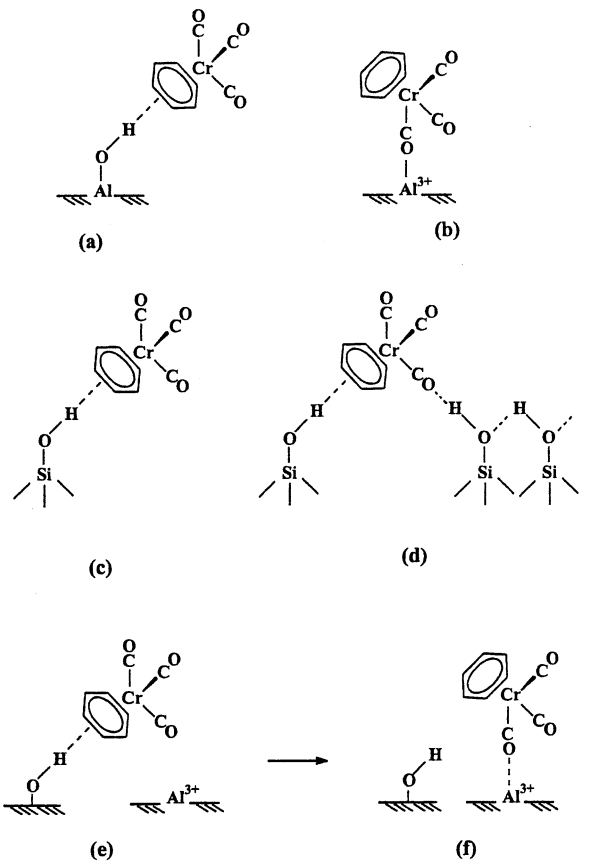

Figure 8. Adsorption of [Cr(CO)$_3$(η^6-C_6H_6)] on alumina (a) and (b), silica (c) and (d), or silica alumina supports (e) and (f).

In addition to the hexacarbonylmolybdenum precursor (vide supra), the lability of the allyl ligands has also been used to anchor a molybdenum fragment on a surface.[165] At 318 K, [Mo(η^3-C_3H_5)$_4$] reacts with silica (pretreated at 823 K under O_2) to yield an anchored species with a Mo/C ratio of 1/6. This result is in agreement with the bis-allyl molybdenum(IV) [(≡SiO)$_2$Mo(η^3-C_3H_5)$_2$] species observed by Iwasawa in pentane solutions.[166] ESCA measurements performed after samples reduction at 823 K indicate the presence of Mo^{2+} surface species.

Ozin and co-workers have examined the vapor-phase impregnation of [(η^5-C_5H_5)Ir(CO)(H)$_2$] onto various M_{56}Y zeolites where M is an alkaline metal present in the framework as cation.[167] This study shows that for the small Li^+ and Na^+ cations, the bonding involves the simultaneous interaction of the CO and the cyclopendienyl ligands with two cations. However, with the larger K^+, Rb^+, and Cs^+ cations, the interaction occurs only between a cation and the two hydrides. At saturation, two iridium molecules can be incorporated in the α-cage of the zeolite.

E. Conclusion

It appears from this analysis of the literature that the fate of a metal complex approaching a solid surface obviously depends on the nature of that surface. The most recent physicochemical investigations on oxide supports, show clearly the main role of the surface hydroxyl groups and the presence of Lewis acidic sites in coordinating the metal precursor and then stabilizing any subcarbonyl species. These intermediate complexes, in which the support acts as a ligand, have in certain cases been fully characterized. Further removal of the primary ligand requires heating and, in some cases, the presence of a reactive gas.

When, in the first step, molecular or quasi-molecular species are obtained, the resulting material consists mainly either in an oxide or in zerovalent metallic aggregates. Here also the noninnocent nature of the support needs to be underlined. Unfortunately, the second step of decomposition has been poorly investigated, particularly the nucleation step.

Besides zerovalent carbonyl complexes which have been mainly studied, a few complexes containing other ligands than CO, such as allyl or acetylacetonato, that show good volatility properties deserve more investigation, not only to understand more deeply all the steps of a surface-organometallic chemistry but also to have at one's disposal a large range of metallic precursors.

III. Preparation and Surface Properties of CVD Catalysts

After the first part of this review devoted to the interactions between the surface of the support and a precursor, we examine the various gas-phase methods that can be used to elaborate heterogeneous catalysts. We have focused on the various strategies that have been adopted to prepare catalysts with a controlled morphology. The structural and physicochemical characterization of the resulting materials will be emphasized. Finally, their catalytic performance will be analyzed and compared with those of the corresponding catalysts prepared by conventional impregnation methods.

In this section, we will distinguish between two kinds of gas-phase methods: (i) the two-step process that consists of the gas-phase adsorption of the precursor on the support followed by the thermal treatments required to obtain the active catalyst, and (ii) the one-step process in which the sublimated precursor is simultaneously adsorbed and decomposed on the heated support. This latter process which is similar to the chemical vapor deposition one used for film elaboration in microelectronics will be specifically called CVD. As the two-steps process is often named in the literature CVD, atomic layer epitaxy (ALE), grafting or anchoring, we will call it here for clarity reasons "gas-phase impregnation-decomposition" (GPI-D). Additionally, a dry-mix method has also been reported in which the precursor is physically mixed with the support, heated for gas-phase impregnation and then decomposed.

While most of the studies deal with the fixed bed technique, the use of a fluidized bed has proved its efficiency to obtain a narrow distribution of the particle size on the surface of the grains together with a homogeneous dispersion on the whole surface of the porous support. Omata et al.[168] were the first to report the use of a fluidized bed reactor to decompose nickel tetracarbonyl in a two-step reaction. Due to the high vapor pressure of $[Ni(CO)_4]$, a low-temperature gas-phase impregnation is followed by a decomposition stage under a nitrogen atmosphere. The same two-step procedure was used by Dossi et al. to prepare, in a U-shaped tube, Pd and Pt particles supported on zeolites.[169] We have reported the design of a CVD reactor that allows the vapor of a precursor to come into contact with the support in a fluidized bed under reduced pressure, as well the small sizes obtained for highly dispersed noble metal agregates, easily produced at relatively low temperatures of decomposition.[170] Generalization of this method has appeared and we can mention the work of Pakkanen and his group,[171] who describes the use of a fluidized bed to obtain structurally well-defined catalysts by a controlled gas-phase deposition which involves successive GPI-D cycles, similar to the ALE process described by Lakomaa et al.[172] A similar approach has been used by Baerns et al. who prefer to define their method as "CVD and decomposition".[173]

For reasons of clarity, we have chosen to classify the different catalysts prepared by gas-phase techniques according to the metal precursor that has been used. The choice of the metal precursor for catalyst preparation is mainly governed by some well-known general criteria, which can be summarized as follows: good volatility and thermal stability under transport conditions, simple preparation, high purity, easy and clean decomposition, reduced-toxicity, and stability under storage conditions over a long period.

A. Zerovalent Metal Precursors

1. Chromium, Molybdenum, and Tungsten

Several zerovalent carbonyl precursors especially $[Cr(CO)_6]$, $[Mo(CO)_6]$, and $[W(CO)_6]$ have been used by Brenner et al. to prepare γ-Al_2O_3 or TiO_2-supported catalysts.[174−178] These catalysts have been prepared by GPI-D and the influence of various pretreatments of the support on the catalytic activity in the hydrogenation of ethylene has been studied.[174−176] Low-temperature decomposition (473−573 K under He) leads to the formation of well-dispersed subcarbonyl species more active than catalyst activated at 873 K. The decrease of activity is explained as resulting from the oxidation of the metal by the remaining surface hydroxyl groups at high temperature. When a dehydroxylated alumina (1223 K) is used, the metal oxidation is less pronounced and a much more active catalyst is produced. On titania support, the oxidation degrees of Cr, Mo, and W deposited by GPI-D from the hexacarbonyl precursors depends also on the dehydroxylation level of the support.[179] From TPD experiments performed until

1073 K, it appears that dehydroxylated titania at 773 K provokes less oxidation than the same support dehydroxylated at 523 K. All these latter catalysts are active for ethylene hydrogenation and the reactivity increases in the order Cr < W < Mo as in the case of alumina-supported catalysts.

$[Mo(CO)_6]$-based catalysts supported on TiO_2, Al_2O_3, ZrO_2, or MgO after dehydration at 773 K have been characterized by TPD, XPS, and the catalytic activities evaluated for various reactions, as propene metathesis and 1,3-butadiene hydrogenation.[180] Molybdenum catalysts supported on TiO_2 show the highest catalytic activity, and the oxidation degree of molybdenum is lower on this support than on the others. It is worth noting that the GPI-D method does not allow grafting of molybdenum on a silica support.

When $[Mo(CO)_6]$ is encaged at room temperature in MY zeolites, a very active catalyst for hydrogenation of butadiene (423 K) is produced, the grafting of the complex being accompanied by CO evolution. Treatment at 473 K, corresponding to a complete decarbonylation, has a negative effect on the activity of this catalyst.[181]

Recently, molybdenum dimer oxycarbides entrapped in NaY supercages and prepared by GPI-D cycles from $[Mo(CO)_6]$ have shown a specific activity for the methanol decomposition reaction to produce CH_4, CO_2, and H_2.[182] After exposure to $[Mo(CO)_6]$ vapors at room temperature, the supercages are filled with two $[Mo(CO)_6]$ molecules. Decarbonylation at 573 K under vacuum results in the evolution of 5.5 equiv of carbon per molybdenum atom and in the formation of $Mo_2(C)O_x$ dimers as shown by TPD, EXAFS, XPS, and XRF analyses. Oxidation at 623 K induces Mo−Mo bond breaking and formation of tetrahedral monomeric MoO_4 species with evolution of the remaining carbon atoms. Further reduction at 723 K under H_2 produces clusters, which contain both Mo−O and Mo−Mo bonds. The catalysts have been tested in the methanol decomposition reaction at each step of their preparation; the oxycarbide dimer species is the only one to produce CH_4, CO_2, and H_2, whereas the oxidized and reduced samples produce only dimethyl ether.

Although less common than the gas-phase impregnation process, the dry-mix method is described here since it would seem to involve the diffusion of the precursor in the gaseous state. For instance, $[Mo(CO)_6]$ has been mixed in the solid state with alumina, treated under vacuum at low temperature, and then heated slowly until 573 K to achieve a complete decarbonylation. Dispersions obtained by this way are significantly lower than those observed for the catalysts prepared by impregnation of $[Mo(CO)_6]$ in hexane solution.[183]

Finally, photoactivation of $[Mo(CO)_6]$ or $[W(CO)_6]$ has been reported as an effective method for the preparation of active catalysts for but-1-ene metathesis.[184] Sublimation of the metal carbonyl at 333 K followed by irradiation at room-temperature induces the formation of subcarbonyl species that could be active catalyst precursors. Alumina-supported subcarbonyl tungsten species prepared by GPI from $[W(CO)_6]$ or $[W(CO)_5L]$ (L = PPh_3, $P(OPh)_3$, or PBu_3] are active catalyst precursors in the *cis*-2-pentene metathesis.[185]

2. Nickel, Iron, Cobalt, Ruthenium, and Rhenium

a. Nickel. Due to its high toxicity, $[Ni(CO)_4]$ has been relatively rarely employed as precursor for catalyst preparation. Gas-phase impregnation at 298 K of $[Ni(CO)_4]$ on γ-Al_2O_3, alumina fibers (Saffil), or HY and NaY-zeolites has been performed by Derouane et al.[186] On alumina fibers, decomposition of the impregnated material at 473 K affords Ni metal crystallites (5−15 μm) consisting of 50−200 nm Ni particles. Active Ni/C* catalysts for methanol carbonylation can also be prepared by GPI-D from $[Ni(CO)_4]$.[168] The GPI step is performed either at 325 K or at 423 K in a fluidized bed reactor, and the decomposition occurs at 523 K under N_2 in the same reactor. Although the nickel particles are much larger for the GPI-D catalyst (7% Ni w/w) than for a wet impregnated catalyst (10% Ni w/w from aqueous solution of nickel acetate), both exhibit very similar catalytic activities for methanol carbonylation. Furthermore, no activation step, such as H_2 reduction, is needed in the case of the GPI-D catalyst.

b. Iron. Iron-based catalysts supported on γ-alumina, dehydrated at 473 K, have been prepared from $[Fe(CO)_5]$ vapor, followed by decomposition under vacuum at 673 K.[187] They present a poor activity in the hydrogenation of ethylene. However, when KOH-doped γ-alumina is used as a support, this method of preparation leads to higher activities than a classical promoted-iron ammonia catalyst.

c. Cobalt. Suvanto and Pakkanen have studied the preparation of cobalt particles dispersed on silica support by the GPI-D method starting from $[Co_2(CO)_8]$ in a fluidized bed reactor.[171] Prior to impregnation, silica having a 320 $m^2\ g^{-1}$ surface area has been sieved to 200−500 μm to ensure an easy fluidization (elimination of fine particles); then, the support has been dehydrated at 573 K under vacuum for 10 h. Cobalt carbonyl, which has a high volatility even at low temperature (80 Pa at 323 K), has been reacted with silica powder in the fluidized bed, either under a CO atmosphere providing orange brown silica particles, or under nitrogen, giving rise to black or black-brown powders. In a second step, heating at 373 K under nitrogen assists the decarbonylation. After 25 h of contact, a loading of 2.5% w/w of cobalt is obtained. The authors show also that on a MCM-41 support much larger amounts of $[Co_2(CO)_8]$ are adsorbed compared to SiO_2.[188] After one GPI-D cycle, the monolayer coverage is ca. 20% Co w/w, the metal loading increases up to 41% Co w/w by using a sequential pulse GPI-D technique. Further comparison of SiO_2 and MCM-41 supports and of two GPI methods (direct or pulsed) on the ease of reduction of the supported cobalt is also reported.[189] The results reveal that samples in which $[Co_2(CO)_8]$ has been deposited on MCM-41 via the pulsed method are more easily reduced or oxidized.

By the same process, tungsten and bimetallic tungsten−cobalt particles have been prepared on γ-alumina supports.[190,191] Loading of tungsten has been realized through successive pulses of $[W(CO)_6]$;

typical sequences are 2 h of sublimation at 363 K, 10 h of decarbonylation at 473 K, and then a second pulse under the same conditions followed by a final reduction step at 723 K under hydrogen for 5 h. To prepare the bimetallic catalysts $[Co_2(CO)_8]$ has been added by a similar pulse sequence to the tungsten-supported catalyst. The preparation has been monitored by infrared spectroscopy in parallel to TPD measurements, mainly to measure the efficiency of the decarbonylation: $[Co_2(CO)_8]$, $[Co_4(CO)_{12}]$, as well as $[Co(CO)_4]$ have been identified as surface-adsorbed complexes. The particle size, their dispersion, and the potential presence of carbonaceous deposits are not indicated. However, these bimetallic catalysts show higher activity than a commercial Co/Mo catalyst for the hydrodesulfurization reaction (HDS) of thiophene. As shown by temperature programmed reduction experiments, after an oxidation pulse at 523 K tungsten catalysts present reduction peaks at temperatures significantly lower than traditional tungsten oxide catalysts. These results are consistent with a good dispersion of the particles on the surface of the alumina supports. $CoMo/Al_2O_3$ [192] and $CrCo/Al_2O_3$ [193] have been also prepared by a similar GPI-D method and tested in thiophene HDS. In the case of $CoMo/Al_2O_3$ samples, the order of metal deposition has been found to moderately affect the catalytic activities, the better results being obtained when cobalt is deposited before molybdenum. For $CrCo/Al_2O_3$, a pronounced promoting effect of Co has been noticed for thiophene conversion: 51.1% with Cr/Al_2O_3 and 86.6% with $CrCo/Al_2O_3$.

The catalytic performances of the well-characterized $[Co^{II}]_4/Al_2O_3$ catalytic species (see part II of this review) prepared from $[Co_2(CO)_8]$ by Iwasawa et al. have been studied.[194] This catalyst presents a much higher catalytic activity than a conventionally prepared impregnated catalyst in the NO−CO reaction.

A dry-mix method has been used to prepare Co/SiO_2 from $[Co_2(CO)_8]$: contrary to other preparation methods as liquid-phase impregnation or physical mixtures, it allows one to obtain a very small metallic particle size (<2 nm).[195]

Finally, the preparation of cobalt containing zeolites catalysts via a microwave discharge method has also been reported.[196,197] The compound $[Co_2(CO)_8]$ has been sublimed onto a dehydrated NaX zeolite and the argon plasma (1−3 W) ignited to decompose $[Co_2(CO)_8]$. The highly dispersed metal clusters located both on the surface and in the bulk of the zeolite are active catalysts in the Fischer Tropsch reaction.

d. Ruthenium. The volatile cluster $[Ru_3(CO)_{12}]$ can be used to deposit ruthenium on various supports. Ichikawa et al.[198,199] use a dry-mix method to incorporate $[Ru_3(CO)_{12}]$ in the α-cages of a NaY zeolite at 333 K under vacuum. A binding site model is proposed[198] that involves the interaction of the oxygen atoms of two cis-carbonyl ligands with a single extraframework Na^+ α-cage cation. The reaction of this $[Ru_3(CO)_{12}]/NaY$ material with dihydrogen at 363 K produces the single hydride species $[H_4Ru_4(CO)_{12}]/NaY$.

When dry mixing is carried out at 403 K under argon at atmospheric pressure with NaY or FSM-16 (amorphous silicate) supports, a black material is obtained[200] indicative of $[Ru_3(CO)_{12}]$ decomposition. After reduction under hydrogen at 723 K, small Ru particle sizes are measured by TEM and H_2 chemisorption (Ru/NaY: 2.4 nm and Ru/FSM-16: 3.6 nm), which can be compared to those of Ru/Y prepared by ion exchange (2.6 nm) but are smaller than those of Ru/NaY prepared from $[Ru(NH_3)_6]Cl_3$ aqueous solutions. The catalytic activity of these dry-mix catalysts has been compared to that of impregnated and ion-exchanged samples in the CO_2 hydrogenation reaction at 423 K and 3 MPa total pressure (CO_2/H_2 = 1:3). On NaY support, no significant difference in activity has been measured whatever the catalyst; however, the ion-exchanged sample shows a higher selectivity for methanol production. It is concluded that the preparation method rather than the metal particle size influences the reactivity.

Pakkanen et al. have used a GPI-fluidized bed method to prepare ruthenium-bipyrydine catalysts supported on SiO_2, silica gel, or alumina, starting from $[Ru_3(CO)_{12}]$.[201] Sublimation of the ruthenium precursor has been performed between 408 and 418 K and the vapors carried out to the fluidized bed maintained at lower or higher temperatures. At 373 K, $[Ru_3(CO)_{12}]$ is mainly physisorbed on the silica support. At higher temperatures, infrared analyses of the fluidized bed, allow to propose the following surface reaction:

$$[Ru_3(CO)_{12}] + HOSi\equiv \rightleftharpoons HRu_3(CO)_{10}\text{-}OSi\equiv + 2CO \quad (1)$$

Further reaction of this species with bipyridine at 373 K results in the formation of an unknown surface species whose infrared bands indicate a compound containing two carbonyl groups. These as-prepared catalysts have been shown to be active in hex-1-ene hydroformylation and water gas shift reactions. In this latter reaction, the GPI-D catalysts are 2−2.5 times more active than the corresponding impregnated catalysts.[201]

On planar model TiO_2 (110) surfaces, $[Ru_3(CO)_{12}]$ can be used for depositing nanosized metallic ruthenium particles under UHV conditions.[202] The precursor decomposition proceeds through some intermediate subcarbonyl species which are completely decomposed at 573 K; however, the metal particles show some residual carbon contamination.

Finally, a series of ruthenium, molybdenum, and ruthenium−molybdenum catalysts supported on Al_2O_3 have been prepared from $[Ru_3(CO)_{12}]$ and $[Mo(CO)_6]$ by GPI-D or wet impregnation (hexane solutions) and tested for thiophene HDS.[203] In HDS tests, the mono- and bimetallic GPI-D catalysts give better thiophene conversion than the corresponding catalysts produced by liquid-phase impregnation. These results clearly demonstrate the benefits of the absence of solvent during supported catalyst preparation.

e. Rhenium. The $[Re_2(CO)_{10}]$ complex has been used to prepare Re/NaY and RePt/NaY catalysts by GPI-D.[204,121] The precursor can be easily deposited by sublimation in flowing He at 363 K onto the zeolite or on a Pt/NaY prereduced support. This behavior

contrasts with that observed on dehydrated SiO_2, on which no deposition takes place as in the case of $[Mo(CO)_6]$.[180] Reductive decomposition of $[Re_2(CO)_{10}]$ is assisted by the presence of platinum particles and complete decarbonylation has been achieved at 723 K, whereas, in the absence of platinum, the required temperature is 773 K. Furthermore, when prereduced Pt particles are present on NaY, the decomposition pathway of $[Re_2(CO)_{10}]$ changes, and complete decarbonylation and aggregation to bimetallic PtRe particles occur in one step. On NaHY support,[121] $Re(CO)_x$ subcarbonyl species are formed that interact with acidic Brönsted sites, so that diffusion inside the zeolite is slow. In this case, a two-step decomposition of $[Re_2(CO)_{10}]$ is observed to obtain PtRe bimetallic particles. The high activity shown by these PtRe/NaY catalysts in the cyclopentane hydrogenolysis reaction is characteristic of a large concentration of platinum−rhenium bimetallic particles.[204]

Active Re/γ-Al_2O_3 catalysts for thiophene HDS have been prepared through GPI-D cycles in a fluidized bed reactor.[205,206] The gas-phase impregnation has been performed at 388 K and the metal loading (1−11% Re w/w) controlled by adjusting the exposure time (4−17 h) or by doing successive GPI-D cycles of 6 h. TPD experiments for different rhenium loadings have shown that a complete decarbonylation occurs between 773 and 873 K, and that whatever the metal content the first step of the decarbonylation corresponds to the formation of $Re(CO)_3$ species. Temperature programmed oxidation and reduction profiles allow to conclude that, for a given metal loading, the dispersion of the resulting particles is better when successive deposition/decarbonylation cycles are performed: a 43% dispersion is obtained for a 11% Re w/w catalyst in one cycle, whereas a 68% dispersion characterizes a 11% w/w Re catalyst prepared by GPI-D cycles.

3. Miscellaneous

Chemical vapor deposition of MnO nanoparticles from $[Mn_2(CO)_{10}]$ has been carried out on platinum(111) surfaces.[207] At 473 K, in the presence of water vapor under UHV conditions, pure ultrathin films of MnO are obtained in a first stage. XPS reveals the presence of MnO, and the absence of any carbon incorporation, presumably due to a catalytic role of the platinum substrate. Careful deconvolution of the XPS spectra for the deposits obtained in the early stages shows the presence of MnO and zerovalent manganese. Longer contact time produces three-dimensional nanoclusters, which grow epitaxially. MnO is known to present a first-order phase transition at 118 K from para- to anti-ferromagnetism; however, performances of this material in catalysis have not been reported.[207] Such a catalytic effect of the metallic support has clearly been observed in recent studies on GPI-D of $[Cr(CO)_6]$ on Pd(100) under UHV conditions. Indeed, infrared measurements have shown that $[Cr(CO)_6]$ can be decomposed on the palladium surface after physisorption and then chemisorption, whereas on a copper (100) surface $[Cr(CO)_6]$ is physisorbed and desorbs without any decomposition.[208]

Finally, it is worth mentioning a recent study on the homogeneous gas-phase decomposition of $[Mo(CO)_6]$ for the preparation of unsupported catalysts.[209] The homogeneous gas-phase decomposition between 773 and 1373 K of $[Mo(CO)_6]/H_2S$ mixtures produces bulk catalysts of molybdenum sulfides characterized by high surface area (16−120 $m^2\ g^{-1}$). This method has been extended to $[Mo(CO)_6]/NH_3$, $[Mo(CO)_6]/[Fe(CO)_5]/NH_3$ mixtures.

4. Conclusion

It appears from these reports that whereas zerovalent carbonyls are convenient precursors for metallic catalyst preparation, some questions remain unanswered concerning the characterization of the resulting materials, especially the chemical purity, the morphology of the deposits, and the particle size distribution. In addition, films deposited by MOCVD starting from carbonyl precursors, in other scientific fields than catalysis, have been reported to be contaminated by substantial amounts of carbon and oxygen.[210]

B. Other Non-Noble Metal Precursors

1. Iron

Two catalytic materials have been extensively studied in the literature due to their high catalytic performances: FeMo heterobimetallic systems and Fe/ZSM5 materials.

Iron−molybdenum bimetallic catalysts supported on borosilicate molecular sieves have been prepared by GPI-D through sublimation of the corresponding chlorides, and their catalytic activities have been evaluated for the oxidation of alkyl aromatics.[211−217]

The supports used in these studies are previously treated to adjust the silanol content on the sieve surface. Iron chloride and the support, separated by quartz wool plugs, are placed in an horizontal quartz reactor. The chloride is sublimed and transported onto the support with N_2 carrier gas at 733 K for approximately 1 h, until the powder becomes uniformly yellow. The anchoring proceeds through the elimination of 1 equiv of HCl per Fe atom, and presumably a $[Si-O-FeCl_2]$ surface species is formed.[211] The resulting material is washed with deionized water, oven dried at 393 K, and heated under N_2 at 673 K. A similar subsequent procedure has been used for molybdenum deposition starting from MoO_2Cl_2, $MoOCl_4$, or $MoCl_5$. The active catalyst is obtained after air calcination in the 923−963 K temperature range in such a way that the ratio Mo/Fe = 1.6−2.0 is reached. The reaction proceeds through the transient $MoO_3 \cdot 3H_2O$ species, which can sublime under the reaction conditions.[212]

This active catalyst has been characterized by X-ray diffraction, X-ray photoelectron spectroscopy, electron microscopy, Raman spectroscopy, and in situ synchrotron radiation studies.[213] In addition, the effect of iron and molybdenum deposition on the surface area has been examined. The two main phases on DBH, i.e., deboronated borosilicate molecular sieves, are $Fe_2(MoO_4)_3$ and MoO_3. High-resolution electron microscopy has revealed that molybde-

num and iron are deposited as rodlike small particles inside the two microporous channel systems characteristic of the support.[213] Concerning the surface area, deposition of ca. 2% of iron has no effect, whereas after addition of 5% more molybdenum a small but definite decrease in both surface area and pore volume is noticed.[212]

The activity of these catalysts in the gas-phase (oxygen[214−217] or N_2O[215]) oxidation of alkyl aromatics has been investigated. For the oxidation of benzene by N_2O to produce phenol,[215] the GPI-D Fe/Mo/DBH catalysts exhibit a significantly higher catalytic activity than their impregnated counterparts prepared from aqueous solutions of iron nitrate and ammonium paramolybdate. TEM observations show clearly a uniform and well-dispersed deposit for the GPI-D catalysts, whereas large aggregates are deposited nonuniformly and mostly on the external surface for the impregnated samples.

For the oxidation of alkyl aromatics by oxygen, the effect of the para-substituents in toluene derivatives has been studied[217] to understand the para-selective oxidation properties of the GPI-D catalysts. For the selective synthesis of terephthaldehyde from *para*-xylene, the authors show that further deposition of SiO_2 from $[Si(OMe)_4]$ vapors on the previous catalysts (1.4% Si w/w) has a positive effect.[216] The use of other supports than DBH, such as a ZSM-5 zeolite or a silicalite, for the GPI-D preparation of the Fe/Mo catalysts has been reported.[214] On a silicate support, the limited number of silanol groups restricts the possible metal loading: 0.58% Mo w/w and 0.13% Fe w/w, vs 7% Mo w/w and 1.3% Fe w/w for the DBH support. Furthermore, a partial destruction of the silicalite and the ZMS-5 structure occurs during the catalyst preparation as observed on TEM micrographs.[47]

For the selective oxidation of *para*-fluorotoluene to produce para-fluorobenzaldehyde, an FeMo/Boralite catalyst, prepared by a GPI-D method similar to that described by Yoo et al., shows a higher selectivity at low conversion, than bulk $Fe_2(MoO_4)_3$.[218] This reactivity is correlated to the presence of nanosized iron-molybdate particles inside the zeolite channels.

As reported by Sachtler et al.,[219−224] an iron-containing zeolite, Fe/ZSM-5 prepared by GPI-D from $FeCl_3$ catalyzes very efficiently the reduction of NO by hydrocarbons, in the presence of high concentrations of water at temperatures as low as 623 K. The catalyst is prepared by sublimation of $FeCl_3$ into the cavities of a H/ZSM-5 zeolite under an argon flow at 593 K in a U-shaped reactor. The reactions between $FeCl_3$, or Fe_2Cl_6, that prevail in the gas phase and the Brönsted acidic sites of the zeolite result in the formation of one HCl molecule per iron atom. The samples are then washed with water and further calcinated in flowing O_2 at 773−873 K, resulting in the removal of most of the remaining chlorine. XRD measurements and HREM observations demonstrate that the GPI-D process does not cause any damage to the zeolite structure. Furthermore, only few particles have been observed and identified as iron oxides, while most of the iron is located inside the cavities and molecularly dispersed.[219] Even if a structural identification of the active species has not been performed, the cross-checking of various experimental results provided by H_2 and CO TPR, oxygen TPD, and catalytic activity for different Si/Al ratios have allowed the proposal of the formation of a binuclear iron complex $[(HO)Fe-O-Fe(OH)]^{2+}$.[219,220] The presence of binuclear ionic species with a bridging oxygen ligand is also indicated by ESR spectroscopy.[223]

A similar method has been used by Centi et al. to prepare, without any calcination step, iron supported onto NaZSM-5.[218,225,226] The comparison with an ion-exchanged catalyst, calcinated at 873 K, in the N_2O reduction reaction with the simultaneous presence of propane and oxygen has been done. The activity for N_2O reduction to N_2 is higher for the GPI-D catalyst even at lower loading (GPI-D: 1% Fe w/w, impregnation: 5% Fe w/w), but lower for propane oxidation. Both catalysts present isolated Fe^{3+} ions or small clusters. Besides these species, diffuse reflectance spectra indicate that the impregnated sample contains highly clustered Fe^{3+} and Fe_2O_3 particles. In our opinion, the high-temperature calcination step performed for the impregnated catalyst should be at the origin of the differences in reactivity.

Additional studies concerning Sachtler catalyst have confirmed the excellent performances of this GPI-D materials for selective catalytic reduction of NO_x.[227−229] Particularly, the wide temperature range (600−800 K) of catalytic activity and stability has been demonstrated.[227] Compared with a commercial vanadia catalyst, the Fe/ZSM-5 catalyst is five times more active at 673 K and produced only N_2 and H_2O in the selective reduction of NO with ammonia.[228] ESR analyses have shown that the GPI-D catalyst contain mainly Fe^{3+} ions in tetrahedral and distorted tetrahedral sites.[229]

2. Nickel

The deposition of nickel on alumina spheres by CVD from nickel chloride vapors at 1073 K followed by a reduction step has been investigated.[230] The use of a fixed bed reactor induces inhomogeneities in the deposit between the upper and the lower part of the bed. Moreover, the intraparticle nickel concentration profile shows a limited diffusion of the metal in the case of the 3.5-mm diameter alumina spheres, despite a modal pore diameter of 9 nm. TEM observations show a mean particle size ranging from 500 to 650 nm. This catalyst has been tested after a reduction step in the acetylene hydrogenation reaction and is more active than an impregnated one.

A mathematical modeling of $NiCl_2$ chemical vapor infiltration into a porous catalyst support has been developed by Moulijn et al.[231] This model shows that the intraparticle metal profile depends on (i) the associative or dissociative adsorption mode of the precursor and (ii) the decomposition rate of the adsorbed metal precursor.

The growth mechanism and reactivity of nickel particles has been studied in the sequential preparation of Ni/Al_2O_3 catalyst via GPI-D (the authors use the term of atomic layer epitaxy) by bringing $[Ni(acac)_2]$ vapors into contact with a stationary bed

of alumina.[232,233] During the first impregnation cycle (3−4% Ni w/w), at 473 K and 10 kPa under nitrogen, the grafted nickel species retain acetylacetonate ligands with the ring structure intact. However, the C/Ni atomic ratios were 5 and 8 for alumina supports preheated at 473 and 1073 K, respectively. An atomic dispersion of nickel is obtained after the first impregnation cycle. Such dispersion is maintained after oxidation at 673 K and reduction at 773 K; however, this catalyst shows no activity for toluene hydrogenation. During the 2 to 4 cycles to prepare 5−10% Ni w/w, low-energy ion scattering (LETS) and XPS analyses reveal a growth of nickel that occurs preferentially on the nucleation centers. The best catalytic activity is obtained for 10% w/w of Ni and further increase of the amount of nickel by additional cycles does not improve the performance of the catalyst.

3. Cobalt

An extensive study of Co/SiO_2 catalysts prepared by a similar sequential GPI-D technique (once again called atomic layer epitaxy) has been performed by Backman et al. (see Figure 9).[234−236] The organometallic complex $[Co(acac)_3]$ is adsorbed at 453 K and 6−10 kPa under nitrogen on a fixed bed of silica, preheated at 873 K. The first impregnation cycle allows the deposition of around 5% Co w/w, and after seven cycles metal loading as high as 20% can be reached. The reducibility of these catalysts is low (max 30%) when compared to a classically cobalt nitrate impregnated catalyst (85−90%).[234] However, if the calcination step after the last sequence is omitted, the reducibility increased up to 60%. The authors explain this phenomenon by the presence of more easily reduced cobalt species that enhance, by spillover, the easier reducibility of silicate CoO_x-SiO_2 species, which are more abundant on GPI-D catalysts than on a impregnated catalyst. The existence of higher quantities of silicates on the former catalyst is related to a higher dispersion compared to impregnated catalysts. The presence of these silicate species has been confirmed by XRD and XPS analyses.[235]

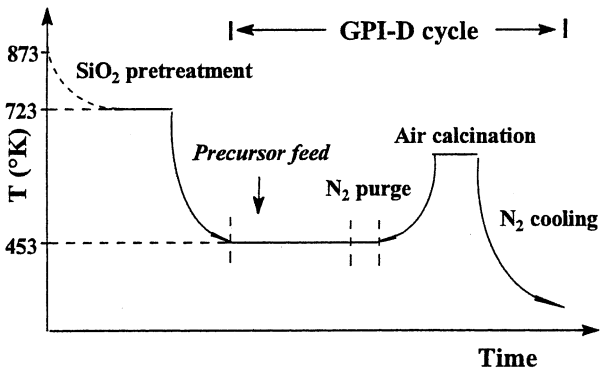

Figure 9. Catalysts preparation using GPI-D cycles (adapted from ref 234).

The resulting catalysts have been characterized and a slight decrease of the surface area and pore size has been observed when increasing the metal loading from 6 to 20% Co w/w. In parallel, the particle size increases from 5 to 25 nm, but the catalytic activity in toluene hydrogenation is not very sensitive to these variations.[235]

These Co/SiO_2 catalysts have been compared to Co/Al_2O_3 samples prepared in a similar way starting from $[Co(acac)_2]$[236] to investigate the effect of the support on the properties of the final material. Smaller quantities of metal are deposited after the first cycle on alumina support: 3 and 5% Co w/w for Al_2O_3 and SiO_2 respectively, and, for each cycle, the cobalt loading increases more slowly on alumina than on silica. In all cases, highly reducible silicates or aluminates are formed, essentially during the first cycle of the preparation. After reduction between 773 and 873 K (41 to 78% of reduction), better dispersions have been observed on alumina support for a comparable metal loading. However, no significant differences have been noticed in the toluene hydrogenation reaction. The Co/SiO_2 catalyst is three times more active than a classically impregnated catalyst (prepared from $Co(NO_3)_2 \cdot 6H_2O$) in the ethylene hydroformylation reaction.[237] This result has to be directly connected to the smaller particle size obtained with the gas-phase process: 4.3 nm for a 5% w/w Co/SiO_2 GPI-D catalyst and 11.3 nm for a 4% w/w Co/SiO_2-impregnated catalyst.

4. Molybdenum

Supported molybdenum catalysts are used in a wide variety of reactions and have been prepared by using different gas-phase methods and precursors.

The early works of Sonnemans and Mars[238] have shown that a monolayered $Al_2O_3 \cdot MoO_3$ catalyst can be obtained by adsorbing $MoO_2(OH)_2$ from the gas phase on alumina. In this process, the volatile precursor is formed by flowing water/air mixtures at 868 K through a fixed bed of MoO_3 particles. The $MoO_2(OH)_2$ vapors react with the alumina in another fixed bed at 873 K to produce an aluminum molybdate layer $Al_2O_3 \cdot MoO_3$. Metal oxide loadings as high as 20% w/w have been reached for reaction times of several days. At high coverage, MoO_3 is also present on the catalyst. This material shows similar catalytic activity in the dehydrogenation of cyclohexane reaction than a catalyst prepared from the liquid phase from ammonium molybdate.

The chemically well-defined Mo^{2+}/SiO_2 catalyst prepared by GPI-D from the alkyl molybdenum precursor $[Mo_2(\eta\text{-}C_3H_5)_4]$[239,240] (Figure 10) is four

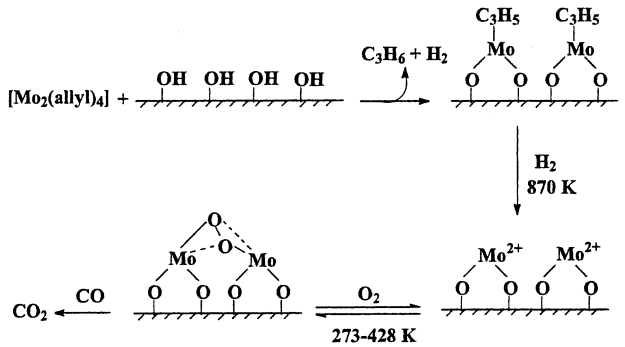

Figure 10. Surface organometallic chemistry of $[Mo_2(allyl)_4]$ on silica.

times more active in ethene hydrogenation at 293 K than a classically impregnated catalyst.[239] It has also been shown that the same Mo^{2+}/SiO_2 catalyst can reversibly fix oxygen in the temperature range 273−428 K. The oxidation of CO to CO_2 by this $Mo_2{\cdot}O_2/SiO_2$ catalyst has also been reported.[240]

Che and co-workers have extensively studied Mo/SiO_2 catalysts prepared from $MoCl_5$ vapor on dehydrated silica by a GPI-D method called "grafting".[241−243] The photoluminescence behavior of this catalyst has been investigated to get information about the structure of the surface species and their reactivity, and to compare them to impregnated catalysts.[241,242] Dynamic photoluminescence spectroscopy studies revealed that the GPI-D catalyst contains only one type of Mo emitting site, whereas the impregnated one, obtained from the same precursor in cyclohexane solutions, contains at least two kinds of sites. The presence of isolated tetrahedral Mo species for the GPI-D catalyst and the additional presence of aggregated Mo and/or polymolybdate species on the impregnated one could be an explanation of this result.[241] The GPI-D catalyst has been tested in the photoinduced methatesis of propylene and compared with an impregnated catalyst prepared from aqueous solutions of ammonium heptamolybdate. The GPI-D catalyst presents a greater activity than its impregnated counterpart. These good performances result from the higher dispersion and the same environment for all the Mo ions (tetrahedral) on the GPI-D catalyst.[242] In the structure sensitive methanol oxidation reaction, good activities and selectivities have been obtained with the GPI-D catalyst. However, contrasting results have been obtained when using the impregnated catalyst, probably due to the lack of reproducibility of its preparation and to its lower metal dispersion.[243]

Silica-supported molybdenum oxide catalysts have also been prepared from the acetylacetonato precursor $[MoO_2(acac)_2]$ by a similar procedure.[244,245] The gas-phase impregnation has been carried out under vacuum, between 393 and 433 K on a dehydroxylated silica (973 K) and is followed by a calcination step at 773 K. A comparison of the dispersion and of the anchoring of the complex with a conventionally prepared catalyst (aqueous impregnation of ammonium heptamolybdate) has been presented.[245] The use of the organometallic precursor allows the formation of Si−O−Mo bonds via ligand loss and leads to larger molybdenum network (Mo−O−Mo bonds) than the impregnated catalyst. XRD shows the presence of orthorombic MoO_3 crystals for both catalysts.

Molybdenum carbide catalysts[246] have been prepared on alumina by using a vapor mixture of $MoCl_5$, benzene, and H_2 under a total pressure of 0.12 kPa. The activity of this catalyst in the reduction of CO_2 has been compared to that of a molybdenum carbide catalyst prepared by impregnation. After a reduction step at 923 K in flowing hydrogen, the catalytic activity of the GPI-D catalyst is 20 times higher than that of its impregnated counterpart. XPS measurements reveal that the valency of molybdenum changes from II for the GPI-D carbide to IV for the impregnated one.

Finally, steam-deposited MoO_3/SiO_2 catalysts have been prepared from MoO_3 and water at high temperature (around 973 K).[247] The presence of water allows the formation of volatile molybdenum hydroxyoxides and the transient formation of Si−OH groups that permit the attachment of molybdenum species.

5. Vanadium

First, the reactivity of VCl_4 vapors with different oxide surfaces (Al_2O_3, SiO_2) has been used to get insight on the hydroxyl groups distribution on these surfaces.[248] Then, vanadium-supported catalysts have been studied because of their activity and selectivity in oxidation reactions of organic compounds.[249,250]

The reaction at room temperature of $VOCl_3$ vapors with hydroxylated anatase followed by a calcination step at 670 K allows a loading of V_2O_5 substantially lower than the value expected for a complete monolayer. Four additional GPI-D cycles are necessary to obtain a catalyst corresponding to one monolayer, which gave a very high selectivity to phthalic anhydride in the *o*-xylene oxidation reaction. Such selectivity is noticeable for a low loading V_2O_5 catalyst and without the aid of any promoter.[249] However, it is worth noting that a similar catalyst can be prepared by a standard procedure that consists of wet impregnation of $VOCl_3$ in different organic solvents.[250]

More recently, it has been shown that $VOCl_3$ can be introduced in the channels of MCM-41 by a GPI-D process.[251] Gas-phase impregnation of $VOCl_3$ at 375 K under nitrogen, followed by purging in N_2 to remove physisorbed $VOCl_3$, affords chemically bonded vanadium species. Previous studies on silica support have allowed proposing $Si-O-VOCl_2$ species.[252] Hydrolysis at 375 K and calcination in dry oxygen at 675 K produces predominantly mononuclear V^{5+} oxide in tetrahedral coordination VO_4^{3-} together with easily reducible polynuclear V^{5+} oxide species.

Photoassisted (300−450 nm) chemical vapor deposition of $VOCl_3$ at 273 K on porous Vycor glass allows one to obtain the chemically anchored $Si-O-VOCl_2$ species via reaction with hydroxyl groups and HCl elimination.[253] Further hydrolysis and calcination steps give a tetrahedral V^{5+} mononuclear species that presents photoluminescent properties. These anchored vanadium oxide catalysts show a much higher activity for the photocatalytic isomerization of 2-butene than that of oxides prepared by conventional impregnation.

Vanadyl alkoxides precursors have also been used with success to prepare supported V_2O_5 catalysts.[254−258] The $[VO(OC_2H_5)_3]$ vapors react at 423 K under a pressure of 13 Pa with the OH groups of a high surface area silica to produce two surface species:

$$VO(OC_2H_5)_3 + \equiv Si\text{-}OH \xrightarrow[423\ K,\ 1\ hr]{10^{-1}\ Torr} \equiv Si\text{-}O\text{-}VO(OC_2H_5)_2 + C_2H_5OH \quad (2)$$

$$VO(OC_2H_5)_3 + 2 \equiv Si\text{-}OH \xrightarrow[423\ K,\ 1\ hr]{10^{-1}\ Torr} (Si\text{-}O)_2\text{-}VO(OC_2H_5) + 2\ C_2H_5OH \quad (3)$$

as suggested by ethanol evolution measurements and changes in the OH region of the IR spectra during GPI-D cycles. Further treatments at 623 or

723 K under vacuum produce highly dispersed V_2O_5 overlayers (thin film or small sized nanoparticles) as indicated by XPS from semiquantitative measurements of the V to Si ratio (I_v/I_{Si}).[254,255] After seven GPI-D cycles, V_2O_5 loading as high as 18% w/w are reached with a high I_v/I_{Si} ratio (0.7) compared to a conventional prepared impregnated catalyst ($I_v/I_{Si} = 0.2$). The as-prepared GPI-D catalyst is 3−4 times more active than the impregnated one in the oxidative dehydrogenation of ethanol reaction at 493 K.[254]

The same authors have studied by EXAFS the influence of the preparation method (GPI-D or impregnation) and of the nature of the support on the structure of the overlayers.[256] The GPI-D method leads to thin films of V_2O_5 (5−10% w/w) on SiO_2 (2 OH nm^{-2}) and on Al_2O_3 (10 OH nm^{-2}), whereas liquid-phase impregnation produces crystallites, defined by the authors as entities, detectable by XRD on silica and thin films on alumina. In the same oxidative dehydrogenation of ethanol reaction the catalytic activity decreases in the order V_2O_5/Al_2O_3-(GPI-D) > V_2O_5/Al_2O_3(imp) > V_2O_5/SiO_2(GPI-D) > V_2O_5/SiO_2(imp). The conclusion is that the activity of the thin films is greater than that of crystallites.

Vanadyl triisopropoxide [VO(*i*-$C_3H_7)_3$] (VOTIP) has been used to prepare vanadia catalysts on different supports.[257,258,245,173] On titania, a support that presents low surface area and low OH concentrations, low loadings of metal are obtained by a cyclic GPI-D process. After three cycles (GPI at 300 K and calcination under O_2 or decomposition under N_2 at 573 K), a V_2O_5 loading of 3.5% w/w is obtained, whereas for an impregnated catalyst (immersion of the support in VOTIP) 5% w/w is obtained in one operation. Raman spectroscopy and ^{51}V NMR spectrometry have been used to characterize the structure of the vanadia species as a function of the dehydroxylation degree of the support. Tetrahedral coordinated vanadia species predominate on highly dehydoxylated surfaces, whereas octahedral coordinated vanadia ions are present on fully hydroxylated supports.[257] Silica, alumina, and zircona supports have also been investigated,[258] and the catalytic properties of the final material have been reported for the reduction of NO by NH_3. The intrinsic activity decreases following the sequence: V_2O_5/TiO_2 > V_2O_5/ZrO_2 > V_2O_3/Al_2O_3 > V_2O_5/SiO_2 and is correlated to the various distributions of the Lewis- and Brönsted-bound ammonia sites on the supported vanadia catalysts.

The preparation of vanadium oxide on different supports from the vanadium acetylacetonates [V(acac)$_3$][173] and [VO(acac)$_2$][245] has been reported. The complex [V(acac)$_3$] is adsorbed on dehydrated silica or alumina at 400 K under N_2 in a fluidized bed reactor.[173] On silica, the chemisorption involves a partial precursor decomposition via acetylacetone evolution, which is more complete on the alumina support. Further decomposition of the surface species in air produces V_2O_5 at 470 K on SiO_2 support and at 570 K on Al_2O_3 support. The [VO(acac)$_2$] precursor has been adsorbed on silica gel by GPI (called "molecular designed dispersion") and by impregnation in toluene.[245,259] In the liquid-phase impregnation at room temperature, hydrogen bonding occurs through an hydroxyl group of the support and an acetylacetonato ligand (Figure 11).

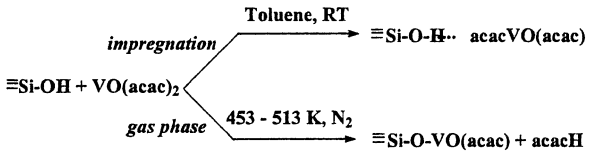

Figure 11. Surface reaction of [VO(acac)$_2$] with silica.

For the gas-phase impregnation at 453−513 K and under nitrogen a ligand exchange mechanism prevails (Figure 11), whereas at 403−443 K under vacuum both hydrogen bonding and exchange mechanism coexist. On alumina, a more reactive support, the reaction of [VO(acac)$_2$] proceeds exclusively by a ligand exchange mechanism. It has been demonstrated from infrared investigations that the environment of the vanadium atoms changes slightly according to the preparation method and to the supports: it is essentially tetrahedral with some fraction of octahedral sites in the case of GPI-D of [VO(acac)$_2$] on silica support. These catalysts present a significant activity for the oxidation of methanol.[259] To obtain the vanadium oxide catalyst; the precursors are thermally converted by oxidation in air at 773 K.

On new mesoporous MCM-48 silica support, the same GPI-D procedure has been applied and after calcination of the grafted complex the supported vanadium species are present in a tetrahedral configuration, mainly as linked tetrahedra and not as isolated species. The final catalyst, 8.7% V w/w, still presents a narrow pore size distribution and a high surface area (S_{BET} = 800 m^2 g^{-1}) compared to the original support (S_{BET} = 1000 m^2 g^{-1}).[260] Modified MCM-48 supports have also been used to obtain larger amounts of anchoring sites and a better anchoring of the vanadium species.[261] An extremely stable catalytic material (under hydrothermal conditions) is produced in which isolated tetrahedral V^{5+} species are dominant.

6. Chromium

The preparation of CrO_x/Al_2O_3 catalysts has been studied by several authors, mainly because of their catalytic activity in dehydrogenation reactions.[173,262−264] The [Cr(acac)$_3$] precursor has been employed for gas-phase impregnation under N_2, and decomposition has been performed under air between 673 and 873 K. The metal loading is adjusted either by using a repeated pulse technique[262,263] (1.3 to 12.5% Cr w/w), or by adjusting the gas-phase impregnation duration (1.2 to 16.9% Cr w/w).[262] Adsorption of [Cr(acac)$_3$] on alumina between 400 and 473 K seems to proceed via a dissociative pathway as reported by Baerns et al.[173] and Kytökivi et al.;[262,263] however, Vansant et al.[264] report that adsorption proceeds in a molecularly dispersed form without acac ligand elimination. Air oxidation of the impregnated samples produces both Cr^{3+} and Cr^{6+} amorphous species.[262,263] The CrO_x dispersion decreased from 77 to 22% when increasing CrO_x loading from 0.9% w/w to 11.8% w/w.[6] The activity and selectivity of the GPI-D catalysts for

isobutane dehydrogenation to butene is very similar to those of impregnated catalysts.[263]

C. Noble Metals

Due to the wide use of mono- or bimetallic supported noble metals catalysts, their preparation by gas methods will retain particularly our attention. In this group of elements, many complexes have been prepared and characterized, so that organometallic chemistry affords a large variety of potential precursors. However, in the platinum group metal, no zerovalent carbonyl complexes are stable enough to be used in a gas-phase preparation process.

1. Gold

Although it is well established that the surface of gold is intrinsically inert, it has been shown that the control of a high metal dispersion (particle size around 2−5 nm) through a strong interaction between the gold particles and the support can give highly active catalysts for a large variety of reactions.[265−269]

Haruta et al. have compared different methods for the preparation of gold catalysts on various oxide supports (TiO_2, Al_2O_3, SiO_2, MgO, ZnO, or Fe_2O_3): three different liquid-phase methods using $HAuCl_4$ as starting reagent and one GPI-D method using $[Au(CH_3)_2(acac)]$ as volatile precursor.[265−267] It results from these studies that, only the GPI-D technique allows the deposition of active gold nanoparticles with relatively high dispersion whatever the investigated supports (2−6 nm gold nanoparticles), even on acidic ones.[266] The main drawbacks of the liquid-phase methods are interpreted by the authors as being due to (i) a weak interaction between the $HAuCl_4$ precursor and acidic supports giving rise to large gold particles and/or (ii) the partial embedding of gold nanoparticles in the bulk of Al_2O_3 in the coprecipitation preparation methods.

The GPI-D method consists of (i) contacting overnight $[Au(CH_3)_2(acac)]$ vapors at 306 K with the pretreated support (dehydration for hours at 473 K and oxidation under 2.6 kPa O_2 at 473 K), and (ii) a calcination step in air in the temperature range 473−773 K to decompose the precursor into metallic gold particles. The highly dispersed gold nanoparticles deposited on SiO_2 are particularly active for CO oxidation at low temperatures.[269]

2. Palladium

In 1991, Sachtler and Faly[270] have shown that chlorine treatments at 623 K of Pd/NaY or Pd/HY impregnated catalysts lead to a redispersion of the palladium. The redispersed species are palladium(II) halides that sublime and transport the metal from the external surface to the interior of the zeolite support. Further H_2 reduction produces HCl and highly dispersed (<12 Å) Pd^0 particles. Although this study would suggest the potentiality of $PdCl_2$ as a volatile precursor, later studies report only the use of organometallic palladium precursors.

The palladium complex $[Pd^{II}(\eta^3\text{-}C_3H_5)(\eta^5\text{-}C_5H_5)]$ has been used by Dossi et al. to prepare Pd/NaY or Pd/NaHY catalysts by GPI-D.[169,271−273] These studies highlight some advantages of gas-phase processes compared to wet impregnation. The gas-phase impregnation of the support is carried out in a U-shaped tube under argon at 298 K and atmospheric pressure. After impregnation, the organometallic precursor is decomposed into metal by heating under a 95% He/5% H_2 atmosphere. The thermal decomposition has been monitored until 773 K by temperature programmed reductive decomposition technique (TPRD) for both NaY and NaHY supports.[272] On both supports, the authors observe the formation of propane and cyclopentane resulting from the hydrogenation of the two allyl and cyclopentadienyl ligands on the metal. However, the evolution of cyclopentane is significantly lower and spread out over a much larger temperature range on NaHY than on NaY support. The authors explain this phenomenon by the presence of intrazeolite protons, probably favoring cationic polymerization of the cyclopentadienyl ligand prior to its hydrogenation.

On NaY support, a clean decomposition to metallic palladium is assumed to be achieved at 473 K. This catalyst presents a bimodal particle size distribution[273] with maxima corresponding to the supercage diameters: 1.3 and 2.5 nm. Thus, the GPI-D technique allows the reduction of the surface migration of metal clusters to the surface of the zeolite by using mild reduction conditions. Pd/NaY catalysts produced by GPI-D or conventional wet impregnation methods have also been studied at 573 K in the methylcyclopentane reforming reaction, leading to ring opening products, ring enlargement products, and coke deposition. The GPI-D catalysts are characterized by a lower deactivation rate compared to the conventional ones. Another advantage of GPI-D is the absence of solvent that prevents the precursor molecule from entering inside the zeolite cages. Similarly, the authors have shown that, on a MgO support, GPI-D catalysts prepared from $[Pd(\eta^3\text{-}C_3H_5)(\eta^5\text{-}C_5H_5)]$ are more active and selective than the impregnated one for methylcyclopentene aromatization.[274]

The same precursor has been used by Ying et al.[275,276] to graft palladium on mesoporous molecular sieves by GPI-D. The precursor has been contacted under reduced pressure at 358−393 K with MCM-41 (997 $m^2\ g^{-1}$, pore size 27.4 Å) and in a second step reduced under a hydrogen stream at 573−623 K. The resulting black material consists of 15−25% Pd w/w, with dispersions around 30%. The authors have also reported the use of a fluidized bed to scale-up the preparation of the catalyst and to ensure a uniform exposure of the large amounts of support with the precursor during the gas-phase process. Impregnated catalysts have also been prepared starting from different precursors, including $[Pd(\eta^3\text{-}C_3H_5)(\eta^5\text{-}C_5H_5)]$ in hexane solutions; all of them present lower dispersions, and lower activities in the Heck carbon−carbon coupling reaction.

A one-step CVD process has been reported to prepare Pd/SiO_2 catalysts in a fluidized bed reactor.[277−279] Preliminary CVD experiments have been performed on model planar supports in an horizontal hot-wall reactor. The CVD process consists of carrying the vapor of the palladium precursor toward the support

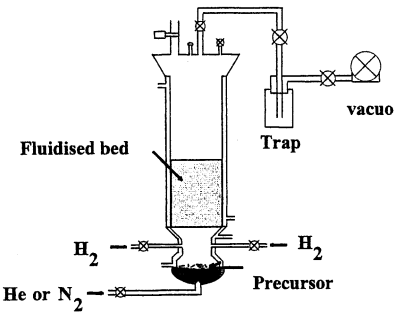

Figure 12. Fluidized bed CVD reactor for the preparation of supported catalysts.

that is heated to a temperature able to ensure metal deposition and ligand removal. A reactive gas such as hydrogen can be introduced to activate this reaction via ligand hydrogenation.

The two complexes [Pd(η^3-C_3H_5)(η^5-C_5H_5)] (**1**) and [Pd(η^3-C_3H_5)(hfa)] (**2**) (hfa = $CF_3COCHCOCF_3$) have been heated between 303 and 323 K and carried by a helium stream toward the support under a total pressure of 6.6 kPa. In these conditions, precursor **1** decomposed at 533 K and precursor **2** at 683 K. The addition of controlled amounts of hydrogen as reactive gas in the precursor and helium mixtures allows one to decrease dramatically the decomposition temperatures to 333 K for **1** and **2** and to produce pure metallic films as evidenced by X-ray diffraction and XPS analyses.[277] On-line MS analyses of the gas phase at the exit of the reactor confirm the role of hydrogen and show the autocatalytic behavior of the reaction. The decomposition products are cyclopentane and propane as already reported by Dossi et al.[273] plus cyclopentene and cyclopentadiene resulting from a partial hydrogenation due to the low partial pressure of hydrogen introduced in the gas phase. The same tuned conditions have been applied to the preparation of Pd/SiO_2 catalysts in a fluidized bed reactor (Figure 12) from [Pd(η^3-C_3H_5)(η^5-C_5H_5)].[277] Homogeneous deposits of pure palladium have been observed by TEM that consist in 2−4 nm nanoparticles for metal leading ranging between 1 and 4% Pd w/w. These catalysts show high activities in cyclohexane dehydrogenation[278] and octene hydrogenation[279] reactions.

Palladium acetylacetonate [Pd(acac)$_2$] has been used to prepare Pd/MgO catalysts by the dry-mix method[280] or Pd catalytic monoliths by CVD.[281]

In the first case, the support consists of ultrafine single crystals (100 nm and S_{BET} = 144 $m^2\ g^{-1}$) that are uniformly mixed by ultrasonic vibrations with [Pd(acac)$_2$] and heated at a temperature higher than the melting point of the precursor, i.e., around 473 K. Then, the acetylacetonate ligand is decomposed at 523 K and finally the catalysts are calcinated from 1023 to 1773 K to test their thermal stability. The catalysts present surface area as large as 60 $m^2\ g^{-1}$ after calcination and show a high activity for methane combustion. Similar results have been obtained for Pt/MgO and Ru/MgO starting from [Pt(acac)$_2$] and [Ru(acac)$_3$] respectively.

In the second case, palladium catalytic monolith with a nonuniform distribution of the active metal is produced by CVD. The sublimation temperature (373−393 K) and the decomposition temperature (403−423 K) are ensured by the temperature profile of the furnace. The reaction takes place under atmospheric pressure for 2−4 h and leads to nonuniformly distributed nanoparticles (0.01−0.03% Pd w/w). The particle size in the entry region of the monolith is centered at 4−5 nm. A nonuniform distribution has been shown theoretically to offer good performance in automotive catalysis.[281]

3. Platinum

Platinum acetylacetonates [Pt(acac)$_2$] and [Pt(hfa)$_2$] have been extensively used to prepare platinum-based catalysts.

A dry-mix method has been developed by Davis et al. to load [Pt(acac)$_2$] into aluminosilicate and aluminophosphate supports.[282] A dry mixture of the precursor and the molecular sieve is kept under vacuum in a sealed tube at 418 K for 16−34 h. The resulting material is analyzed by ^{13}C-MAS NMR and TEM and compared to an [Pt(acac)$_2$]/acetone impregnated catalyst. For the dry-mix method, the ^{13}C-MAS NMR spectra are similar to those of the free complex, suggesting that it remain located on the outer surface of the support. For Pt/$AlPO_{4-5}$ catalysts, the TEM observations confirm the localization of the particles (well dispersed over the support) with a mean particle size of 2−3 nm for the dry-mix catalyst, and 20 nm for the impregnated catalysts with most of the particles being located on the outer surface. The authors propose that, in the liquid phase, the metal complex can be solvated by acetone and, with such a solvation sphere, may be too large to enter the pores of the supports.

Using the same apparatus as for the GPI-D preparation of palladium-based catalysts (see above), Dossi et al. have prepared 1% w/w Pt/KL or Pt/HL zeolites catalysts.[271,272,283−285] The precursor is sublimed at 343 K under argon and decomposed to metal by heating in flowing H_2 at 523 K. Once the precursor has being encaged in the zeolite, TPRD (H_2) studies revealed different behaviors for [Pt(hfa)$_2$]/KL and [Pt(hfa)$_2$]/HL. One peak (m/z = 69, hfaH) is observed at 559 K for [Pt(hfa)$_2$]/KL, whereas two peaks at 433 and 553 K are present for [Pt(hfa)$_2$]/HL. On KL support, the decomposition follows the pathway:

$$[Pt(hfa)_2]/KL \xrightarrow{H_2} Pt^0/KL + 2\ hfaH \quad (4)$$

On HL zeolites, the presence of protons induces the intermediate step:

$$[Pt(hfa)_2]/HL \xrightarrow{H^+\ (zeolite)} "[Pt(hfa)]^+"O^{2-}(zeol) + hfaH \quad (5)$$

From EXAFS experiments, the authors propose that the precursor molecule is entrapped within the channels of the KL support, and that, after decomposition, the size of the metal particles is not influenced by the zeolite protons and do not exceed 0.7−0.8 nm in size.[283,284] The activity of these two catalysts in the reaction of conversion of methyl cyclopentane (MCP) to benzene at 773 K has been reported. The Pt/KL catalyst is characterized by unique properties, i.e., activity and selectivity to benzene formation,

Table 3. Atom Number of Platinum in the Cluster Formed on HMOR and KLTL

preparation procedure of 2% (w/w) Pt/support	average number of Pt atoms per cluster	
	HMOR	KLTL
dry-mix: $[Pt(acac)_2]$ + support (318 K, vacuum, 2 h)	45	10
wet impregnation: $[Pt(acac)_2]$ + support (acetone, 300 K, + drying overnight 383 K)	230	15
ion-exchange: $[Pt(NH_3)_4]Cl_2$ + sup. (water + NH_3 (pH = 11), 353 K, + drying overnight 383 K)	45	< 10

Table 4. Effect of the Addition of Hydrogen to the Carrier Gas for the Decomposition of Platinum Precursors

precursor/H_2	$T_{sublim}/T_{decomp.}$ (K)	impurities (XPS and EDX)	metal loading % (w/w)/ mean particle size (nm)[a]
$[PtMe_2(COD)]$	343−353/513	C (high amounts)	
$[PtMe_2(COD)]/H_2$	343−353/363−393	C (1%)	2.3/3
$[Pt(hfa)_2]$	328−348/673	F, C (10%), O	
$[Pt(hfa)_2]/H_2$	328−348/413−423	C (10%), O (1%)	1.7−5.7/10−100

[a] On SiO_2 powders.

while Pt/HL activity drops rapidly to 10% after 30 min and continuously decreases. It is assumed that this deactivation is due to a preferential deposition of carbonaceous residues onto acidic sites.

Similar Pt/KL catalysts have been prepared by the dry-mix method starting from $[Pt(acac)_2]$ and compared to impregnated catalysts in the reaction of conversion of MCP.[286] The solid mixture of zeolite and $[Pt(acac)_2]$ is heated under vacuum between 333 and 403 K to ensure a complete and homogeneous repartition by sublimation of the precursor, and then calcinated under air at 623 K to decompose the precursor. TEM and EXAFS show that the dry-mix catalysts results in smaller particles than the catalyst prepared by impregnation with an aqueous solution of tetraamine platinum(II) nitrate. Such morphology induces an improvement of the performance of the dry-mix catalyst under clean and sulfur-poisoned conditions, enhancing the catalyst resistance to coke formation and decreasing the sintering.

On unidimensional molecular sieves (MOR, KLTL), the influence of the preparation procedures has been confirmed by EXAFS and XANES.[287] The number of atoms per cluster of platinum after calcination and reduction is reported in Table 3 according to the preparation procedure.

On neutral molecular sieves, the authors note that larger clusters are obtained, but the dry-mix method still gives better results than wet impregnation.

A fluidized bed GPI-D process has been used by Baerns et al. to deposit platinum on SiO_2 and Al_2O_3 from $[Pt(acac)_2]$.[173] After adsorption on the support at 400 K under N_2 at atmospheric pressure, DRIFT spectra of the adsorbed precursor show that (i) on SiO_2, the adsorbate consists of the entire $[Pt(acac)_2]$ molecule, H-bridges between silanol groups and the delocalized π-electrons of an oxygen of the acac ligand and (ii) on Al_2O_3, a partial decomposition of $[Pt(acac)_2]$ occurs leading to acetylacetone adsorbed as an enolate and to surface carbonate formation. Upon decomposition under N_2 between 420 and 570 K, CO is the main gaseous decomposition product whatever the support, as well as some acetylacetone and acetone on silica support. Carbonates and carboxylate species are present on the alumina support after complete decomposition of the platinum precursor. It is reported that, on silica supports, the dispersion of the final catalyst can be affected by the atmosphere used to perform the decomposition (N_2 or air).

A one-step CVD process in fluidized bed reactor has been used by Kalck et al. to prepare Pt/SiO2,[278,279] Pt/C*,[288,289] and Pt−Pd/SiO_2 catalysts.[290] In the case of Pt/SiO_2, $[Pt(hfa)_2]$ and $[Pt(CH_3)_2(COD)]$ have been investigated as potential precursors. A preliminary study on planar SiO_2 substrates in a classical horizontal CVD reactor as well as TGA analyses have allowed the determination of the temperatures of decomposition and to demonstrate their significant decrease when a partial pressure of hydrogen is added to the gas phase. XPS and EDX analyses have demonstrated that H_2 also improves the purity of the final deposit (Table 4).

The disappointing results obtained starting from $[Pt(hfa)_2]$ have to be interpreted as resulting directly from the stability of the complex and from the difficulty of decomposition, even in the presence of hydrogen. In the case of $[Pt(CH_3)_2(COD)]$, a clean decomposition is observed under H_2, giving rise to methane, cyclooctane, cyclooctene, and cyclooctadiene as organic products.

Furthermore, the authors have demonstrated the crucial role of a high supersaturation regime to obtain a high nucleation rate with regard to the growth rate. Indeed, for a high supersaturation of the $[Pt(CH_3)_2(COD)]$ precursor ($T_{sublimation}$ = 468 K, vapor pressure = 4.6 Pa) a mean particle size of 2−6 nm is obtained, whereas for a low supersaturation ($T_{sublimation}$ = 402 K, vapor pressure = 0.48 Pa) the mean particle size is around 60 nm.

On activated carbon or carbon nanospheres,[288,289] the platinum dispersion, starting from $[Pt(CH_3)_2(COD)]$, depends strongly on the amount of anchoring sites. On commercial activated carbon, a mean particle size of 10−15 nm has been measured. Oxidative treatments (HNO_3 or O_2) of the supports lead to a dramatic increase of surface oxygen containing groups that result in a better dispersion of the platinum with a mean particle size of 4−5 nm. On carbon nanospheres, a support that does not present anchoring sites, no deposition is observed in the absence of oxidative treatment. After oxidation, a mean particle

Table 5. Main Characteristics of the Rh/SiO_2 (1% w/w) Catalysts Starting from Various Complexes

precursor/H_2	T_{sublim}/ T_{decomp} (K)	impurities (XPS) w/w	mean particle size (nm)
$[RCl(CO)_2]_2$	326/398	Cl (23%)	
$[RCl(CO)_2]_2/H_2$	326/348	Cl (1.5%)	1.8
[Rh(allyl)$_3$]	313/373	C (19%)	
[Rh(allyl)$_3$]/H_2	313/333	C (7%)	1.5
$[Rh(CO)_2(acac)]$	328/408	C (32%)	
$[Rh(CO)_2(acac)]/H_2$	328/358	C (14%)	1.7

size of 5 nm is measured on this support of low surface area (10 $m^2\ g^{-1}$).

Bimetallic Pt/Pd nanoparticles have also been produced on silica support in a fluidized bed reactor by two successive CVD runs starting from $[Pt(CH_3)_2(COD)]$ at 393 K and then $[Pd(\eta^3\text{-}C_3H_5)(hfa)]$ at 333 K in the presence of a low partial pressure of H_2.[290] The selective deposition of palladium on preformed platinum nanoparticles is observed that leads to a layered, pure bimetallic structure (mean particle size 5−15 nm). Catalytic dehydrogenation of cyclohexane tests have shown the high activity and stability of these bimetallic catalysts.

4. Rhodium, Iridium, Ruthenium, and Osmium

Although the surface chemistry of $[RhCl(CO)_2]_2$ and $[Rh(\eta^3\text{-}C_3H_5)_3]$ on oxide supports has been deeply investigated (see part II), the direct preparation of metallic rhodium catalysts by CVD has only been reported by Kalck et al.[291−295] Three rhodium complexes $[Rh(\eta^3\text{-}C_3H_5)_3]$, $[RhCl(CO)_2]_2$, and $[Rh(CO)_2(acac)]$ have been identified as convenient precursors for the one-step preparation of rhodium-supported catalysts on SiO_2 or activated carbon (C*) in the fluidized bed reactor already described.[112] To control the molar ratio and the metal loading of the catalysts, the vapor pressure laws have been determined.[294] A precursor/helium molar ratio of around 10^{-3} has been used under a total pressure of 13 kPa, corresponding to temperatures of sublimation ranging between 307 and 338 K according to the complex. The temperatures of decomposition decrease significantly upon addition of hydrogen (∼10%) in the gas phase and ligand hydrogenation allows a decrease in the amount of impurities in the final deposit (Table 5). The results of ligand removal on silica supports can be summarized as:

$$[RhCl(CO)_2]_2\ (g) \xrightarrow[100°C\text{ - support}]{H_2} [Rh^0 + \varepsilon\ Cl]/support + CO + HCl\ (g) \quad (6)$$

$$[Rh(C_3H_5)_3]\ (g) \xrightarrow[80°C\text{ - support}]{H_2} [Rh^0 + \varepsilon\ C]/support + C_3H_8 + C_3H_6 \quad (7)$$

$$[Rh(CO)_2(C_5H_7O_2)]\ (g) \xrightarrow[110°C\text{ - support}]{H_2} [Rh^0 + \varepsilon\ C]/support + CO + C_5H_8O_2(g) \quad (8)$$

It is worth mentioning that, contrary to the GPI-D process, in this one-step CVD process, the fast kinetics of the reactions does not allow the identification of the intermediate rhodium surface species. Furthermore, gas-phase reactions could occur, but in the case of the $[RhCl(CO)_2]_2$ precursor all attempts to identify gaseous intermediate species have been unsuccessful.[296] The presence of metallic rhodium in all the samples has been evidenced by XRD and XPS analyses.

In the case of $[RhCl(CO)_2]_2$, the mean particle size increases from 1.2 nm for 0.5% Rh/SiO_2 w/w to 3.0 nm for 5% Rh/SiO_2 w/w. On activated carbon, a larger mean particle size of 4−5 nm is measured for a 2% Rh/C* w/w. These CVD Rh/C^* catalysts are efficient for the hydrocarbonylation of acetic acid into higher acids (mainly propionic) at 20 MPa and 493 K.[295]

Basset and co-workers have studied the GPI-D and the wet impregnation and decomposition processes of $[Ir(acac)_3]$ on silica supports by infrared spectroscopy.[297] In a first step, at room temperature, both methods produce physisorbed $[Ir(acac)_3]$ on the surface. Upon oxidation under oxygen at 573 K, it seems that the decomposition of the physisorbed complex occurs by complete oxidation of the acetylacetonate groups into CO, CO_2, and carbonates. Upon reduction under hydrogen, CO, CO_2, acetylacetone, and hydrocarbon have been detected. The mean particle size has been found in the case of the wet impregnation, to be 0.7−4 nm after the reduction step.

Due to its high volatility, ruthenocene has been used by Miura et al. to prepare Ru/SiO_2 catalysts or Ru/Pt wire gauze materials.[298,299] On silica support, a GPI-D process has been used: ruthenocene is sublimed under hydrogen at 360 K and is further reduced at 500 K in flowing H_2. The Ru dispersion in the final catalyst has been found to be very low (2−3%), presumably due to a weak interaction between the precursor and the silanol groups that induces the ruthenium atoms migration across the support during the reduction step. On platinum wire gauze, chemical vapor deposition is optimal at 450 K under hydrogen and leads to selective deposition on the platinum substrate, while at higher temperatures deposition occurs also on the Pyrex walls of the reactor.

Finally, osmium carbonyl clusters have been entrapped in Y zeolite by exposure of the support to $[H_2Os(CO)_4]$ vapors at room temperature.[300] This material has been found to be a selective and stable catalyst for CO hydrogenation at 573 K and 2 MPa to give C_2-C_4 hydrocarbons.

5. Bimetallics

As the catalytic performances, and particularly the selectivity, of supported metal catalysts can be substantially modified by tin addition, the deposition of tin has been used for the production of Rh/Sn, Pt/Sn, and Ni/Sn bimetallic catalysts. Alkyl tin precursors have been particularly investigated.

Iwasawa et al. have prepared highly active Rh−Sn/SiO_2 catalysts for NO/H_2 and ketone hydrogenation reactions.[301−306] The Rh/SiO_2 catalyst has been prepared by classical wet impregnation of $RhCl_3$, followed by a reduction step. The mean particle size of this Rh/SiO_2 catalyst is 2.5 nm. Then, GPI of $[Sn(CH_3)_4]$ has been performed in a closed circulating system at low pressure and 423 K. The vapors of $[Sn(CH_3)_4]$ react exclusively with the rhodium nanoparticles and two molecules of methane per tin atom evolve, probably via OH groups activation. By further

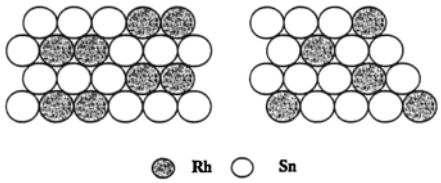

Figure 13. Bimetallic Rh−Sn structure model of Rh−Sn/SiO_2.

reduction at 573 K under hydrogen, two more molecules of methane are formed, leading to complete elimination of carbon on the surface. The rhodium loading has been fixed at 14% w/w, while the Sn/Rh ratio ranges from 0 to 1. A mean particle size of 2.5 nm has been measured for Rh−Sn/SiO_2 (Sn/Rh = 0.45) and of 3 nm for Rh−Sn/SiO_2 (Sn/Rh = 0.9). The structure of these catalysts has also been studied by EXAFS as a function of the Sn/Rh ratio. The Sn atoms in the bimetallic particles remain located in the first layer as long as Sn/Rh < 0.4, whereas above this value Sn atoms intrude into Rh metal particles. Bimetallic ensemble models have been proposed for Sn/Rh = 0.2[306] and Sn/Rh = 0.4[302] (Figure 13). For a surface composition of Sn_{surf}/Rh_{surf} = 1.5 (Sn/Rh = 0.2 at.), two atoms of Rh are surrounded by 8 atoms of Sn. For a surface composition of Sn_{surf}/Rh_{surf} = 3 (Sn/Rh = 0.4), one rhodium atom is surrounded by six tin atoms. These two different environments confer different reactivity to the catalysts. For example, in the NO/H_2 reaction the best activitiy has been obtained for Sn/Rh = 0.4,[301] and for the ketone hydrogenation,[306] the best results have been obtained for Sn/Rh = 0.2. In the case of coimpregnated catalysts, the particular Rh−Sn bimetallic surface structure (Sn/Rh = 0.4) is not present, and these catalysts are six times less active in the NO/H_2 reaction than the one obtained by GPI-D.[301]

A PtSn/SiO_2 catalyst has been prepared by the same group in a similar way[307] by reacting [$Sn(CH_3)_4$] vapors at 423 K with a Pt/SiO_2 catalyst prepared by the usual impregnation method using H_2PtCl_6 solutions. For a Sn/Pt ratio of 0.2 (Sn_{surf}/Pt_{surf} = 1.5) the same surface structure model than for rhodium has been proposed from EXAFS analyses. These PtSn/SiO_2 catalysts are active in the synthesis of unsaturated nitriles from NO and alkanes or alkenes.

The surface reaction of [$Sn(i\text{-}C_4H_9)_4$] with Rh/SiO_2[308] or Ni/SiO_2[309] catalysts has been studied and the deposits characterized by different analytical methods. The Rh/SiO_2 and Ni/SiO_2 catalysts have been prepared by a cationic exchange between [$RhCl(NH_3)_5]^{2+}$ or [$Ni(NH_3)_6]^{2+}$ and ≡SiO−NH_4^+ groups, followed by oxidation and reduction. In the absence of Rh or Ni, the tin precursor does not interact with the silica surface, even upon heating at 573 K. When the tin precursor reacts with the metallic surface under an hydrogen atmosphere (30 kPa), a controlled hydrogenolysis of [$Sn(i\text{-}C_4H_9)_4$] on M/SiO_2 has been evidenced. This reaction, which produces butane and ethene on Rh catalysts or butane and butene on Ni catalysts, is controlled both by the Sn_{surf}/M_{surf} ratio and by the temperature. At a given temperature (<373 K) and for a high surface coverage, there is incomplete hydrogenolysis and surface organometallic fragments are stable. At low coverage, the organometallic fragments are fully dealkylated. An MSn/SiO_2 catalyst is obtained at 473 K on Rh or 373 K on Ni. The particle size varies slightly before and after tin deposition: 1−2 nm for Rh/SiO_2 and 2−3 nm for RhSn/SiO_2 as well as 3−4 nm for Ni/SiO_2 and 4−5 nm for NiSn/SiO_2.

Miura and Itoh have also studied the selective deposition of tin on Pt/$ZnAl_2O_4$.[310] The Pt/$ZnAl_2O_4$ catalyst (0.6% w/w) has been prepared by liquid-phase impregnation from H_2PtCl_6 and tin introduced either by a CVD technique or by a liquid-phase impregnation. The two volatile precursors, [$Sn(CH_3)_4$] and [$Sn(i\text{-}C_4H_9)_4$], have been dissolved in cyclohexane and vaporized at temperature ranging between 423 and 523 K, to deposit selectively Sn on Pt in a flow of dihydrogen. The two nonvolatile precursors [$SnCl(acac)_2$] and [$Sn(C_6H_5)_4$] have been used to deposit tin nonselectively by acetone impregnation, followed by a reduction step under H_2 at 673 K. On the $ZnAl_2O_4$ support, the CVD process does not allow the deposition of tin, whatever the temperature. On Pt/$ZnAl_2O_4$, the amounts of deposited tin have been fixed between 0.5 and 0.6% w/w in the 423−473 K temperature range. At deposition temperature beyond the melting point of tin (523 K), the amount of deposited tin increases sharply, and it entirely covers the catalyst. The selective deposition of tin on platinum particles achieved by the CVD technique has been evidenced by CO chemisorption measurements, whereas liquid-phase impregnation leads to a distribution of tin both on the support and on the metal. The addition of tin to platinum improves the activity of the catalyst in the isobutane dehydrogenation reaction whatever the preparation method. However, higher amounts of tin are needed for the impregnated catalyst than for the CVD catalyst, e.g., 3−4% w/w instead of 0.1% w/w.

Rhodium−tin bimetallic particles entrapped in NaY zeolites have been obtained by Psaro et al. by GPI-D of SnR_4 (R = C_2H_5 or C_6H_5) onto Rh/NaY catalysts that have been prepared either by GPI-D from [$Rh(CO)_2(acac)$] or by ion-exchange from [$RhCl(NH_3)_5]^{2+}$.[311] The main difference between the two Rh/NaY catalysts (1% w/w Rh) is the presence (ion-exchange preparation) or not (GPI-D preparation) of significant amounts of protons. The gas-phase impregnation of tin has been performed at 328 K for [$Sn(C_2H_5)_4$] or 508 K for [$Sn(C_6H_5)_4$], and the decomposition performed under H_2 at 773 K. The selective deposition of tin on the rhodium particles as shown by TPRD profiles occurs only if the monolayer capacity is not overcome. The mechanism of decomposition is influenced by the presence of protons and by the nature of the tin precursor. On GPI-D Rh/NaY catalysts, the reaction is as follows:

$$[\text{Rh-Sn}(C_2H_5)_4]/\text{NaY} + 2\,H_2 \longrightarrow \text{Rh}^0\text{-Sn/NaY} + 4\,C_2H_6 \quad (9)$$

On impregnated catalysts, methane formation has also been demonstrated, and a relevant mechanism for its formation involving the presence of protons on the Rh/NaY support has been proposed. In the case of [$Sn(C_6H_5)_4$]/RhNaY, whatever the Rh/NaY catalyst used, the only product of decomposition is methane (573−673 K). In the case of the GPI-D

catalyst, DRIFT spectra of adsorbed CO clearly evidence a bimetallic Rh−Sn interaction. The selective hydrogenation of citral (3,7-dimethyl-2,6-octadienal) to the corresponding unsaturated alcohol has been observed only for RhSn/NaY catalysts entirely prepared by GPI-D.

Finally, the selective deposition of tin by GPI-D on Ni/SiO_2 has been reported by Komatsu et al.[312] Ni_3Sn particles have been obtained by GPI of $[Sn(CH_3)_4]$ on Ni/SiO_2 (5% w/w, prepared by impregnation of a $Ni(NO_3)_2$ solution) at temperatures ranging from 373 to 523 K, followed by a decomposition in hydrogen at 873−1173 K. The amounts of deposited tin on Ni/SiO_2 are much more important than on SiO_2. In particular, no appreciable deposition of tin is observed on SiO_2 below 423 K. The mean particle size of Ni_3Sn/SiO_2 is about 18 nm as shown by TEM and XRD. These GPI-D Ni_3Sn/SiO_2 catalysts are 500 times more active than nonsupported ones.

Besides these bimetallic catalysts, SnO_2 nanoparticles encapsulated in zeolites have also been prepared by GPI-D to study their properties as sensors of reducible gases.[313] The SnO_2/NaY material has been prepared from $SnCl_4$ previously adsorbed on NaY that has been hydrolyzed and then oxidized. The loading of the support leads to very small SnO_2 particles, not detectable by TEM (<1.5 nm) that are too small for applications as sensor materials. Attempts to increase the Sn loading up to 3% w/w induces the zeolite framework to be destroyed due to the formation of HCl that reacts with aluminum atoms.

D. Miscellaneous

A dry-mix method has been used by Kwak and Sachtler[314,315] to produce Ga/HZSM-5 catalysts. The preparation method includes the dry mixing of $GaCl_3$ with the zeolite and further heating in a quartz tube up to 773 K. The Brönsted acidity of the HZSM-5 support is markedly lowered after this treatment and HCl is released without destruction of the zeolite framework. At high Ga loading (3−4% w/w), the formation of GaO^+ cations that replace zeolitic protons prevails, whereas at low loading (≈ 1% w/w) significant amounts of highly dispersed Ga_2O_3 (mean particle size < 0.5 nm by high-resolution analytical electron microscopy) are also formed. As protons are replaced by gallium cationic species, this Ga/HZSM-5 material acts as a bifunctional catalyst for C_3 conversion to aromatics. A similar preparation method has been used to produce Zn/ZSM-5,[223] where isolated Zn^{2+} cations are present. The Zn ions are stabilized in this state and cannot be reduced below 1073 K.

Deposition of B_2O_3 on alumina or silica by CVD produces highly active catalysts for the Beckmann rearrangement of cyclohexanone oxime into ϵ-caprolactam.[316−318] Vapors of $[B(OC_2H_5)_3]$ are contacted in air between 523 and 673 K with SiO_2 or γ-Al_2O_3, and directly deposited as B_2O_3 (2−34% w/w). The higher catalytic activity and selectivity of these catalysts, when compared to impregnated ones obtained from aqueous solutions of H_3BO_3 and calcination at 623 K, should be attributed to a larger amount of effective acid sites in addition to more uniform acid strength. Such characteristics should result from a more uniform deposition of B_2O_3 by CVD; in particular, large crystals of B_2O_3 (50 μm) have been observed by SEM on impregnated catalysts.[318] An amorphous, highly dispersed silica-supported boron phosphate catalyst has been prepared by CVD using mixtures of boron triethoxide and phosphoryl trimethoxide.[319] The choice of convenient CVD conditions taking into account the temperature and the P/B molar ratio allows the production of more active catalysts for the isomerization of 1-butene and simultaneous oligomerization of 1-butane than conventional ones.

Niobia (6−8% w/w) has been deposited on γ-Al_2O_3 powders by GPI-D from niobium pentachloride at 423 K under vacuum in a closed vessel followed by hydrolysis at 423 K and a 723 K thermal treatment with steam.[320] To remove chlorine contamination, further hydrothermal treatments are required. Specific surface area of the material decreases slightly depending on the treatments (from 246 to 170 m^2 g^{-1}), but no details are given concerning the morphology of the deposits (particles or film). Deposition of niobia on alumina up to a level of 6.5% w/w results in a slight increase both in the ammonium adsorption capacity and in the catalytic activity for cumene dealkylation.

Chemical vapor deposition has been employed to prepare films of tungsten or niobium nitride on γ-Al_2O_3 pellets that have been used as catalysts for thiophene hydrodesulfurization.[321,322] Metal chlorides (WCl_6 or $NbCl_5$) vapors are carried in an argon flow together with NH_3 and H_2 at reduced pressure and decomposes on γ-Al_2O_3 at temperatures ranging between 773 and 973 K. Nitride films of several micrometers characterized by high surface area (150−180 m^2 g^{-1}) are obtained. These metal nitride films deposited on γ-Al_2O_3 are active catalysts in the thiophene HDS reaction at 673 K at atmospheric pressure. However, for NbN/Al_2O_3 a deactivation of the catalyst occurs due to replacement of N by S atoms.

Copper(II) acetylacetonate has been employed to deposit, under oxygen, copper oxides onto fiber glass in a classical horizontal hot-wall CVD reactor; producing a novel catalyst for oxidation reactions.[323] The decomposition temperature 588−613 K has a strong effect on both the crystallinity and the composition of the film. The authors have shown that the films deposited between 593 and 613 K consist in a mixture of Cu_2O and CuO, and present remarkable properties for the oxidation of ethanol at temperatures below 473 K.

Mn/MCM-41 catalysts have been prepared by a dry-mix method and compared to impregnated catalysts.[324] Four different volatile manganese precursors have been used: $[Mn_2(CO)_{10}]$, $[MnBr(CO)_5]$, $[Mn(CO)_3(\eta^5\text{-}C_5H_5)]$, and $[Mn(\eta^5\text{-}C_5H_5)_2]$. Each precursor is dry-mixed in a Schlenk tube with the support, and then the tube is evacuated, sealed, and heated between 393 and 423 K for 2 days. After removal of the excess of precursor, no more than one monolayer remains attached to the support, and surface species have been analyzed by FTIR and EXAFS.[325] After calcination in flowing air at 573 K,

Table 6. Selected Catalytic Studies Using GPI-D and CVD Catalysts

catalytic system	metal loading (%)	particle size (nm)[a]	reaction	catalytic activity	ref
Fe/Al_2O_3 (KOH doped)			ethylene		20
GPI-D ($[Fe(CO)_5]$)	7		hydrofomylation	GPI-D > commercial	
commercial catalyst	10	(iron oxide)			
Fe/ZSM5					58
GPI-D ($FeCl_3$)	1.1	(Fe^{3+} nanoclusters)	NO_x reduction	GPI-D > ion ex.	
ion exchange (Fe^{3+} aqueous sol.)	2.5 and 5	(Fe^{3+} highly clustered + Fe_2O_3)			
FeMo/DBH					48
GPI-D ($FeCl_3 + MoO_2Cl_2$)	Fe 1.4 − Mo 4.6	(well dispersed)			
impregnation ($Fe(NO_3)_3{\cdot}xH_2O$ + $(NH_4)_2(MoO_4)$)	Fe 1.5 − Mo 4.5	(large aggregates)	benzene oxidation	GPI-D > imp. (x2)	
Co/Al_2O_3					27
GPI-D ($[Co_2(CO)_8]$)	2.2	-	NO−CO reaction	GPI-D > imp. (x23)	
impregnation (−)	3				
Co/SiO_2					70
GPI-D ($[Co(acac)_3]$)	5	4.3 (23%)	ethylene	GPI-D > imp. (x2)	
impregnation ($Co(NO_3)_2{\cdot}6H_2O$)	4	11.3 (8.5%)	hydrofomylation		
Ni/C*					1
GPI-D ($[Ni(CO)_4]$)	7	(GPI-D > imp.)	methanol	GPI-D = imp.	
impregnation ($[Ni(OAc)_2]$)	10		carbonylation		
Mo/Al_2O_3					36
GPI-D ($[Mo(CO)_6]$)	2.7		hydrodesulfurization		
impregnation ($[Mo(CO)_6]$)	0.9			GPI-D > imp.	
Mo/SiO_2					75
GPI-D ($MoCl_5$)	0.01−0.37	(isolated Td Mo species)	propene metathesis		
impregnation ($(NH_4)_6(Mo_7O_{24})$)	0.01−0.1	(idem + agregates of Mo and polymolybdate)		GPI-D > imp.	
MoO_3/Al_2O_3					71
CVD ($MoO_2(OH)_2$)	15	-	cyclohexane	CVD = imp.	
impregnation ($(NH_4)_2(MoO_4)$)	22	-	dehydrogenation		
$Mocarbide/Al_2O_3$					79
CVD ($MoCl_5 + C_6H_6$)	1−6	1.4 (Mo^{II})	CO_2 reduction	CVD > imp. (x 20)	
impregnation ($(NH_4)_2(MoO_4) + CH_4$)		Mo^{IV}			
Ru/NaY					33
dry mix ($[Ru_3(CO)_{12}]$)	2	2.2−2.4	CO_2 hydrogenation	dry mix = imp. = i.e.	
impregnation ($[Ru(NH_3)_6]Cl_3$)	3	4.7−13			
ion exchange (Ru/Y)	3	2.6			
Ru/FSM16					33
dry mix ($[Ru_3(CO)_{12}]$)	2	3.3	CO_2 hydrogenation	dry mix > imp. (x2)	
impregnation ($[Ru(NH_3)_6]Cl_3$)	3	8			
Ru/Al_2O_3					36
GPI-D ($[Ru_3(CO)_{12}]$)	1.1	-	hydrodesulfurization	GPI-D > imp.	
impregnation ($[Ru_3(CO)_{12}]$)	1.6	-			
$RuMo/Al_2O_3$					36
GPI-D ($[Ru_3(CO)_{12}]$ + $[Mo(CO)_6]$)	Ru 2 Mo 2.7	-	hydrodesulfurization	GPI-D > imp.	
impregnation ($[Ru_3(CO)_{12}]$ + $[Mo(CO)_6]$)	Ru 1.8 Mo 0.7	-			
Mn/MCM41					157
dry mix ($[Mn_2(CO)_{10}]$)	8.2	(lower particle size)	trans-stilbene oxidation	dry mix > imp.	
impregnation ($[Mn(acac)_3]$)	8.6				
B_2O_3/SiO_2			Beckmann		151
CVD ($B(OEt)_3$ + air)	25	(uniform deposition)	rearrangement of cyclohexanone oxime	CVD > imp.	

Table 6 (Continued)

catalytic system	metal loading (%)	particle size (nm)[a]	reaction	catalytic activity	ref
impregnation (H_3BO_3 + water)	19	(large B_2O_3 crystallites)			
V_2O_5/SiO_2					87
GPI-D cycles ($[VO(OC_2H_5)_3]$)	19.4	(overlayer or nanoparticles)	oxidative ethanol dehydration	GPI-D > imp. (x4)	
impregnation (−)	19.4				
Pd/MgO					107
GPI-D Pd(η^3-C_3H_5)(η^5-C_5H_5)	2	-	methylcyclopentene aromatization	GPI-D > imp.	
impregnation ($Pd(NO_2)_2(NH_3)_2$)	2	-			
Pd/MCM41					108, 109
GPI-D Pd(η^3-C_3H_5)(η^5-C_5H_5)	22.3	(32%)	Heck reaction	GPI-D > imp.	
impregnation Pd(η^3-C_3H_5)(η^5-C_5H_5)	4.4	(17%)			
Pt/KL					119
dry mix ($[Pt(acac)_2]$)	0.5−2.5	(better dispersion)	hexane aromatization	dry mix > imp.	
impregnation ($(NH_3)_4Pt(NO_3)_2$)	0.5−2.5				
Rh/C*					128
CVD ($[RhCl(CO)_2]_2$)	2	4−5 (chlorine free)	acetic acid hydrocarbonylation	CVD > imp.	
impregnation ($RhCl_3 \cdot 3H_2O$)	2	4−5 (remaining chlorine)			
Rh−Sn/SiO_2					134−138
GPI-D ($[Sn(CH_3)_4]$)	Rh 1 − Sn/Rh 0.45	2.5	NO/H_2	GPI-D > coimp. (x6)	
coimpregnation ($RhCl_3 \cdot 3H_2O$−$SnCl_2$)	Rh 1 − Sn/Rh 0.45	-			

[a] Between parentheses are given either the dispersion (%) either available information concerning the catalytic material.

the surface area of the calcinated samples does not significantly decrease contrary to the case of calcinated wet impregnated samples: MCM41, 1236 m^2 g^{-1}; dry-mix samples, 1050−1200 m^2 g^{-1}; impregnated samples, 550−950 m^2 g^{-1}. These results show that the gas-phase method generates small particles that anchor onto the channel walls without blocking the pores. TPR experiments performed on all the calcinated samples suggest that dry-mix samples contain more reactive Mn-oxygen species than the impregnated catalysts. Moreover, some differences in the TPR profiles of the dry-mix samples have been noted according to the nature of the volatile precursor. Finally, the dry-mix catalysts show different, but in any case higher, activity than the impregnated samples in the oxidation of trans-stilbene to trans-stilbene oxide reaction.

Manganese-promoted rhodium/NaY catalysts[326] have been prepared by successive GPI-D from $[Rh(CO)_2(acac)]$ (sublimation at 353 K − decomposition at 673 K under H_2) and $[Mn_2(CO)_{10}]$ (sublimation at 378 K − decomposition at 673 K under H_2). A detailed FTIR study indicates that no discrete monometallic Mn aggregates are present upon decomposition of $[Mn_2(CO)_{10}]$ on the prereduced rhodium particles, consistent with the formation of bimetallic particles.

Surface reactions between vapors of $[ZrCl_2(\eta^5\text{-}C_5H_5)_2]$ (temperature of sublimation = 503 K) and SiO_2 (300−340 m^2 g^{-1}) have been studied by preparing different samples by GPI (ALE method) at 573 K, to synthesize heterogeneous metallocene catalysts.[327] The $[ZrCl_2(\eta^5\text{-}C_5H_5)_2]$ complex reacts mainly with the isolated silanol groups. The effect of dehydroxylation of silica on $[ZrCl_2(\eta^5\text{-}C_5H_5)_2]$ reactivity has been followed by NMR and FTIR analyses. On partially dehydroxylated SiO_2 (573 K − 2.6 isolated OH nm^{-2}), ^{13}C NMR spectra reveal the presence of triply, doubly, and singly bonded Zr species on the silica, while on highly dehydroxylated SiO_2 (873 K − 0.2 isolated OH nm^{-2}), Zr is mainly monofunctionally bonded to the surface. Due to the surface saturation through chemisorption, the controlled deposition is an attractive method for fabrication of metallocene catalysts.

The $Se(CH_3)_2$ precursor has been used to dope impregnated Rh-supported catalysts for ethene hydroformylation reaction.[328−330] On zirconia support,[328] adsorption of vapors of $Se(CH_3)_2$ has been performed at 373 K. The reactivity of $Se(CH_3)_2$ with ZrO_2 or Rh/ZrO_2 has been studied by TPD, and the results show that $Se(CH_3)_2$ preferentially reacts with the hydrogen atoms adsorbed on the Rh metal surface to form CH_4 rather than with the surface OH groups of ZrO_2. From TEM observations, the mean particle size is not altered after Se deposition (around 4 nm), and similar observations have been made for silica-supported catalysts.[329] Whatever the support used, ZrO_2,[328] SiO_2,[329] or MgO,[330] the addition of Se promotes the hydroformylation of ethene. On zirconia, the activity enhancement is more pronounced for the GPI-D catalyst than for a coimpregnated one. EXAFS experiments performed for all the GPI-D-supported catalysts show that Se is selectively bound to Rh with bond distances of 2.41 Å on SiO_2 or ZrO_2 and 2.43 Å on MgO.

Pt−Ge intermetallic compounds supported on HZSM-5 have been prepared by CVD of $[Ge(acac)_2Cl_2]$ at 493 K on impregnated Pt/HZSM-5 and subsequent hydrogen reduction at 823 K.[331] XRD measurements have shown that, according to the Pt/Ge molar ratio, Ge reacts with Pt particles (34 nm) to form different Pt−Ge intermetallic phases. The particles are located

on the external surface of the zeolite whose structure, and specific surface areas are not affected by the deposit. These intermetallic compounds show higher selectivity toward aromatic hydrocarbons than HZSM-5 or Pt/HZSM-5 in the aromatization reaction of butane.

E. Conclusion

As shown in Table 6 the results reported in the literature are rather spread out. However, from the great variety of metal or metal oxides deposits that have been described, it is possible to draw general trends about the potentialities of such methods.

Generally speaking, two main gas-phase methods for the preparation of supported catalysts have to be distinguished.

Most of the studies concern the GPI-D two-step process, and very often the authors carry out several cycles to increase the loading of the deposited metal. The growth of the aggregates becomes the dominant phenomenon after the first GPI-D cycle is completed. Preferential deposition on the metallic phase rather than on the support has been systematically observed during the preparation of heterobimetallic catalysts. Such a method allows control of the metal loading, and produces well-dispersed catalysts.

The one-step process has been less widely used, maybe because it is necessary to fine-tune the operating conditions, especially the vapor pressure of the precursor, the reactor temperature, and the presence of an additional reactive gas to the carrier gas. The main advantage of this method lies in the possibility to control the particle size for a given metal loading by adjusting the precursor supersaturation, which governs the nucleation rate.

In both cases, the fluidized bed technology allows the easy preparation of homogeneous deposits.

Compared to the conventional wet impregnation methods, the absence of any solvent favors the diffusion of the precursor inside the pores and precludes the drying step during which redistribution of the active phase can occur. In addition, for the impregnation methods, when water is used as solvent, the possibility to adjust the concentration of the OH surface groups no longer exists. Compared to the coprecipitation method, the partial embedding of nanoparticles in the bulk of the support does not occur.

It should be underlined that the use of organometallics complexes as metal precursors provides an efficient way to produce deposits at relatively low temperatures. However, in many papers that have been examined in this review, analyses to determine the chemical purity of the deposits are lacking. Additionally, the problems of weak interactions between an acidic precursor and an acidic surface (or basic precursor/basic surface), which often give rise to large particles in the wet impregnation technique, do not occur.

Most of the time, catalytic materials resulting from gas-phase methods preparation show good dispersion and high catalytic activities.

IV. Overlayers, Thin Films, and Surface Modifications

A. Introduction

In heterogeneous catalysis, the nature and the morphology of the support contribute greatly to the performances of the catalyst. Modifications of the surface of the support can be carried out to adjust the acido-basic characteristics and/or the pore opening size. For such a purpose, the gas-phase methods proved to be efficient. Therefore, the resulting material can either be used directly as a catalyst—this is, for instance, the case of zeolites—or as a support that will require further treatments to deposit the catalytic phase. We have to point out that the deposits reported in this part do not present the same morphology than the supported catalysts described in the previous parts of this review. Thus, layered deposits as well as thin films are frequently described. Moreover, we will include in this part the incorporation of noble metals on membranes to design catalytic membrane reactors.

B. Gas-Phase Deposition of SiO_2, GeO_2, Carbon, ZrO_2, and TiO_2

First, we will mention that gaseous-phase interactions between different molecules and a silica surface have been widely investigated by infrared and Raman spectroscopy in attempts to elucidate the molecular nature of the silica surface.[332−338] Thus, silanes, diboranes, or boron, titanium, and germanium halides have been frequently used as probes to study the number and the nature of the surface hydroxyl groups. Some of these molecules seem to be hydroxyl specific, and a distinction between free and bridged hydroxyl groups is achievable. For example, Vansant et al.[337,338] have shown that trichlorosilane reacts differently with bridged and free (or terminal) hydroxyl groups, whereas diborane does not allow one to distinguish between these two kinds of groups because it reacts easily with siloxane bridges. When metal chlorides are used as probe molecules, the main reaction is

$$MCl_x + \equiv SiOH \longrightarrow \equiv SiO\text{-}MCl_{x-1} + HCl \quad (10)$$

that is, in some cases, accompanied by a direct concurrent chlorination of the surface[334] by formation of ≡Si−Cl bonds.

1. Gas-Phase Deposition of SiO_2 on Al_2O_3

To obtain a novel and alternative catalyst and to compare it to the usual silica−alumina oxides, chemical vapor deposition of tetraalkoxysilane has been applied to prepare thin layers of silica on alumina.

Starting from $Si(OMe)_4$ (∼2 Torr at 273 K), Niwa and co-workers have prepared a silica monolayer by repeated CVD cycles at 593 K followed by hydrolysis with water vapor[339,340]or oxygen calcination.[341−343] A monolayer of silica that fully covers the alumina support (∼165 $m^2\ g^{-1}$) is obtained with 20% w/w SiO_2/Al_2O_3. From chemical titration,[344] it has been shown that this monolayer presents concentrations of 12 Si

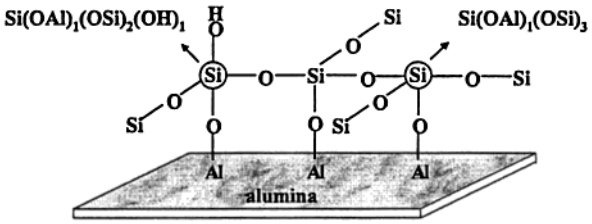

Figure 14. Monolayered structure of a Si−O−Si network covering the surface of alumina.

nm^{-2} and 1.5 OH nm^{-2} that remain quite stable upon heating to 1100 K. These observations as well as NMR studies are consistent with the predominance of $Si(OAl)_1(OSi)_3$ species with regard to $Si(OAl)_1(OSi)_2(OH)_1$ species.[343] On the basis of IR, gravimetry, and products analyses, a mechanism of decomposition has been proposed:[342] $Si(OMe)_4$ is deposited quickly on alumina until the silicon alkoxide and a fraction of methanol would cover the surface; at high temperature, water contaminating the support hydrolyses the silicon alkoxide into silanol, which reacts with another $Si(OMe)_4$. The successive deposition processes create a monolayer with a network of Si−O−Si covering the surface almost completely (Figure 14).

The silicon atoms bonded to alumina behave as weak Brönsted acid sites compared to silica−alumina commercial catalysts prepared by co-gelation or kneading method. The Lewis acidic sites of alumina are completely converted into strong Brönsted acid sites. The final material presents a sharp distribution of acidic sites with a homogeneous strength of the acidity.[340] These SiO_2 monolayered CVD catalysts present a remarkable thermal stability and a high resistance to sintering compared to conventional mixed oxides catalysts.[341] They are active for cumene cracking, but-1-ene and cyclopropane isomerization and alcohol dehydration.[340,341,345−347] The maximum conversion for these various reactions is attained at different SiO_2 loadings, corresponding to one or less than one monolayer. The catalytic activities are comparable to those of a commercial SiO_2/Al_2O_3 catalyst.

Deposition of silica from $Si(OEt)_4$ onto an amorphous silica alumina support has also been reported to give active cumene cracking catalyst.[348] It has been demonstrated by TPD that, in this case also, the strong Lewis acid sites of the original support are converted into strong Brönsted acid sites.

SiO_2/Al_2O_3 materials[340] have also been used as supports to prepare active palladium-based catalysts for complete oxidation of methane.[349,350] The Al_2O_3 surface is not fully covered by silica, and the palladium is preferentially deposited ($PdCl_2$, liquid impregnation) on the remaining part of the alumina. With 5% w/w SiO_2 on Al_2O_3 a strong influence on the sintering behavior is noted, the deposited SiO_2 preventing the palladium metal from sintering.

2. Gas-Phase Deposition of SiO_2 on Other Oxides

Similar deposition of silica from $Si(OCH_3)_4$ on TiO_2 and ZrO_2 have been reported by the same authors.[351] The highest loadings of silica on titania or on zirconia were 8.81% w/w (surface concentration 17.5 Si nm^{-2}) and 8.77% w/w (13.2 Si nm^{-2}), respectively, and correspond to a coverage of around 90%. The authors suggest that the silica overlayers present a structure similar to the support surface up to these concentrations, with however a little alteration in the case of titania. The formation of weak Brönsted acidic sites is evidenced by the IR spectra of adsorbed gases on this monolayers. The catalytic activity for the dehydration of ethanol into ethene decreases with the silicon content, while isomerization of but-1-ene and dehydration of *tert*-butyl alcohol are both enhanced, reaching a maximum rate for Si surface concentrations around 14% w/w on TiO_2 and 9% w/w on ZrO_2, respectively.

The deposition under UHV conditions of SiO_2 by CVD from $Si(OCH_2CH_3)_4$ onto ZrO_2, TiO_2, MgO, SiO_2, and Al_2O_3 has been studied by TPD and Auger electron spectroscopy.[352] The precursor adsorbs at 300 K and decomposes during TPD to give ethene and H_2O on every support except SiO_2, where it adsorbs physically and then desorbs by evacuation at 300 K. On ZrO_2, a uniform SiO_2 film free from carbon contamination is obtained, with a thickness of about 10 Å (four monolayers), while carbon contamination occurs on the other supports. On TiO_2,[353] the formation of small clusters of SiO_2 and/or a mixed metal oxide layer has been proposed.

Yamaguchi and al.[354] have tested several methods to prepare acid−base hybrid catalysts by the combination of typical solid-base and solid-acid materials or by deposition of SiO_2 overlayers on MgO from $Si(OCH_3)_4$. Gaseous $Si(OCH_3)_4$ is adsorbed on MgO (preheated at 773 K) at room temperature, and the adsorption is followed by oxidation and evacuation at 773 K, this cycle being repeated 4 or 8 times. This GPI-D method allows the preparation of a SiO_x/MgO catalyst that is twice more active for the decomposition reaction of $(C_2H_5)_3N$ to produce acetonitrile than a conventionally prepared $SiO_2-Al_2O_3$/MgO catalyst. This result indicates clearly the generation of acidic sites on the MgO surface.

Si-modified Pd/SiO_2 or Pd/Al_2O_3 have been prepared by CVD of SiH_4/H_2 mixtures at 523 K followed by exposure to O_2 at room temperature.[355] The Si/Pd atomic ratio is fixed between 0.1 and 0.2 and, due to Pd-catalyzed silane decomposition, the Si deposits selectively on Pd as Si or SiO_2 patches. The deposition does not affect the pore size distribution and XPS and CO chemisorption measurements have shown that it modifies the palladium surface geometrically but not electronically. The geometric modifications improve the performance of the catalyst that presents higher ethene selectivity and longer catalytic lifetimes in the selective hydrogenation of acetylene.

Iwasawa et al. have used a surface silica modification reaction to prepare a new supported iron carbonyl cluster $[Fe_3(CO)_6]$.[356] The surface modification has been carried out by GPI-D of $SiCl_2R_2$ ($R = CH_3$, C_6H_5) or $SiCl_3R$ at 343 K followed by heating to 473 K in a vacuum, exposure to water at 273−373 K and evacuation at 473 K to convert the SiCl into SiOH groups. The gas-phase impregnation of $[Fe_3(CO)_{12}]$ (room temperature, evacuation at 393 K) on this modified hydrophobic SiR_x/SiO_2 surface leads to the

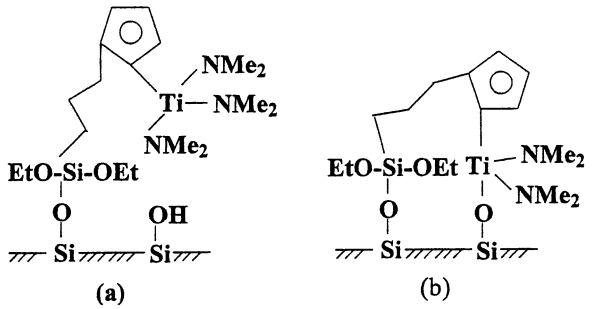

Figure 15. Surface reaction of $[Ti(NMe_2)_4]$ with a modified silica.

supported $[Fe_3(CO)_6]$ cluster that presents an unusual Fe−Fe bond length as shown by EXAFS studies. The iron clusters on $SiMe_2/SiO_2$ showed a higher activity for propene hydrogenation (by a factor of 200) than $[Fe_3(CO)_{12}]$.

Such a strategy to modify a silica surface has been extended by Pakkanen and co-workers[357−359] to the grafting of a cyclopentadienyl ligand through a spacer bond to a siloxane surface group as shown in eq 11:

$$\text{Surf.-SiOH} + \text{Si(OEt)}_3(\text{CH}_2)_3\text{C}_5\text{H}_4 \xrightarrow{-\text{EtOH}} \text{Surf.-Si-O-Si(OEt)}_2(\text{CH}_2)_3\text{C}_5\text{H}_4 \quad (11)$$

Surface Si−O−Si termini react similarly to provide the same functional group and a surface $Si-O(C_2H_5)$ function. Further reaction in the liquid phase with butyllithium and then with $[(\eta^5\text{-}C_5H_5)ZrCl_3]$ allows the grafting of the zirconium complex onto the support through a surface $Si-O-Si(OEt)_2CH_2CH_2\text{-}CH_2(\eta^5\text{-}C_5H_4)$ bond.[357] Such an anchored complex is an active precursor in the presence of the methylating methylaluminoxane agent for the polymerization of ethene. Its catalytic activity is twice that of $[(\eta^5\text{-}C_5H_5)ZrCl_3]$ in purely homogeneous conditions.

The same authors have grafted titanium by using $[Ti(NMe_2)_4]$ in hexane solutions onto a silica, chemically modified by $C_5H_4(CH_2)_3Si(OEt)_3$.[358] The metal center is either bonded to the surface through the spacer or attached directly onto the surface (Figure 15).

The surface can be methylated after functionalization of silica to reduce the Si−OH surface group concentrations. These catalysts present the same activity for the polymerization of ethene as the homogeneous counterpart $[(\eta^5\text{-}C_5H_4SiMe_3)Ti(NMe_2)_3]$. Analogous zirconium systems have been prepared and tested in ethene polymeryzation.[359]

3. Gas-Phase Deposition of GeO_2 and Carbon

GeO_2-modified silica prepared by GPI-D has been used to prepare new rhodium-supported catalysts.[360−364] The reaction in a closed circulating system of gaseous $Ge(OMe)_4$ with isolated OH groups of SiO_2 at 393 K, followed by calcination at 693 K induces the deposition of monolayered GeO_2.[360] The characterization of this material has been performed by FTIR, XRD, and EXAFS. After one cycle of impregnation, the coverage of GeO_2 at saturation, which corresponds to the disappearance of the Si−OH groups as monitored by FTIR, is estimated to be 1/5 monolayer (7.4% Ge w/w). After calcination, isolated GeO_2 and SiOH groups are formed, and those permit further GeO_2 deposition. The local structure of germanium in GeO_2/SiO_2 has been characterized by EXAFS and is similar to that of hexagonal GeO_2. Neither Brönsted nor Lewis acidic sites have been detected on GeO_2/SiO_2. A 2% w/w Rh/GeO_2-SiO_2 catalyst has been prepared by impregnating at room temperature $CHCl_3$ solutions of $[Rh_6(CO)_{16}]$ on 7.4% w/w GeO_2/SiO_2 followed by a reduction step.[361−364] Before reduction, EXAFS experiments have shown that the supported $[Rh_6(CO)_{16}]$ cluster interacts preferentially with the Ge−OH groups and remains unchanged. Upon reduction at 423−523 K, the carbonyl ligands partially desorb and metallic rhodium particles (2.6 nm) are formed. RhGe alloys are also produced when starting from the rhodium complex $[Rh(\mu\text{-}CH_2)(CH_3)(\eta^5\text{-}C_5Me_5)]_2$ and by using a similar procedure.[364] By further reduction at 623−723 K RhGe alloy particles (2.8 nm) are formed. The catalyst that has been reduced at 423−523 K shows high activity and selectivity for hydrogenation of ethyl acetate to ethanol, while Rh/GeO_2 and Rh/SiO_2 are inactive for this reaction. These studies demonstrate the significance of the use of support surface modifications on the metal activity for catalytic reactions.

Finally, thick (20−50 nm) porous diamond coatings have been deposited on silica−alumina pellets by using voltage-based, hot filament CVD from CH_4/H_2 mixtures.[365] The resulting material presents the same BET surface, the same pore size distribution and the same catalytic activity for methanol dehydration reaction than uncoated pellets. However, the diamond coating measurably enhanced the thermal conductivity, and the temperature gradient for a fixed bed reactor could be reduced.

4. Gas-Phase Deposition of SiO_2 on Zeolites

Acidity and pore size are the main characteristics of zeolites as catalysts. Generally speaking, the acidity is dependent on the components or impurities that they contain; on the other hand, the size of the channels is determined by the zeolite structure. Chemical vapor deposition of SiO_2 from different precursors as silicon alkoxydes, silanes, or disilanes has been used to control the pore-opening size or/and the physicochemical properties of zeolites.

a. Gas-Phase Deposition of SiO_2 on Mordenite. Niwa and his group have used $Si(OMe)_4$ as a precursor to deposit SiO_2 to control the pore-opening size of mordenite (H form) without affecting the acid sites. Indeed, the molecular size of this silicon alkoxide is too large to enter the pores of the mordenite; thus, it interacts only with the external surface.[366−368] $Si(OMe)_4$ has been deposited at 598 K on dehydrated HM zeolite followed by calcination at 673 K in flowing oxygen to remove carbon contamination.[367] TPD experiments with ammonia show no change in the acidity whatever the temperature and the amount of deposition, and adsorption of water indicates the conservation of the internal surface. Thus, it is proposed that $Si(OMe)_4$ does not interact with the inside surface of the pores but is deposited only on the external surface of the zeolite. The pore-opening size of the zeolite is effectively reduced by 0.1 and 0.2 nm upon formation of 1−2 and 3 molecular layers

of SiO_2 respectively. The mechanisms of CVD from $Si(OMe)_4$ on HM has also been investigated;[368] it involves first the reaction of $Si(OMe)_4$ with the hydroxyl groups of the external surface to yield an anchored trimethoxide and methanol. Second, the trimethoxide is hydrolyzed by remaining water to form hydroxide groups, which further react with the gaseous alkoxide or with vicinal trimethoxide. The products of the reaction are methanol and dimethyl ether produced by methanol dehydration. Si−HM yields better results than HM for the selective disproportionation of toluene to *p*-xylene.[366]

On NaM, that does not present strong acid sites that could catalyze the dehydration of methanol, deposition of SiO_2 from $Si(OMe)_4$ is possible by performing repeated cycles of deposition and hydrolysis;[369] indeed, deposition at 593 K was possible, but readily saturated at low surface concentration. Therefore, water vapor has been admitted at 593 K into the zeolite that is saturated with methoxide deposit residue. The deposit is converted into hydroxide, and thus, further deposition can occur. On the basis of the competitive cracking of octane isomers as test reaction, it has been found that adjusting the extent of the deposition controlled the pore-opening size of the zeolite.

On Ba-dealuminated mordenite Ba(DM), a low coverage of SiO_2 has also been obtained from $Si(OMe)_4$ at 593 K.[370] In the conversion of methanol to gasoline reaction, differences in selectivity toward heavy aromatics have been noticed between Si−Ba(DM) and Ba(DM) catalysts. The deposition of SiO_2 results in a decrease of the yield of heavy aromatics and a complementary increase of the yield of small molecules (C_1−C_4), indicating a decrease of the pore opening size.

Silane, disilane, and diborane have been used with success to modified H-mordenite zeolites.[371,372] In the case of Si_2H_6, the disilane reacts with OH groups, either at high temperature (373−473 K) on the zeolite external surface or at low temperature (253−303 K) throughout the zeolite (both internal and external surface). The authors have developed a method for fine-tuning of the pore size without affecting the internal acid sites and volume. Introduction of small amounts of Si_2H_6 at around 423 K followed by hydrolysis at 473 K and dehydration at 733 K results in a narrowing of the pore diameter as evidenced by a study of sorption rate of different gas mixtures and their separation. The cracking reaction of hexanes has also been investigated to confirm the fine control of the pore-opening size without affecting the catalytic active sites. The remarkable increase in propane productivity compared to isobutane indicates the shape selectivity of the catalyst.[41]

b. Gas-Phase Deposition of SiO_2 on ZSM-5 and other Zeolites. On ZSM-5 support, Niwa and his group have used different precursors[373−375] to modify both the external pore opening and the acidity. By deposition of $Si(OMe)_4$[373,374] at 593 K followed by calcination in flowing oxygen at 673 K, SiO_2 is formed on the external surface. Repeated cycles allow depositing between 4.5 and 12% w/w of SiO_2. As $Si(OMe)_4$ is too large (0.89 nm) to enter the pore of the zeolite (0.54−0.56 nm), SiO_2 is depleted as about six monolayers (12% w/w SiHZSM-5) on the external surface, reducing significantly the pore-opening size. TPD of ammonia has shown no significant modifications of the strength and amount of acidity of the SiO_2 modified zeolite.[373] However, it gives information on the acidity of the whole material, and further catalytic reaction studies[374] have shown that the number of active sites on the external surface can be reduced. The authors have also shown that the nature of the silicon compound precursor $Si(OCH_3)_2(CH_3)_3$, $Si(OCH_3)_2(CH_3)_2$, $Si(OCH_3)_3CH_3$, or $Si(OCH_3)(C_3H_7)_3$ affects the extent of inactivation of the external acid sites of HZSM-5.[375] Among the various silicon compounds used, the $Si(OCH_3)(C_3H_7)_3$ is particularly effective for the selective inactivation of acid sites on the external surface of HZSM-5, without affecting its void space. In the case of the reaction of methylation of toluene with methanol, the enhancement of para-selectivity is connected to the control of the pore-opening size rather than to acid site modification. By using $Si(OCH_3)_4$ or $Si(OCH_3)_2(CH_3)_2$ to deposit SiO_2 or HY zeolite,[376] Niwa et al. have indicated that the pore-opening size, which is controlled by the deposition, is affected by the aluminum concentration of the zeolite. Pore-openings in HY are completely closed at high aluminum concentration, while pore-opening size could be controlled with low aluminum concentration.

The $Si(OC_2H_5)_4$ precursor has been used by different groups to modify HZSM-5 zeolites.[377−381] The modified zeolites have been used for different catalytic reactions and compared to zeolites modified by liquid-phase impregnation.[377−379] The influence of preparation parameters importance on the external acidity of the modified zeolites is noticeable.[377] The deposition of $Si(OC_2H_5)_4$ has been performed either by static vapor phase or flow systems followed by calcination, or by liquid phase mixing of the zeolite with solutions containing ethanol or hexane, water, and $Si(OC_2H_5)_4$. In the case of the static vapor-phase system, it has been shown that physisorbed species must be removed by evacuation or calcination to reexpose active sites to obtain an almost complete (97%) passivation of the external surface activity. In the vapor flow system, continuous $Si(OC_2H_5)_4$ deposition is observed if water is added at relatively high temperature. For liquid impregnation, the presence of a diluent is necessarily to obtain 86% passivation. In any case, a more uniform coverage is obtained by gradual deposition process. Si/HZSM5 modified catalysts have been prepared from $Si(OC_2H_5)_4$ by the vapor phase flow method (373 K deposition temperature − calcination in air at 773 K), and the Si loading has been controlled by adjusting the number of deposition cycles.[378] The isomerization, disproportionation, and cracking of various molecules have been used to probe the effects of SiO_2 deposition on the external surface acidity and the pore-opening size.

A reactive CVD method has been used to deposit SiO_2 on H-ZSM5 from 50% toluene−45% MeOH−5% $Si(OC_2H_5)_4$ [379,380] mixture vapors at 473−483 K. During the reaction, methanol converts to dimethyl ether

and water on acidic sites of the support, leading to hydrolysis of the $Si(OC_2H_5)_4$ precursor. FT-IR, MAS NMR, and catalytic test reactions have shown that this treatment passivates the external surface of the zeolite and that the concentration of Brönsted acid sites increases at the cost of Lewis sites.[379] By using the same preparation procedure, Wang et al.[380] have prepared a Si-modified ZSM-5 catalyst that shows better activity and better durability in various reactions of preparation of para-alkylbenzenes than a catalyst modified by the conventional impregnation method. It has also been shown that an additional coking of the modified catalyst is a good technique for achieving para-selectivity for extended time on stream.[381]

Si-modified zeolites have also been used as support for metal-supported catalyst preparation.[382,383] The synthesis of pyridine-bases on Pb, Tl, or Ca/Si-ZSM5 catalysts has been investigated by Abe et al.,[382] and it has been shown that repeated CVD cycles induce a decrease in activity because the entrance pore size becomes smaller. SiO_2 has been deposited on a nonacidic KL zeolite by GPI from $Si(OC_2H_5)_4$ or $(Me)_3Si-O-Si(Me)_3$ vapors at room temperature followed by a calcination step under O_2 at 673 K.[383] Contrary to H-type zeolites, the framework oxygen ion is the deposition site. Due to the appearance of new basic sites, the interaction between platinum and the Si-modified zeolite is strengthened, and electron-rich platinum particles are obtained after dry impregnation with *cis*-$[Pt(NH_3)_2Cl_2]$.

Finally, some authors have also deposited SiO_2 on zeolite-supported metal catalysts to modify their properties.[384−390] Chemical vapor depositon of $Si(OC_2H_5)_4$ on Cu/HZSM-5 catalyst has been used to modify its pore-opening size to allow a selective combustion of hydrogen in a gas mixture containing isobutene.[384] Silicon tetraethoxide is deposited on Mg/ZSM-22 at 423 K and then calcined at 723 K.[385] The deposition of SiO_2 leads to a decrease in the amount of external acid sites (TPD of NH_3 and trimethyl pyridine) and also reduces the pore-opening size (*n*-hexane chemisorption). The increase of selectivity in the isomerization of 1-butene to iso-butene appears to be the result of passivation of strong acidic sites and narrowing of the pore-opening.

Silica modified Pt-supported zeolites have been prepared from $Si(OC_2H_5)_4$ [386] or $Si(C_6H_5)_2(OC_2H_5)_2$.[387] It has been demonstrated that a high regioselective hydrogenation of unsaturated hydrocarbons can be achieved with this catalytic system. Similarly, treatment of a Ga-MFI zeolite with $Si(OC_2H_5)_4$ enhances the para-selectivity during toluene alkylation.[388]

On Pt-loaded mordenite catalysts,[389] silica has been selectively deposited on the external surface of the zeolite without affecting the internal acidic sites. This narrowing of the zeolite pores can be tuned by controlling the extent of surface modification; it induces a shape selectivity for the hydrocracking of paraffins.

An interesting effect of deposited silica on Pd/HZSM-5 is the recovery of the activity for the reaction of NO-methane-oxygen that is suppressed by water vapor.[390] Indeed, without SiO_2 deposition, palladium migrates from the inside pores to the surface and sinters into large particles. This phenomenon, accelerated by the presence of water vapor, may be suppressed by SiO_2 deposition from $Si(OCH_3)_4$ and heating at 773 K under He. Water adsorption experiments have shown that the equilibrium amount of adsorbed water is reduced by SiO_2 deposition on the external surface.

5. Gas-Phase Deposition of GeO_2 or ZrO_2 on Zeolites

The deposition of germanium dioxide on different zeolites (H-mordenite, Z-HM10 or ZSM-5) from $Ge(OCH_3)_4$ or $Ge(OC_2H_5)_4$ affords similar results than for SiO_2 deposition.[391,392] The GeO_2 thin film is located mainly on the external surface of the support; it is unstable to moisture and reconstructs by heating at 773 K to give GeO_2 particles with size above 5 nm, leading to heterogeneous narrowing of the pore-opening size.[391] On ZSM-5 zeolite,[393] the reduction of pore-opening and the passivation of the outer surface acidity is less drastic with GeO_2 than with SiO_2.

An one-atomic layer ZrO_2/ZSM-5 catalyst has been prepared by reaction of $[Zr(OC_2H_5)_4]$ vapors at 473 K with surface OH groups of the zeolite, followed by heating at 503 K to complete the reaction, exposure to H_2O vapor at room temperature, and calcination at 773 K in air.[394] This GPI-D cycle allows the preparation of 1.7% w/w Zr/ZSM-5 that corresponds to 1/3 atomic layer and can be repeated to obtain a full monolayer coverage. The reduction of the pore size and volume of the ZSM-5 is not observed, indicating that $[Zr(OC_2H_5)_4]$ reacts only with the external OH groups of the support. EXAFS measurements show that this one-atomic layer of ZrO_2 grows epitaxially in a [111] direction of tetragonal ZrO_2. This particular structure could explain the unique behavior of this catalyst for methanol conversion reactions during which isopentane is obtained selectively, and CO hydrogenation where C_4H_8 hydrocarbons are obtained selectively (mainly isobutene).

6. TiO_2 Deposition from the Gas Phase

The gas-phase reactions between $TiCl_4$ or $[Ti(OR)_4]$ precursors and high surface area oxides supports have been studied extensively over the last two decades.[395,396] First, $TiCl_4$, like $SiCl_4$, has been used as a probe molecule to study the surface chemistry (OH groups) of silica. Then, catalytic applications have merged: TiO_2-supported overlayers have been shown to exhibit special surfaces properties as metal catalyst support; titania-silica materials have been used as acidic catalysts and supported TiO_2 is known to be an effective photocatalyst.

The gas-phase reaction of $TiCl_4$ with the surface of silica has been studied by several groups[332−334,397−401] by infrared, NMR, and chemical analysis. The possible reactions of $TiCl_4$ with the surface of the silica surface are presented in Figure 16. The results of these different studies show that monofunctional, bifunctional, or siloxane-based reaction become more or less important according to the pretreatment temperature of the silica, or to the reaction temperature.

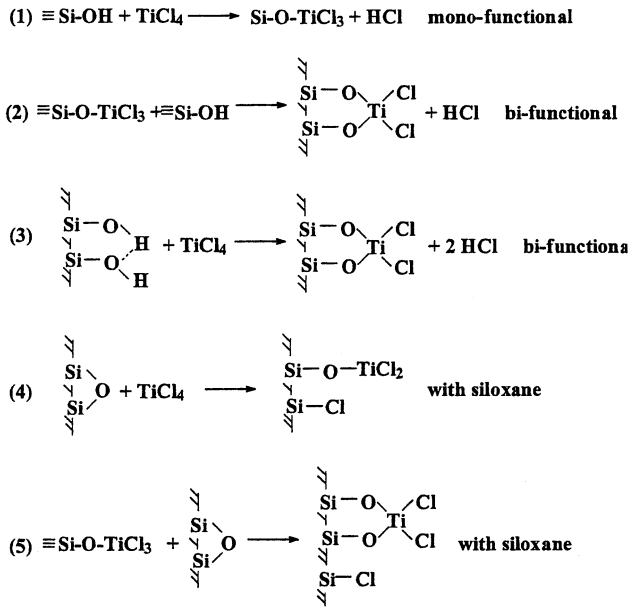

Figure 16. Possible surface reaction between $TiCl_4$ and a silica surface.

a. Preparation of Supported TiO_2 Photocatalysts. Kinney and Staley have shown by using Fourier transform infrared photoacoustic spectroscopy that, on dehydrated (673 K) SiO_2, $TiCl_4$ reacts first (at room temperature) with siloxane bridges (reaction 4 in Figure 16) and then with silanol groups.[397] Other authors have completely excluded this reaction pathway[400] or have proposed only a certain contribution for high-temperature treatment of the silica (>873 K).[398] The amount of bidentate species grafted on the surface increases with increasing concentration of hydroxyl groups and with reaction temperature. The maximum number of grafted groups is sterically limited for low-temperature pretreatment (high OH concentration) and decreases by high-temperature treatment.

Deposition of TiO_2 on silica can be performed by water vapor treatment of the above grafted titanium species at high temperature.[399−401] If the reaction with water is performed at 373 K, no crystalline phase is detected by XRD whatever the titanium content (up to 21% w/w). Raman spectra performed after three GPI-D cycles indicate the presence of a TiO_2 anatase-liked structure. After calcination of the sample at 773 K, a reorganization of the layer occurs and XRD indicates that anatase is present.[399] If the reaction with water is carried out at 448 K, both ^1H MAS NMR and FTIR analyses show that anatase-like Ti−OH groups are formed.[400] After reaction with water above 723 K, XRD has revealed a mixture of rutile and anatase crystalline phase.[401]

Li et al. have also observed different titanium species during the preparation of Ti/SiO_2 catalysts for the styrene epoxidation reaction.[402,403] From UV−Raman spectra and XRD experiments, they have demonstrated that the temperatures of both the silica pretreatment and the $TiCl_4$ gas-phase impregnation influence the titanium loading and the nature and structure of the supported species.

Deposition of titanium oxide species on zeolites has been reported.[404] $TiCl_4$ chemisorption, followed by hydrolysis at 373 or 773 K, affords either TiO_x mononuclear species at low temperature, or bulk anatase at 773 K.

The use of supported titanium oxide as photocatalysts for degradation of different toxic organic compounds in water or air is of current interest to solve environmental problems. A TiO_2/Vycor glass catalyst has been prepared from $TiCl_4$, followed by a hydrolysis and a calcination step in O_2. Due to the presence of well-dispersed titanium ions, it presents photoluminescent properties, distinct from bulk or impregnated TiO_2 catalysts.[405] This catalyst is active for the photocatalytic reduction of CO_2 with H_2O in CH_4.

Supported anatase TiO_2 particles on hollow glass micro-beads have been prepared by reacting $TiCl_4$ vapors between 573 and 773 K with the support, followed by hydrolysis at the same temperature.[406] The final material has been tested in the photo-assisted oxidation of ethanol to acetaldehyde and compared to TiO_2-supported catalyst prepared by different methods. Anpo and Che have prepared by a similar method highly dispersed TiO_2 anchored on a porous Vycor glass to investigate photocatalytic reaction mechanisms.[407,408] This preparation method allows the control of the deposit homogeneity and the degree of coordinative insaturation on the surface. The photocatalytic activity of the GPI-D catalyst in the photohydrogenation reaction of $CH_3-C\equiv CH$ with H_2O is much higher than that of the bulk TiO_2, by about 2 or 3 orders of magnitude. This catalyst has also been used for the photoformation of N_2 from N_2O.

A silica gel supported TiO_2 photocatalyst has been prepared by a CVD method from titanium tetra-isopropoxide. This precursor is characterized by a high vapor pressure and a high reactivity with water adsorbed on the support.[409] An anatase form of TiO_2 is produced at 573 K, but a further calcination in air is necessary to obtain better results. TiO_2 loadings around 6% w/w have been reached, and the deposit is located mainly on the external surface of the support with a minor alteration of the total surface area. The photocatalytic activity of this material for phenol aqueous solution oxidation has been evaluated and compared to a commercial TiO_2 catalyst (Degussa P25). Its activity is lower than that of P25, but it can be easily separated from the reaction medium and recycled without loss of activity.

Fine TiO_2 particles have been prepared by homogeneous phase CVD, starting from $[Ti(OC_3H_7)]$.[410] The tuning of some parameters as the temperature of the process, the precursor concentration, and the residence time allows the control of properties such as surface area, particle diameter, crystallinity, and porosity. Surface area as large as 270 $m^2\ g^{-1}$ can be reached, and the particles are amorphous up to 673 K and crystallized in the anatase form above this temperature.

b. Preparation of Modified Supports. Development of new catalysts for deep hydrodesulfurization (HDS) of gas oil is possible by using a CVD method to create new composite supports for metal deposition that associate the advantageous properties of both alumina and titania.[411−414] Surface modification of a porous γ-Al_2O_3 support (186 $m^2\ g^{-1}$) has been realized

by depositing $TiCl_4$ at 473 K on the dehydroxylated support (773 K), then hydrolyzed at the same temperature, and finally calcinated under O_2 at 773 K. From IR measurements, it has been shown that almost all the bands of Al−OH groups disappear for 11% w/w of TiO_2, indicating a high dispersion of Ti-species on alumina. TiO_2 deposition allows one to obtain a material in which Al_2O_3 is almost completely covered by TiO_2 (14% w/w) without significant modification of the specific surface area and of the pore volume. After preparation of Mo-supported or Ni−Mo-supported catalyst by liquid-phase impregnation, it has been shown by XPS that the state of molybdenum on $Mo/TiO_2-Al_2O_3$ catalyst is closer to the state of molybdenum on Mo/TiO_2 than to the molybdenum-supported on Al_2O_3. After sulfurization (H_2S/H_2), similar results are obtained. The conversion rates for dibenzothiophene derivatives HDS obtained over $Mo/TiO_2-Al_2O_3$ are much higher than that obtained over Mo/Al_2O_3, and in some cases higher than that obtained over Mo/TiO_2. When a composite type $TiO_2-Al_2O_3$ support prepared by classical impregnation method is used, the catalytic activity for HDS is lower than with the GPI-D prepared support.

TiO_2 deposition on highly porous supports such as alumina[415] or silica[416] has been investigated to prepare high surface area supports that could present strong metal support interaction (SMSI) properties. Anderson and Foger[415] have prepared titania surface layer on γ-Al_2O_3 by using the same method as Segawa et al.[411−414] with very similar results. A significant difference between samples prepared by this method and samples prepared by liquid (hexane)-phase impregnation is the presence of TiO_2 monolayer. Then, highly dispersed (∼1 nm) iridium particles have been deposited by liquid-phase impregnation.[415] These catalysts are active for *n*-butane and 2,2-dimethylpropane conversion, and it has been shown that, for GPI-D catalysts, a SMSI phenomenon occurs and is more pronounced when increasing the amount of deposited TiO_2 (1−3 layers).

Iwasawa et al. have studied by EXAFS the structure of one atomic layer TiO_2 on SiO_2[416] as well as its restructuration through the reduction mediated by Pd and Pt deposition. The modified TiO_2-SiO_2 support has been prepared by the gas-phase deposition of $[Ti(OC_3H_7)_4]$ at 353 K followed by hydrolysis at room temperature and calcination at 773 K. Two cycles are necessarily to prepare a TiO_2 monolayer. No X-ray diffraction pattern has been observed indicating no TiO_2 crystallite formation on SiO_2. The EXAFS and XANES results indicate that TiO_2 is present as anatase on the SiO_2 support. Thus, one atomic layer TiO_2 is much less reducible (H_2 − 773 K) than when dispersed or than bulk TiO_2, possibly because of a direct TiO_2 bonding. The deposition by liquid-phase impregnation of Pd or Pt followed by calcination and reduction at 773 K affects the structure of the TiO_2 layer in a different way. The Pt-one atomic layer TiO_2 (Pt mean particle size 2 nm) retains the anatase structure, whereas this structure is transformed to rutile in the Pd-one atomic layer TiO_2 (Pd mean particle size 5 nm). It has been proposed that the larger size of the Pd particles plays a role in this structural change. These two catalysts do not present SMSI, probably because of the presence of Ti−O−Si bonds.

C. Gas-Phase Preparation of Catalytic Membranes

The application of porous ceramic membranes in catalytic reactors has started in the 1980s with some studies in the engineering of reactors. Two classes of catalytic reactors based on ceramic membranes have to be distinguished: (i) inert membranes reactors where the role of the membrane is to allow the specific introduction of compounds and the catalyst is located apart from the membrane, and (ii) catalytic membrane reactors where the membrane itself is catalytic, or becomes catalytic.[417]

Porous ceramic membranes are made of alumina, silica, titania, zirconia, zeolites, etc., and composite membranes can be obtained by depositing a metal or an oxide on the surface or in the porosity of the ceramic.

Beside recent advances in chemical vapor deposition of thin ceramic films (SiO_2, Al_2O_3, TiO_2, or B_2O_3) on porous alumina membranes to develop hydrogen-permselective membranes,[418−422] noble metal deposits have been investigated, especially palladium deposits which are particularly efficient to sorb hydrogen.

Palladium(II) acetate has been used as precursor by Morooka et al.[423,424] to deposit metallic palladium by a low-pressure CVD process between 573 and 773 K on a porous α-alumina membrane, which presents an average pore size of 150 nm. Palladium films of 2 μm consisting of 80 nm crystallites have been deposited on the alumina membrane surface at 573 K, and the palladium deposit layer extends as far as 8 μm from the top surface to the inside of the support. At 773 K, the penetration is only of 2 μm due to the fast decomposition of the precursor at this temperature. In all cases, the top 2 μm layer is defective and does not separate the gas. The best H_2 permeability is observed with the palladium membrane prepared at 573 K.

Palladium(II) chloride has been deposited at around 723 K by CVD on α-Al_2O_3 (pore size 200 nm) and γ-Al_2O_3 coated α-Al_2O_3 (pore size 3−6 nm) in the presence of hydrogen.[425] On α-Al_2O_3, thick (50 μm) and defective Pd films (grain size: 15−20 nm) are obtained on the surface, and the major part of palladium is supposed to lie inside the γ-Al_2O_3 pores. An explanation of this result could be given either by differences in Knudsen diffusivity of H_2 and $PdCl_2$ vapors, or by a different reaction rates in the α- and γ-pores. The Pd/γ-Al_2O_3/α-Al_2O_3 membranes present a substantial H_2 permeation rate. The same authors have also studied the deposition of palladium from $[Pd(acac)_2]$ on a γ-Al_2O_3 membrane under low pressure, and in the presence or not of hydrogen.[426] In the absence of H_2, the deposit obtained at 623 K is poorly crystallized (grain size < 5 nm) and is present inside the γ-Al_2O_3 layer (until 6 μm depth) with a maximum concentration near the γ-Al_2O_3 surface. The presence of hydrogen allows a clean decomposition of the palladium precursor, and a well-crystallized pure palladium film is obtained (0.8 μm thick-

ness − grain size 30−50 nm), but the fast reaction rate prevents a deep penetration. This latter Pd-modified membrane exhibits substantial selective permeability for H_2.

Palladium, as well as ruthenium, rhodium, iridium, and platinum acetylacetonates have been used as CVD precursors to prepare asymmetric membranes by coating a tubular γ-Al_2O_3. This membrane consists of a 10 μm γ-Al_2O_3 layer with a mean pore size of 200 nm supported on the outer surface of a matrix having a pore size of 10 μm.[427,428] The CVD conditions leading to the optimal membrane efficiency in hydrogen permeation have been determined. Metal deposition occurs in the outer thin γ-Al_2O_3 layer, and the effective thickness of this deposit ranges between 3 and 10 μm. These membranes are thermally stable up to 773 K. The palladium membrane gives the best results and shows a H_2 flux around 1.6 times higher than that of a dense palladium membrane prepared by electroless-plating and having a thickness of 4.5 μm. These CVD membranes have also been used for steam reforming of methane at 773 K in a membrane reactor and compared to 8 μm palladium electroless-plating membranes.[429] In this case, the CVD platinum and Pd electroless-plating membranes give excellent performances. However, the advantages of the CVD Pt membrane are (i) a lower metal loading and thus a lower cost, and (ii) a lower tendency toward hydrogen embrittlement.

Catalytic membranes have also been prepared by CVD techniques for other applications. Thus, a CVD Ni/Al_2O_3 membrane catalyst is active for methanol reforming.[430] The preparation of this material consists of depositing NiO at 1023 K and at atmospheric pressure in the pores of an alumina filter of mean pore diameter 1 μm from $NiCl_2$ and oxygen. The deposition must operate by a reaction limited regime to allow a suitable mass transfer of the reactant and to fill deeply (along 1 mm), and homogeneously the Al_2O_3 pores. After reduction by hydrogen at 623 K, this Ni/Al_2O_3 catalyst has been employed for methanol decomposition.

A bimetallic Pd−Sn/α-Al_2O_3 catalytic membrane has been prepared by CVD and used for the hydrogenation of nitrates in water.[431] The preferred sequence for precursor deposition is to deposit first tin, from [$Sn(hfa)_2$] under H_2, and then palladium from [$Pd(hfa)_2$] at 523 K under reduced pressure. Typical palladium concentration profiles across the asymmetric membrane, as determined by EPMA/WDX, indicate that Pd is located mainly in the first 50 μm depth, and that the Pd/Sn atomic ratio remains constant over the whole depth. XRD patterns show that metallic palladium is deposited and Auger electron spectroscopy reveals high carbon contamination presumably due to the absence of hydrogen during the palladium deposition. TEM observations show that the deposit consists of particles with diameter around 8−10 nm. Pore size distribution of the catalytic top layer decreases from 64 to 48 nm. These catalytic membranes offer a high activity and fair selectivity to nitrogen for selective hydrogenation of nitrates and are thus an interesting material for nitrates removal from drinking water. The influence of the preparation method on the distribution of Pd and Sn in the deposit has also been reported.[432,433] The palladium-to-tin ratio on the surface, as measured by XPS, is significantly higher when the material is prepared by CVD than when impregnation is used. It has been proposed that the high temperatures for calcination (773 K)-reduction (623 K) steps performed during the impregnation procedure are responsible for tin enrichment on the surface. These two membranes exhibit a similar activity for nitrate reduction, but their selectivity differs markedly. Indeed, N_2 is produced selectively (91%) on the CVD membrane, whereas NH_4^+ is obtained (68%) on the impregnated Pd-Sn membrane.

Pt-based catalytic membranes are of interest for the removal of volatile organic compounds contained in air, and waste streams. Some attempts to prepare Pt/γ-Al_2O_3 membranes by GPI-D from [Pt(η^3-C_3H_5)-(η^5-C_5H_5)] have been reported.[434] The gas-phase impregnation is performed at room temperature by introducing the organometallic precursor inside the tubular membrane and maintaining the outer side under high vacuum. Further calcination to remove the organic ligands follows. Comparison with impregnated membranes for the combustion of toluene and methylethylketone shows that both catalytic membranes present similar performances.

D. Conclusion

Surface modifications and/or thin films deposition constitute new topics in the field of catalyst preparation. The promising results described in this review open new perspectives for the application of gas-phase methods to elaborate catalytic materials. However, it is worth mentioning that, for layered deposits, most of the time the structure has not been fully determined. The terms submonolayer, monolayer, overlayers do not give any information on the structural characteristics of the deposit but are rather an indication of the coverage of the surface by the deposited material. As far as the catalytic membranes are concerned, the use of gas-phase methods allows a good control of the diffusion of the precursor inside the pores and thus of the deposit depth from the surface to the inside of the support. Additional studies devoted to this subject will be necessary. These preliminary positive results should promote additional studies.

V. Conclusions and Perspectives

This review shows that a wide variety of information on gas-phase deposition methods is available, starting from a large series of precursors to prepare supported catalysts. However, this domain suffers from the dispersion of available data that would permit the clear identification of the fundamentals trends and thus to achieve the complete coverage of the subject. This is certainly because specialists of the molecular approach of catalyst preparation, of CVD, and of chemical engineering have too often carried out independent investigations. Indeed, the first stage of the preparation related to the interaction of the gaseous precursor and the surface has

been deeply studied for a limited number of carbonyls; the chemical role of the surface has been clearly explained. Unfortunately, the parameters that govern either the germination, or the growth of the aggregates have been rather neglected. In many cases, the composition and the morphology of the deposits have not been systematically determined. The studies of nucleation/growth phenomena, and of solid characterization classically carried out in CVD on planar substrates, need to be applied to catalytic material elaboration. Chemical engineering is also involved in the design of specific reactors, either for the preparation or for the use of the catalysts.

In our opinion, future studies should combine the skills of researcher of these three specialities.

Since most often the performances of these materials are already higher than those of the corresponding catalysts prepared by wet impregnation, such a unified approach will be fruitful for the comprehension of all the phenomena and will promote the development of gas-phase methods of catalyst preparation.

Finally, the easy and reproducible conditions to prepare more active catalysts than by the classical impregnation method should attract the attention of industry. The patent literature seems to give the same indication, as well as a recent paper of K. P. de Jong.[435]

VI. Acknowledgments

At the beginning of our studies on the preparation of metal deposits by CVD in fluidized bed reactors, a Brite Euram European Program allowed us to collaborate with several other scientists from various specialities and to promote the quality of our investigations: Prof. J.-P. Couderc (CVD, chemical engineering, ENSIACET, Toulouse), Prof. R. Morancho (CVD and materials, ENSIACET, Toulouse), Prof. A. Kiennemann (heterogeneous catalysis, ECPM, Strasbourg), Prof. C. Mazzocchia (heterogeneous catalysis and industrial chemistry, Politecnico di Milano, Milano, Italy), and Dr. J.-P. Guerlet and Dr. N. Petit (chemistry of precious metals, Engelhard-CLAL, Paris). We are grateful to them for the quality of our collaboration. This subject led us to undergo further investigations and to initiate new collaborations: we acknowledge Dr. J.-C. Hierso (Ph.D. on Pd and Pt deposition), Dr. B. Caussat (Ph.D. on modelizations on CVD in fluidized beds), Prof. J.-L. Figueiredo and Dr. J.-L. Faria from Porto, Portugal (Pt deposition on carbon), and Dr. Y. Kihn from CEMES, Toulouse (TEM observations). Finally, we are also grateful for financial support from the "Direction de la Recherche, Ministère de la Recherche et de la Technologie", the Région Midi-Pyrénées, The European Economic Community, Engelhard-CLAL, BP Chemicals, and the Agence nationale de la Valorisation et de la Recherche.

VII. References

(1) *Handbook of Heterogeneous Catalysis*; Ertl, G. et al., Eds, Wiley-VCH: New York, 1997.
(2) Iwasawa, Y. In *Handbook of Heterogeneous Catalysis*; Ertl, G. et al., Eds, Wiley-VCH: New York, 1997; p 853.
(3) Impens, N. R. E. N.; van der Voort, P.; Vansant, E. F. *Microporous Mater.* **1999**, *28*, 217.
(4) Psaro, R.; Recchia, S. *Catal. Today* **1998**, *41*, 139.
(5) Yoo, J. S. *Catal. Today* **1998**, *41*, 409.
(6) *Advanced Catalysts and Nanostructured Materials*; Möser, W. R., Ed.; Academic Press: New York, 1996.
(7) Bailey, D. C.; Langer, S. H. *Chem. Rev.* **1981**, *81*, 130.
(8) Yermakov, Y. I.; Kuznetsov, B. N. *J. Mol. Catal.* **1980**, *9*, 13.
(9) Yermakov, Y. I. *J. Mol. Catal.* **1983**, *21*, 35.
(10) Phillips, J.; Dumesic, J. A. *Appl. Catal.* **1984**, *9*, 1.
(11) Schwartz, J. A. *Chem. Rev.* **1995**, *95*, 477.
(12) Iwasawa, Y. *Adv. Catal.* **1987**, *35*, 187.
(13) Lamb, H. H. *Catal. Today* **1993**, *18*, 3.
(14) Candy, J. P.; Didillon, B.; Smith, E. L.; Shay, T. B.; Basset, J. M. *J. Mol. Catal.* **1994**, *86*, 179.
(15) Ichikawa, M. *Adv. Catal.* **1992**, *38*, 283.
(16) Katada, N.; Niwa, M. *Chem. Vap. Deposition* **1996**, *2*, 125.
(17) Mond, L.; Langer, C.; Quincke, F. *J. Chem. Soc.* **1890**, *57*, 749.
(18) Baker, L. L., Jr.; Bernstein, R. B. *J. Am. Chem. Soc.* **1951**, *73*, 4434.
(19) Gunter, P. L. J.; Niemantsverdriet, W. J. H.; Ribeiro, F. H.; Somorjai, G. A. *Catal. Rev.-Sci. Eng.* **1997**, *39*, 77.
(20) Paukshtis, E. A.; Yurchenko, E. N. *Russ. Chem. Rev.* **1983**, *52*, 426.
(21) Chun, W.-J.; Shirai, M.; Tomishige, K.; Asakura, K.; Iwasawa, Y. *J. Mol. Catal.* **1996**, *107*, 55.
(22) Asakura, K.; Shirai, M.; Iwasawa, Y. *Catal. Lett.* **1993**, *20*, 117.
(23) Vansant, E. F.; Van Der Voort, P.; Vrancken, K.C. *Characterization and Chemical Modification of the Silica Surface*; Elsevier: New York, 1995.
(24) Knözinger, H.; Ratnasamy, P. *Catal. Rev.-Sci. Eng.* **1978**, *17*, 31.
(25) Sohlberg, K.; Pennycook, S. J.; Pantelides, S. T. *Chem. Eng. Commun.* **2000**, *181*, 107.
(26) Scokart, P. O.; Rouxhet, P. G. *J. Colloid Interface Sci.* **1982**, *86*, 96.
(27) Hadjiivanov, K. I.; Klissurski, D. G. *Chem. Soc. Rev.* **1996**, 61.
(28) Kresge, C. T.; Leonowicz, M. E.; Roth, W. J.; Beck, J. S. *Nature* **1992**, *359*, 710.
(29) Beck, J. S.; Vartuli, J. C.; Roth, W. J.; Leonowicz, M. E.; Kresge, C. T.; Schmitt, K. D.; Chu, T. W.; Olson, D. H.; Sheppard, E. W.; McCullen, S. B.; Higgins, J. B.; Schlenker, J. L. *J. Am. Chem. Soc.* **1992**, *114*, 10834.
(30) Corma, A. *Chem. Rev.* **1997**, *97*, 2373.
(31) Ying, J. Y.; Mehnert, C. P.; Wong, M. S. *Angew. Chem. Int. Ed. Engl.* **1999**, *38*, 56.
(32) Inagaki, S.; Guan, S.; Fukushima, Y.; Ohsuna, T.; Terasaki, O. *J. Am. Chem. Soc.* **1999**, *121*, 9611.
(33) Melde, B. J.; Holland, B. T.; Blanford, C. F.; Stein, A. *Chem. Mater.* **1999**, *11*, 3302.
(34) Asefa, T.; MacLachlan, M. J.; Coombs, N.; Ozin, G. A. *Nature* **1999**, *402*, 867.
(35) Rodriguez-Reinoso, F. *Carbon* **1998**, *36*, 159.
(36) Boehm, H. P. *High Temperatures-High Pressures* **1990**, *22*, 275.
(37) Boehm, H. P. *Carbon* **1994**, *32*, 759.
(38) Figueiredo, J. L.; Pereira, M. F. R.; Freitas, M. M. A.; Orfao, J. J. M. *Carbon* **1999**, *37*, 1379.
(39) Coq, B.; Planeix, J. M.; Brotons, V. *Appl. Catal. A* **1998**, *173*, 175.
(40) Basset, J. M.; Choplin, A. *J. Mol. Catal.* **1983**, *21*, 95.
(41) Phillips, J.; Dumesic, J. A. *Appl. Catal.* **1984**, *9*, 1.
(42) Ugo, R.; Dossi, C.; Psaro, R. *J. Mol. Catal.* **1992**, *77*, 257.
(43) Lamb, H. H.; Gates, B. C.; Knözinger, H. *Angew. Chem. Int. Ed. Engl.* **1988**, *27*, 1127.
(44) Bailey, D. C.; Langer, S. H. *Chem. Rev.* **1981**, *81*, 130.
(45) Reddy, K. P.; Brown, T. L. *J. Am. Chem. Soc.* **1995**, *117*, 2845.
(46) Gajda, G. J.; Grubbs, R. H.; Weinberg, W. H. *J. Am. Chem. Soc.* **1987**, *109*, 66.
(47) Howe, R. F. *Inorg. Chem.* **1976**, *15*, 486.
(48) Brown, T. L. *J. Mol. Catal.* **1981**, *12*, 41.
(49) Kazusaka, A.; Howe, R. F. *J. Mol. Catal.* **1980**, *9*, 183.
(50) Kaltchev, M.; Tysoe, W. T. *J. Catal.* **2000**, *193*, 29.
(51) Walter, T. H.; Thompson, A.; Keniry, M.; Shinoda, S.; Brown, T. L.; Gutowsky, H. S.; Oldfield, E. *J. Am. Chem. Soc.* **1988**, *110*, 1065.
(52) Kazusaka, A.; Howe, R. F. *J. Mol. Catal.* **1980**, *9*, 199.
(53) Bilhou, J. L.; Theolier, A.; Smith, A. K.; Basset, J. M. *J. Mol. Catal.* **1977/78**, *3*, 245.
(54) Suvanto, M.; Pakkanen, T. A. *J. Mol. Catal.* **1999**, *138*, 211.
(55) Myllyoja, S.; Pakkanen, T. A. *J. Mol. Catal.* **1998**, *136*, 153.
(56) Brenner, A.; Hucul, D. A. *J. Catal.* **1980**, *61*, 216.
(57) Suvanto, M.; Pakkanen, T. A. *Appl. Catal. A* **1998**, *166*, 105.
(58) Brenner, A.; Burwell, R. L., Jr. *J. Catal.* **1978**, *52*, 353.
(59) Goldwasser, J.; Fang, S. M.; Houalla, M.; Hall, W. K. *J. Catal.* **1989**, *115*, 34.
(60) Zecchina, A.; Platero, E. E.; Arean, C. O. *Inorg. Chem.* **1988**, *27*, 102.
(61) Nakamura, R.; Bowman, R. G.; Burwell, R. L., Jr. *J. Am. Chem. Soc.* **1981**, *103*, 673.

(62) Jaenicke, S.; Loh, W. L. *Catal. Today* **1999**, *49*, 123.
(63) Myllyoja, S.; Suvanto, M.; Kuhrinen, M.; Hirva, P.; Pakkanen, T. A. *Surf. Sci.* **1999**, *441*, 454.
(64) Kurhinen, M.; Venäläinen, T.; Pakkanen, T. A. *J. Phys. Chem.* **1994**, *98*, 10237.
(65) Hunter, G.; Rochester, C. H.; Wilkinson, A. J.; Paton, J. *J. Chem. Soc., Faraday Trans.* **1996**, *92*, 5093.
(66) Hunter, G.; Rochester, C. H.; Wilkinson, A. G.; Paton, J. *J. Chem. Soc., Faraday Trans.* **1997**, *93*, 1205.
(67) Brenner, A.; Hucul, D. A.; Hardwick, S. J. *Inorg. Chem.* **1979**, *18*, 1478.
(68) Guglielminotti, E. *J. Mol. Catal.* **1981**, *13*, 207.
(69) Coluccia, S.; Marchese, L.; Martra, G.; Spoto, G.; Zecchina, A. *J. Mol. Catal.* **1990**, *60*, 71.
(70) Evans, J.; Hayden, B. E.; Lu, G. *J. Chem. Soc., Faraday Trans.* **1996**, *92*, 4733.
(71) Guglielminotti, E.; Zecchina, A. *J. Chim. Phys.* **1981**, *78*, 891.
(72) Abdo, S.; Howe, R. F. *J. Phys. Chem.* **1983**, *87*, 1713.
(73) Okamoto, Y.; Maezawa, A.; Kane, H.; Mitsushima, I.; Imanaka, T. *J. Chem. Soc., Faraday Trans. 1* **1988**, *84*, 851.
(74) Zecchina, A.; Rao, K. M.; Coluccia, S.; Platero, E. E.; Arean, C. O. *J. Mol. Catal.* **1989**, *53*, 397.
(75) Zecchina, A.; Bordiga, S.; Escalona Platero, E.; Otero Arean, C. *J. Catal.* **1990**, *125*, 568.
(76) Okamoto, Y.; Inui, Y.; Onimatsu, H.; Imanaka, T. *J. Phys. Chem*, **1991**, *95*, 4596.
(77) Özkar, S.; Ozin, G. A.; Moller, K.; Bein, T. *J. Am. Chem. Soc.* **1990**, *112*, 9575.
(78) Maezawa, A.; Kane, H.; Okamoto, Y.; Imanaka, T. *Chem. Lett.* **1988**, 241.
(79) Okamoto, Y.; Maezawa, A.; Kane, H.; Imanaka, T. *J. Catal.* **1988**, *112*, 585.
(80) Tway, L.; Apple, T. M. *Inorg. Chem.* **1992**, *31*, 2885.
(81) You-Sing, Y.; Howe, R. F. *J. Chem. Soc., Faraday Trans. I* **1986**, *82*, 2887.
(82) Coudurier, G.; Gallezot, P.; Praliaud, H.; Primet, M.; Imelik, B. *C. R. Acad. Sci. Paris Ser. C* **1976**, *282*, 311.
(83) Abdo, S.; Howe, R. F. *J. Phys. Chem*, **1983**, *87*, 1722.
(84) Okamoto, Y.; Kane, H.; Imanaka, T. *Chem. Lett.* **1988**, 2005.
(85) Okamoto, Y.; Imanaka, T.; Asakura, K.; Iwasawa, Y. *J. Phys. Chem*, **1991**, *95*, 3700.
(86) Yong, Y. S.; Howe, R. F.; Hughes, A. E.; Jaeger, H.; Sexton, B. A. *J. Phys. Chem*, **1987**, *91*, 6331.
(87) Coddington, J. M.; Howe, R. F.; Yong, Y. S.; Asakura, K.; Iwasawa, Y. *J. Chem. Soc., Faraday Trans.* **1990**, *86*, 1015.
(88) Okamoto, Y.; Kobayashi, Y.; Imanaka, T. *Catal. Lett.* **1993**, *20*, 49.
(89) Abdo, S.; Gosbee, J.; Howe, R. F. *J. Chim. Phys.* **1981**, *78*, 885.
(90) Komatsu, T.; Namba, S.; Yashima, T.; Domen, K.; Onishi, T. *J. Mol. Catal.* **1985**, *33*, 345.
(91) Hugues, F.; Basset, J. M.; Ben Taarit, Y.; Choplin, A.; Primet, M.; Rojas, D.; Smith, A. K. *J. Am. Chem. Soc.* **1982**, *104*, 7020.
(92) Hugues, F.; Smith, A. K.; Ben Taarit, Y.; Basset, J. M. *J. Chem. Soc., Chem. Commun.* **1980**, 68.
(93) Jackson, L. J.; Trusheim, M. R. *J. Am. Chem. Soc.* **1982**, *104*, 6590.
(94) Hugues, F.; Dalmon, J. A.; Smith, A. K.; Basset, J. M.; Olivier, D. *J. Phys. Chem.* **1982**, *86*, 5136.
(95) Guglielminotti, E.; Zecchina, A.; *J. Mol. Catal.* **1984**, *24*, 331.
(96) Iwasawa, Y.; Yamada, M.; Ogasawara, S.; Sato, Y.; Kuroda, H. *Chem. Lett.* **1983**, 621.
(97) Phillips, J.; Clausen, B.; Dumesic, J. A. *J. Phys. Chem.* **1980**, *84*, 1814.
(98) Ballivet-Tkatchenko, D.; Coudurier, G. *Inorg. Chem.* **1979**, *18*, 558.
(99) Bein, T.; Jacobs, P. A. *J. Chem. Soc., Faraday Trans.* **1983**, *79*, 1819.
(100) Nagy, J. B.; van Eenoo, M.; Derouane E. G. *J. Catal.* **1979**, *58*, 230.
(101) Brenner, A. *J. Chem. Soc., Chem. Commun.* **1979**, 251.
(102) Brenner, A.; Hucul, D. A. *Inorg. Chem.* **1979**, *18*, 2836.
(103) Bein, T.; Jacobs, P. A. *J. Chem. Soc., Faraday Trans.* **1984**, *80*, 1391.
(104) Ballivet-Tkatchenko, D.; Coudurier, G.; Mozzanega, H.; Tkatchenko, I.; Kiennemann, A. *J. Mol. Catal.* **1979**, *6*, 293.
(105) Rao, K. M.; Spoto, G.; Zecchina, A. *J. Catal.* **1988**, *113*, 466.
(106) Rao, K. M.; Spoto, G.; Guglielminotti, E.; Zecchina, A. *J. Chem. Soc., Faraday Trans.* **1988**, *84*, 2195.
(107) Schneider, R. L.; Howe, R. F.; Watters, K. L. *Inorg. Chem.* **1984**, *23*, 4593.
(108) Iwasawa, Y.; Yamada, M.; Sato, Y.; Kuroda, H. *J. Mol. Catal.* **1984**, *23*, 95.
(109) Asakura, K.; Iwasawa, Y. *Physica B*, **1989**, *158*, 152.
(110) Shirai, M.; Inoue, T.; Onishi, H.; Asakura, K.; Iwasawa, Y. *J. Catal.* **1994**, *145*, 159.
(111) Asakura, K.; Iwasawa, Y. *J. Phys. Chem.* **1989**, *93*, 4213.
(112) Suvanto, M.; Pakkanen, T. A.; Backman, L. *Appl. Catal. A* **1999**, *177*, 25.
(113) Suvanto, S.; Hirva, P.; Pakkanen, T. A. *Surf. Sci.* **2000**, *465*, 277.
(114) Kurhinen, M.; Pakkanen, T. A. *Langmuir* **1998**, *14*, 6907.
(115) Schneider, R. L.; Howe, R. F.; Watters, K. L. *Inorg. Chem.* **1984**, *23*, 4600.
(116) Zecchina, A.; Platero, E. E.; Arean, C. O. *J. Mol. Catal.* **1988**, *45*, 373.
(117) McKenna, W. P.; Higgins, B. E.; Eyring, E. M. *J. Mol. Catal.* **1985**, *31*, 199.
(118) Purnell, S. K.; Xu, X.; Goodman, D. W.; Gates, B. C. *J. Phys. Chem*, **1994**, *98*, 4076.
(119) Papile, C. J.; Gates, B. C. *Langmuir* **1992**, *8*, 74.
(120) Hu, A.; Neyman, K. M.; Staufer, M.; Belling, T.; Gates, B. C.; Rösch, N. *J. Am. Chem. Soc.* **1999**, *121*, 4522.
(121) Dossi, C.; Schaefer, J.; Sachtler, W. M. H. *J. Mol. Catal.* **1989**, *52*, 193.
(122) Keyes, M. P.; Watters, K. L. *J. Catal.* **1986**, *100*, 477.
(123) Keyes, M. P.; Watters, K. L. *J. Catal.* **1988**, *110*, 96.
(124) Frederick, B. G.; Apai, G.; Rhodin, T. N. *J. Am. Chem. Soc.* **1987**, *109*, 4797.
(125) Bowser, W. M.; Weinberg, W. H. *J. Am. Chem. Soc.* **1981**, *103*, 1453.
(126) Belton, D. N.; Dimaggio, C. L. *Surf. Sci.* **1989**, *220*, 96.
(127) Belton, D. N.; Schmieg, S. J. *Appl. Surf. Sci.* **1988**, *32*, 173.
(128) Evans, J.; Hayden, B.; Mosselmans, F.; Murray, A. *J. Am. Chem. Soc.* **1992**, *114*, 6912.
(129) Evans, J.; Hayden, B.; Mosselmans, F.; Murray, A. *Surf. Sci. Lett.* **1992**, *279*, L159.
(130) Evans, J.; Hayden, B.; Mosselmans, F.; Murray, A. *Surf. Sci.* **1994**, *301*, 61.
(131) Hayden, B. E.; King, A.; Newton, M. A. *Chem. Phys. Lett.* **1997**, *269*, 485.
(132) Hayden, B. E. In *Chemisorption and Reactivity on Supported Clusters and Thin Films*; Kluwer Academic Publishers: Norwell, MA, 1997; p 215.
(133) Evans, J. *J. Chem. Soc. Rev.* **1997**, 11.
(134) Hayden, B. E.; King, A.; Newton, M. A. *Surf. Sci.* **1998**, *397*, 306.
(135) Newton, M. A.; Bennett, R. A.; Smith, R. D.; Bowker, M.; Evans, J. *Chem. Commun.* **2000**, 1677.
(136) Newton, M. A.; Bennett, R. A.; Smith, R. D.; Bowker, M.; Evans, J. *Surf. Sci.* **2001**, *487*, 223.
(137) Hayden, B. E.; King, A.; Newton, M. A.; Yoshikawa, N. *J. Mol. Catal.* **2001**, *167*, 33.
(138) Gelin, P.; Ben Taarit, Y.; Naccache, C. *J. Catal.* **1981**, *59*, 357.
(139) Evans, J.; Hayden, B. E.; Newton, M. A. *Surf. Sci.* **2000**, *462*, 169.
(140) Smith, P. B.; Bernasek, S. L.; Schwartz, J.; McNulty, G. S. *J. Am. Chem. Soc.* **1986**, *108*, 5654.
(141) Chang, T.; Bernasek, S. L.; Schwartz, J. *J. Am. Chem. Soc.* **1989**, *111*, 758.
(142) Dufour, P.; Houtman, C.; Santini, C. C.; Nédez, C.; Basset, J. M.; Hsu, L. Y.; Shore, S. G. *J. Am. Chem. Soc.* **1992**, *114*, 4248.
(143) Santini, C. C.; Scott, S. L.; Basset, J. M. *J. Mol. Catal.* **1996**, *107*, 263.
(144) Iwasawa, Y.; Sato, H. *Chem. Lett.* **1985**, 507.
(145) Asakura, K.; Iwasawa, Y.; Kuroda, H. *J. Chem. Soc., Faraday Trans.* **1988**, *84*, 1329.
(146) Dufour, P.; Santini, C. C.; Houtman, C.; Basset, J. M. *J. Mol. Catal.* **1991**, *66*, L23.
(147) Dufour, P.; Houtman, C.; Santini, C. C.; Basset, J. M. *J. Mol. Catal.* **1992**, *77*, 257.
(148) Nédez, C.; Theolier, A.; Lefebvre, F.; Choplin, A.; Basset, J. M.; Joly, J. F. *J. Am. Chem. Soc.* **1993**, *115*, 722.
(149) Quignard, F.; Lecuyer, C.; Bougault, C.; Lefebvre, F.; Choplin, A.; Olivier, D.; Basset, J. M. *Inorg. Chem.* **1992**, *31*, 928.
(150) Rosier, C.; Niccolai, G. P.; Basset, J. M. *J. Am. Chem. Soc.* **1997**, *119*, 12408.
(151) Amor Nait Ajjou, J.; Scott, S. L. *Organometallics* **1997**, *16*, 86.
(152) Ajjou, J. A. N.; Rice, G. L.; Scott, S. L. *J. Am. Chem. Soc.* **1998**, *120*, 13436.
(153) Dufaud, V.; Niccolai, G. P.; Thivolle-Cazat, J.; Basset, J. M. *J. Am. Chem. Soc.* **1995**, *117*, 4288.
(154) Farkas, J.; Hampden-Smith, M. J.; Kodas, T. T. *J. Phys. Chem.* **1994**, *98*, 6753.
(155) Sekine, R.; Kawai, M. *Appl. Phys. Lett.* **1990**, *56*, 1466.
(156) Sekine, R.; Kawai, M.; Hikita, T.; Hanada, T. *Surf. Sci.* **1991**, *242*, 508.
(157) Sekine, R.; Kawai, M.; Asakura, K.; Hikita, T.; Kudo, M. *Surf. Sci.* **1992**, *278*, 175.
(158) Sekine, R.; Kawai, M.; Asakura, K.; Iwasawa, Y. *Mat. Res. Soc. Symp. Proc.* **1991**, *222*, 333.
(159) Shirai, M.; Asakura, K.; Iwasawa, Y. *Chem. Lett.* **1992**, 1037.
(160) Haukka, S.; Lakomaa, E.-L.; Suntola, T. *Appl. Surf. Sci.* **1994**, *75*, 220.
(161) Zecchina, A.; Spoto, G.; Bordiga, S. *J. Chem. Soc., Faraday Trans.* **1989**, *87*, 149.
(162) Hunter, G.; Rochester, C. H.; Wilkinson, A. J.; Paton, J. *J. Chem. Soc., Faraday Trans.* **1996**, *92*, 4763.

(163) Hunter, G.; Rochester, C. H.; Wilkinson, A. J.; Paton, J. *J. Chem. Soc., Faraday Trans.* **1997**, *92*, 5093.
(164) Hunter, G.; Rochester, C. H.; Wilkinson, A. J.; Paton, J. *J. Chem. Soc., Faraday Trans.* **1997**, *93*, 1205.
(165) Aigler, J. M.; Brito, J. L.; Leach, P. A.; Houalla, M.; Proctor, A.; Cooper, N. J.; Hall, W. K.; Hercules, D. M. *J. Phys. Chem.* **1993**, *97*, 5699.
(166) Iwasawa, Y.; Yamagishi, M. *J. Catal.* **1983**, *82*, 373.
(167) Crowfoot, L.; Ozin, G. A.; Özkar, S. *J. Am. Chem. Soc.* **1991**, *113*, 2033.
(168) Omata, K.; Mazaki, H.; Yagita, H.; Fujimoto, K. *Catal. Lett.* **1990**, *4*, 123.
(169) Dossi, C.; Bartsch, A.; Losi, P. In *Proceedings of the Congress Advanced Synthesis and Methodologies in Inorganic Chemistry*; Daolio, S. Ed.; 1991, 83.
(170) Hierso, J.-C.; Serp, P.; Feurer, R.; Kalck, P. *Appl. Organomet. Chem.* **1998**, *12*, 161.
(171) Suvanto, M.; Pakkanen, T. A. *J. Mol. Catal.* **1997**, *125*, 91.
(172) Lakomaa, E.-L. *Appl. Surf. Sci.* **1994**, *75*, 185.
(173) Köhler, S.; Reiche, M.; Frobel, C.; Baerns, M. In *Preparation of Catalysts VI*; Poncelet, G. et al., Eds.; Elsevier Science B. V.: New York, 1995; p 1009.
(174) Hucul, D. A.; Brenner, A. *J. Chem. Soc., Chem. Commun.* **1982**, 830.
(175) Hucul, D. A.; Brenner, A. *J. Phys. Chem.* **1981**, *85*, 496.
(176) Thomas, T. J.; Brenner, A. *J. Mol. Catal.* **1983**, *18*, 197.
(177) Brenner, A.; Hucul, D. A. *J. Am. Chem. Soc.* **1980**, *102*, 2484.
(178) Brenner, A. *J. Mol. Catal.* **1979**, *5*, 157.
(179) Gonzalez, P. F.; Villa Garcia, M. A.; Brenner, A. *J. Catal.* **1989**, *118*, 360.
(180) Masuyama, Y.; Tomatsu, Y.; Ishida, K.; Kurusu, Y.; Segawa, K.-I. *J. Catal.* **1988**, *114*, 347.
(181) Okamoto, Y.; Maezawa, A.; Kane, H.; Imanaka, T. *J. Chem. Soc., Chem. Commun.* **1988**, 380.
(182) Suvanto, S.; Hukkamäki, J.; Pakkanen, T. T.; Pakkanen, T. A. *Langmuir* **2000**, *16*, 4109.
(183) Jaenicke, S.; Loh, W. L. *Catal. Today* **1999**, *49*, 123.
(184) Wada, Y.; Nakaoka, C.; Morikawa, A. *Chem. Lett.* **1992**, 1037.
(185) Bilhou, J. L.; Theolier, A.; Smith, A. K.; Basset, J. M. *J. Mol. Catal.* **1977/78**, *3*, 245.
(186) Derouane, E. G.; Nagy, J. B.; Védrine, J. C. *J. Catal.* **1977**, *46*, 434.
(187) Kazusaka, A.; Suzuki, H.; Toyoshima, I. *J. Chem. Soc., Chem. Commun.* **1983**, 150.
(188) Suvanto, S.; Hukkamäki, J.; Pakkanen, T. T.; Pakkanen, T. A. *Langmuir* **2000**, *16*, 4109.
(189) Suvanto, S.; Pakkanen, T. A. *J. Mol. Catal.* **2000**, *164*, 273.
(190) Suvanto, M.; Räty, J.; Pakkanen, T. A. *Appl. Catal. A* **1999**, *181*, 189.
(191) Suvanto, M.; Räty, J.; Pakkanen, T. A. *Catal. Lett.* **1999**, *62*, 21.
(192) Kurhinen, M.; Pakkanen, T. A. *Appl. Catal. A* **2000**, *194*−*195*, 365.
(193) Myllyoja, S.; Räty J.; Pakkanen, T. A. *J. Mol. Catal.* **2000**, *157*, 245.
(194) Yamaguchi, A.; Asakura, K.; Iwasawa, Y. *J. Mol. Catal.* **1999**, *146*, 65.
(195) Srinivasan, R.; De Angelis, R. J.; Reucroft, P. J.; Dhere, A. G.; Bentley, J. *J. Catal.* **1989**, *116*, 144.
(196) Zerger, R. P.; McMahon, K. C.; Seltzer, M. D.; Michel, R. G.; Suib, S. L. *J. Catal.* **1986**, *99*, 498.
(197) McMahon, K. C.; Suib, S. L.; Johnson, B. G.; Bartholomew, C. H, Jr. *J. Catal.* **1987**, *106*, 47.
(198) Shen, G.-C.; Liu, A. M.; Ichikawa, M. *J. Chem. Soc., Faraday Trans.* **1998**, *94*, 1353.
(199) Chen, J. G. C.; Liu, A. M.; Tanaka, T.; Ichikawa, M. *J. Phys. Chem B*, **1998**, *102*, 7782.
(200) Bando, K. K.; Arakawa, H.; Ichikuni, N. *Catal. Lett.* **1999**, *60*, 125.
(201) Hirva, P.; Venäläinen, T.; Pakkanen, T. A. *J. Catal.* **1994**, *148*, 722.
(202) Rizzi, G. A.; Magrin, A.; Granozzi, G. *Surf. Sci.* **1999**, *443*, 277.
(203) Pinto, P.; Calhorda, M. J.; Straub, T.; Miikkulainen, V.; Räty, J.; Suvanto, M.; Pakkanen, T. A. *J. Mol. Catal.* **2001**, *170*, 209.
(204) Tsang, C. M.; Augustine, S. M.; Butt, J. M.; Sachtler, W. M. H. *Appl. Catal. A* **1989**, *46*, 45.
(205) Räty, J.; Pakkanen, T. A. *Appl. Catal. A* **2001**, *208*, 169.
(206) Räty, J.; Pakkanen, T. A. *J. Mol. Catal.* **2001**, *166*, 275.
(207) Rizzi, G. A.; Zanoni, R.; Di Siro, S.; Perriello, L.; Granozzi, G. *Surf. Sci.* **2000**, *462*, 187.
(208) Clowes, S. K.; Seddon, E. A.; McCash, E. M. *Surf. Sci.* **2000**, *464*, L667.
(209) Close, M. R.; Petersen, J. L.; Kugler, E. L. *Inorg. Chem.* **1999**, *38*, 1535.
(210) Wei, J.-C. J.; Lo, M.-H. *Appl. Organomet. Chem.* **1998**, *12*, 201.
(211) Yoo, J. S.; Lin, P. S.; Elfline, S. D. *Appl. Catal. A* **1993**, *106*, 259.
(212) Yoo, J. S.; Donohue, D. A.; Kleefish, M. S.; Lin, P. S.; Elfline, S. D. *Appl. Catal. A* **1993**, *105*, 83.
(213) Zajac, G. W.; Choi-Feng, C.; Faber, J.; Yoo, J. S.; Patel, R.; Hochst, H. *J. Catal.* **1995**, *151*, 338.
(214) Yoo, J. S.; Choi-Feng, C.; Donohue, D. A. *Appl. Catal. A* **1994**, *118*, 87.
(215) Yoo, J. S.; Sohail, A. R.; Grimmer, S. S.; Choi-Feng, C. *Catal. Lett.* **1994**, *29*, 299.
(216) Yoo, J. S.; Donohue, D. A.; Kleefish, M. S. *Appl. Catal. A* **1994**, *110*, 75.
(217) Yoo, J. S. *Appl. Catal. A* **1996**, *135*, 261.
(218) Centi, G.; Perathoner, S.; Tonini, S. *Catal. Today* **2000**, *61*, 211.
(219) Chen, H.-Y.; Sachtler, W. M. H. *Catal. Today* **1998**, *42*, 73.
(220) Voskoboinikov, T. V.; Chen, H.-Y.; Sachtler, W. M. H. *Appl. Catal. B* **1998**, *19*, 279.
(221) Chen, H−Y; Sachtler, W. M. H. *Catal. Lett.* **1998**, *50*, 125.
(222) Chen, H.-Y.; Voskoboinikov, T.; Sachtler, W. M. H. *Catal. Today* **1999**, *54*, 483.
(223) El-Malki, El-M.; van Santen, R. A.; Sachtler, W. H. M. *J. Phys. Chem. B* **1999**, *103*, 4611.
(224) Chen, H.-Y.; Voskoboinikov, T.; Sachtler, W. M. H. *J. Catal.* **1998**, *180*, 171.
(225) Centi, G.; Vazzana, F. *Catal. Today* **1999**, *53*, 683.
(226) Centi, G.; Misono, M. *Catal. Today* **1998**, *41*, 287.
(227) Ma, A.-Z.; Grünert, W. *J. Chem. Soc., Chem. Commun.* **1999**, 71.
(228) Long, R. Q.; Yang, R. T. *J. Catal.* **1999**, *188*, 332.
(229) Kucherov, A. V.; Montreuil, C. N.; Kucherova, T. N.; Shelef, M. *Catal. Lett.* **1998**, *56*, 173.
(230) Uemera, Y.; Hatate, Y.; Ikari, A. *J. Chem. Eng. Jpn.* **1989**, *22*, 48.
(231) Moene, R.; Makkee, M.; Moulijn, J. A. *Chem. Eng. J.* **1993**, *53*, 13.
(232) Jacobs, J. P.; Lindfors, L. P.; Reintjes, J. G. H.; Jylha, O.; Brongersma, H. H. *Catal. Lett.* **1994**, *25*, 315.
(233) Lindblad, M.; Lindfors, L. P.; Suntola, T. *Catal. Lett.* **1994**, *27*, 323.
(234) Backman, L. B.; Rautiainen, A.; Krause, A. O. I.; Lindblad, M. *Catal. Today* **1998**, *43*, 11.
(235) Backman, L. B.; Rautiainen, A.; Lindblad, M.; Jylhä, O.; Krause, A. O. I. *Appl. Catal. A* **2001**, *208*, 223.
(236) Backman, L. B.; Rautiainen, A.; Lindblad, M.; Krause, A. O. I. *Appl. Catal. A* **2000**, *191*, 55.
(237) Kainulainen, T. A.; Niemelä, M. K.; Krause, A. O. I. *Catal. Lett.* **1998**, *53*, 97.
(238) Sonnemans, J.; Mars, P. *J. Catal.* **1973**, *32*, 209.
(239) Iwasawa, Y.; Yamagishi, M.; Ogasawara, S. *J. Chem. Soc., Chem. Commun.* **1982**, 246.
(240) Iwasawa, Y.; Yamagishi, M.; Ogasawara, S. *J. Chem. Soc., Chem. Commun.* **1980**, 871.
(241) Anpo, M.; Kondo, M.; Coluccia, S.; Louis, C.; Che, M. *J. Am. Chem. Soc.* **1989**, *111*, 8791.
(242) Anpo, M.; Kondo, M.; Kubokawa, Y.; Louis, C.; Che, M. *J. Chem. Soc., Faraday Trans. 1* **1988**, *84*, 2771.
(243) Louis, C.; Tatibouët, J. M.; Che, M. *J. Catal.* **1988**, *109*, 354.
(244) Collart, O.; Van Der Voort, P.; Vansant, E. F.; Gustin, E.; Bouwen, A.; Schoemaker, D.; Rachamandra Rao, R.; Weckhuysen, B. M.; Schoonheydt, R. A. *Phys. Chem. Chem. Phys.* **1999**, *1*, 4099.
(245) Baltes, M.; Collart, O.; van der Voot, P.; Vansant, E. F. *Langmuir* **1999**, *15*, 5841.
(246) Miyao, T.; Shishikura, I.; Matsuoka, M.; Nagai, M. *Chem. Lett.* **1996**, 561.
(247) Patterson, W. R.; Taylor, S. D. *J. Catal.* **1988**, *114*, 460.
(248) Chien, J. C. W. *J. Am. Chem. Soc.* **1971**, *93*, 4675.
(249) Bond, G. C.; König, P. *J. Catal.* **1982**, *77*, 309.
(250) Bond, G. C.; Brückman, K. *Faraday Discuss., Chem. Soc.* **1981**, *72*, 235.
(251) Grubert, G.; Rathousky, J.; Schulz-Ekloff, G.; Wark, M; Zukal, A. *Microporous Mater.* **1998**, *22*, 225.
(252) Hanke, W.; Bienert, R.; Jerschkewitz, H. G. *Z. Anorg. Allg. Chem.* **1975**, *414*, 109.
(253) Anpo, M.; Sunamoto, M.; Che, M. *J. Phys. Chem*, **1989**, *93*, 1187.
(254) Inamuru, K.; Okuhara, T.; Misono, M. *Chem. Lett.* **1990**, 1207.
(255) Inumaru, K.; Okuhara, T.; Misono, M. *J. Phys. Chem*, **1991**, *95*, 4826.
(256) Okuhara, T.; Inamuru, K.; Misono, M.; Matsubayashi, N.; Shimada, H.; Nishijima, A. *Catal. Lett.* **1993**, *20*, 73.
(257) Nickl, J.; Dutoit, D.; Baiker, A.; Scharf, U.; Wokaun, A. *Appl. Catal. A* **1993**, *98*, 173.
(258) Nickl, J.; Dutoit, D.; Baiker, A.; Scharf, U.; Wokaun, A. *Ber. Bunsenges. Phys. Chem.* **1993**, *97*, 217.
(259) Baltes, M.; Van Der Voort, P.; Collart, O.; Vansant, E. F. *J. Porous Mater.* **1998**, *5*, 317.
(260) Van Der Voort, P.; Baltes, M.; Vansant, E. F. *J. Phys. Chem. B* **1999**, *103*, 10102.
(261) Van Der Voort, P.; Morey, M.; Stucky, G. D.; Mathieu, M.; Vansant, E. F. *J. Phys. Chem. B* **1998**, *102*, 585.
(262) Kytökivi, A.; Jacobs, J.-P.; Hakuli, A.; Merilaïnen, J.; Brongersma, H. H. *J. Catal.* **1996**, *162*, 190.

(263) Hakuli, A.; Kytökivi, A.; Krause, A. O. I. *Appl. Catal. A* **2000**, *190*, 219.
(264) Babich, I. V.; Plyuto, Y. V.; Van Der Voort, P.; Vansant, E. F. *J. Chem. Soc., Faraday Trans.* **1997**, *93*, 3191.
(265) Bond, G. C.; Thompson, D. T. *Catal. Rev.-Sci. Eng.* **1999**, *41*, 319.
(266) Okumura, M.; Tanaka, K.; Ueda, A.; Haruta, M. *Solid State Ionics* **1997**, *95*, 143.
(267) Haruta, M. *Catal. Today* **1997**, *36*, 153.
(268) Haruta, M. *Catal. Surv. Jpn.* **1997**, *1*, 61.
(269) Okumura, M.; Nakamura, S.; Tsubota, S.; Nakamura, T.; Azuma, M.; Haruta, M. *Catal. Lett.* **1998**, *51*, 53.
(270) Feeley, O. C.; Sachtler, W. M. H. *Appl. Catal. A* **1991**, *75*, 93.
(271) Dossi, C.; Psaro, R.; Bartsch, A.; Brivio, E.; Galasco, A.; Losi, P. *Catal. Today* **1993**, *17*, 527.
(272) Dossi, C.; Psaro, R.; Ugo, R.; Zhang, Z. C.; Sachtler, W. M. H. *J. Catal.* **1994**, *149*, 92.
(273) Sordelli, L.; Martra, G.; Psaro, R.; Dossi, C.; Coluccia, S. *Top. Catal.* **1999**, *8*, 237.
(274) Dossi, C.; Fusi, A.; Recchia, S.; Anghileri, M.; Psaro, R. *J. Chem. Soc., Chem. Commun.* **1994**, 1245.
(275) Mehnert, C. P.; Ying, J. Y. *J. Chem. Soc., Chem. Commun.* **1997**, 2215.
(276) Mehnert, C. P.; Weaver, D. W.; Ying, J. Y. J. H. *J. Am. Chem. Soc.* **1998**, *120*, 12289.
(277) Hierso, J.-C.; Satto, C.; Feurer, R.; Kalck, P. *Chem. Mater.* **1996**, *8*, 2481.
(278) Hierso, J.-C.; Feurer, R.; Kalck, P. *Chem. Mater.* **2000**, *8*, 2481.
(279) Hierso, J.-C.; Feurer, R.; Kalck, P. *Coord. Chem. Rev.* **1998**, *178*, 8−180, 1811.
(280) Matsuura, I.; Hashimoto, Y.; Takayasu, O.; Nitta, K.; Yoshida, Y. *Appl. Catal. A* **1991**, *74*, 273.
(281) Cominos, V.; Gavriilidis, A. *Appl. Catal. A* **2001**, *210*, 381.
(282) Hong, S. B.; Mielczarski, E.; Davis, M. E. *J. Catal.* **1992**, *134*, 349.
(283) Dossi, C.; Psaro, R.; Bartsch, A.; Fusi, A.; Sordelli, L.; Ugo, R.; Bellatreccia, M.; Zanoni, R.; Vlaic, G. *J. Catal.* **1994**, *145*, 377.
(284) Bellatreccia, M.; Zanoni, R.; Dossi, C.; Psaro, R.; Recchia, S.; Vlaic, G. *J. Chem. Soc., Faraday Trans.* **1995**, *91*, 2045.
(285) Dossi, C.; Psaro, R.; Sordelli, L.; Bellatreccia, M.; Zanoni, R. *J. Catal.* **1996**, *159*, 435.
(286) Jacobs, G.; Ghadiali, F.; Pisanu, A.; Borgna, A.; Alvarez, W. E.; Resasco, D. E. *Appl. Catal. A* **1999**, *23*, 139.
(287) Feast, S.; Englisch, M.; Jentys, A.; Lercher, J. A. *Appl. Catal. A* **1998**, *174*, 155.
(288) Serp, P.; Hierso, J.-C.; Feurer, R.; Kihn, Y.; Kalck, P.; Faria, J. L.; Aksoylu, A. E.; Pacheco, A. M. T.; Figueiredo, J. L. *Carbon* **1999**, *37*, 527.
(289) Serp, P.; Feurer, R.; Kihn, Y.; Kalck, P.; Faria, J. L.; Figueiredo, J. L. *J. Mater. Chem.* **2001**, *11*, 1980.
(290) Hierso, J.-C.; Feurer, R.; Poujardieu, J.; Kihn, Y.; Kalck, P. *J. Mol. Catal.* **1998**, *135*, 321.
(291) Serp, P.; Feurer, R.; Kalck, P.; Molinier, J.; Morancho, R.; Guerlet, J. P. Fr. Patent, 93.08656, 1993.
(292) Serp, P.; Feurer, R.; Morancho, R.; Kalck, P. *J. Mol. Catal.* **1995**, *101*, L107.
(293) Serp, P.; Feurer, R.; Morancho, R.; Kalck, P. *J. Catal.* **1995**, *157*, 294.
(294) Feurer, R.; Reynes, A.; Serp, P.; Kalck, P.; Morancho, R. *J. Phys. IV Colloque C5* **1995**, *5*, 1037.
(295) Serp, P.; Château, L.; Feurer, R.; Kiennemann, A.; Kalck, P. *J. Mol. Catal.* **1998**, *136*, 269.
(296) Serp, P.; Feurer, R.; Morancho, R.; Kalck, P.; Daran, J.-C.; Vaisserman, J. *J. Organomet. Chem.* **1995**, *498*, 41.
(297) Locatelli, F.; Didillon, B.; Uzio, D.; Niccolai, G.; Candy, J. P.; Basset, J. M. *J. Catal.* **2000**, *193*, 154.
(298) Miura, H. *Catal. Today* **1996**, *28*, 215.
(299) Miura, H.; Taguchi, H.; Sugiyama, K.; Matsuda, T.; Gonzalez, R. D. *J. Catal.* **1990**, *124*, 194.
(300) Zhou, P. L.; Gates, B. C. *J. Chem. Soc., Chem. Commun.* **1989**, 347.
(301) Tomishige, K.; Asakura, K.; Iwasawa, Y. *J. Chem. Soc., Chem. Commun.* **1993**, 184.
(302) Tomishige, K.; Asakura, K.; Iwasawa, Y. *Catal. Lett.* **1993**, *20*, 15.
(303) Tomishige, K.; Asakura, K.; Iwasawa, Y. *Chem. Lett.* **1994**, 235.
(304) Tomishige, K.; Asakura, K.; Iwasawa, Y. *J. Catal.* **1994**, *149*, 70.
(305) Tomishige, K.; Asakura, K.; Iwasawa, Y. *J. Catal.* **1995**, *157*, 472.
(306) Yoshikawa, K.; Iwasawa, Y. *J. Mol. Catal.* **1995**, *100*, 115.
(307) Inoue, T.; Tomishige, K.; Iwasawa, Y. *J. Chem. Soc., Chem. Commun.* **1995**, 329.
(308) Didillon, B.; Houtman, C.; Shay, T.; Basset, J. M. *J. Am. Chem. Soc.* **1993**, *115*, 9380.
(309) Lesage, P.; Clause, O.; Moral, P.; Didillon, B.; Candy, J. P.; Basset, J. M. *J. Catal.* **1995**, *155*, 238.
(310) Miura, H.; Itoh, T. *React. Kinet. Catal. Lett.* **1999**, *66*, 189.
(311) Recchia, S.; Dossi, C.; Fusi, A.; Sordelli, L.; Psaro, P. *Appl. Catal. A* **1999**, *182*, 41.
(312) Onda, A.; Komatsu, T.; Yashima, T. *J. Chem. Soc., Chem. Commun.* **1998**, 1507.
(313) Warnken, M.; Lazar, K.; Wark, M. *Phys. Chem. Chem. Phys.* **2001**, *3*, 1870.
(314) Kwak, B. S.; Sachtler, W. M. H. *J. Catal.* **1993**, *141*, 729.
(315) Kwak, B. S.; Sachtler, W. M. H. *J. Catal.* **1994**, *145*, 456.
(316) Sakurai, H.; Sato, S.; Urabe, K.; Izumi, Y. *Chem. Lett.* **1985**, 1783.
(317) Sato, S.; Sakurai, H.; Urabe, K.; Izumi, Y. *Chem. Lett.* **1985**, 277.
(318) Sato, S.; Urabe, K.; Izumi, Y. *J. Catal.* **1986**, *102*, 99.
(319) Sato, S.; Hasegawa, M.; Sodesawa, T.; Nozaki, F. *Bull. Chem. Soc. Jpn.* **1991**, *64*, 516.
(320) Tavares da Silva, C. L.; Loyola Camorim, V. L.; Zotin, J. L.; Rocco Duarte Pereira, M. L.; da Costa Faro, A., Jr. *Catal. Today* **2000**, *57*, 209.
(321) Nagai, M.; Suda, T.; Oshikawa, K.; Hirano, N.; Omi, S. *Catal. Today* **1999**, *50*, 29.
(322) Nagai, M.; Nakauchi, R.; Ono, Y.; Omi, S. *Catal. Today* **2000**, *57*, 297.
(323) Ramirez Ortiz, J.; Ogura, T.; Medina-Valtierra, J.; Acosta-Ortiz, S. E.; Bosch, P.; de los Reyes, J. A.; Lara, V. H. *Appl. Surf. Sci.* **2001**, *174*, 177.
(324) Caps, V.; Tsang, S. C. *Catal. Today* **2000**, *61*, 19.
(325) Burch, R.; Cruise, N. A.; Gleeson, D.; Tsang, S. C. *J. Mater. Chem.* **1998**, *8*, 227.
(326) Beutel, T.; Knözinger, H.; Trevino, H.; Zhang, Z. C.; Sachtler, W. M. H.; Dossi, C.; Psaro, R.; Ugo, R. *J. Chem. Soc., Faraday Trans.* **1994**, *90*, 1335.
(327) Kröger-Laukkanen, M.; Peussa, M.; Leskelä, M.; Niinistö, L. *Appl. Surf. Sci.* **2001**, *183*, 290.
(328) Izumi, Y.; Asakura, K.; Iwasawa, Y. *J. Catal.* **1991**, *127*, 631.
(329) Izumi, Y.; Asakura, K.; Iwasawa, Y. *J. Catal.* **1991**, *132*, 566.
(330) Izumi, Y.; Iwasawa, Y. *J. Phys. Chem.* **1992**, *96*, 10942.
(331) Komatsu, T.; Mesuda, M.; Yashima, T. *Appl. Catal. A* **2000**, *194*−*195*, 333.
(332) Hertl, W.; Hair, M. L. *J. Phys. Chem.* **1971**, *75*, 2181.
(333) Hair, M. L.; Hertl, W. *J. Phys. Chem.* **1973**, *77*, 1965.
(334) Hair, M. L.; Hertl, W. *J. Phys. Chem.* **1973**, *77*, 2070.
(335) Kol'tsov, S. I.; Aleskovskii, V. B. *Russ. J. Chem.* **1968**, *42*, 631.
(336) Morrow, B. A.; Hardin, A. H. *J. Phys. Chem.* **1979**, *83*, 3135.
(337) Van der Voort, P.; Gillis-D'Hamers, I.; Vansant, E. F. *J. Chem. Soc., Faraday Trans.* **1990**, *86*, 3751.
(338) Gillis-D'Hamers, I.; Philippaerts, J.; Van der Voort, P.; Vansant, E. F. *J. Chem. Soc., Faraday Trans.* **1990**, *86*, 3747.
(339) Niwa, M.; Hibino, T.; Murata, H.; Katada, N.; Murakami, Y. *J. Chem. Soc., Chem. Commun.* **1989**, 289.
(340) Niwa, M.; Katada, N.; Murakami, Y. *J. Phys. Chem*, **1990**, *94*, 6441.
(341) Katada, N.; Ishiguro, H.; Muto, K.; Niwa, M. *Chem. Vap. Deposition* **1995**, *1*, 54.
(342) Katada, N.; Toyama, T.; Niwa, M. *J. Phys. Chem.* **1994**, *98*, 7647.
(343) Katada, N.; Fukui, H.; Niwa, M. *J. Chem. Eng. Jpn.* **2001**, *34*, 306.
(344) Katada, N.; Fujii, T.; Iwata, K.; Hibino, H.; Niwa, M. *J. Catal.* **1999**, *186*, 478.
(345) Sato, S.; Toita, M.; Sodesawa, T.; Nozaki, F. *Appl. Catal. A* **1990**, *62*, 73.
(346) Imizu, Y.; Tada, A. *Chem. Lett.* **1989**, 1793.
(347) Sato, S.; Toita, M.; Yu, Y.-Q.; Sodesawa, T.; Nozaki, F. *Chem. Lett.* **1987**, 1535.
(348) Sato, S.; Hiratsuka, M.; Sodesawa, T.; Nosaki, F. *Bull. Chem. Soc. Jpn.* **1991**, *64*, 2214.
(349) Muto, K.; Katada, N.; Niwa, M. *Appl. Catal. A* **1996**, *134*, 203.
(350) Muto, K.; Katada, N.; Niwa, M. *Catal. Today* **1997**, *35*, 145.
(351) Niwa, M.; Katada, N.; Murakami, Y. *J. Catal.* **1992**, *134*, 340.
(352) Okuhara, T.; White, J. M. *Appl. Surf. Sci.* **1987**, *29*, 223.
(353) Jin, T.; Okuhara, T.; White, J. M. *J. Chem. Soc., Chem. Commun.* **1987**, 1248.
(354) Xu, B.-Q.; Yamaguchi, T.; Tanabe, K. *Chem. Lett.* **1989**, 149.
(355) Shin, E. W.; Choi, C. H.; Na, Y. H.; Moon, S. H. *Catal. Today* **1998**, *44*, 137.
(356) Asakura, K.; Ooi, K.; Iwasawa, Y. *J. Mol. Catal.* **1992**, *74*, 345.
(357) Iiskola, E. I.; Timonen, S.; Pakkanen, T. T.; Härkki, O.; Seppälä, J. V. *Appl. Surf. Sci.* **1997**, *121/122*, 372.
(358) Timonen, S.; Pakkanen, T. T.; Iiskola, E. I. *J. Mol. Catal.* **1999**, *148*, 235.
(359) Timonen, S.; Pakkanen, T. T.; Iiskola, E. I. *J. Organomet. Chem.* **1999**, *582*, 273.
(360) Okumura, K.; Asakura, K.; Iwasawa, Y. *Langmuir* **1998**, *14*, 3607.
(361) Okumura, K.; Asakura, K.; Iwasawa, Y. *J. Phys. Chem B* **1997**, *101*, 9984.
(362) Asakura, K.; Okumura, K.; Inoue, T.; Kubota, T.; Chun, W. H.; Iwasawa, Y. *Mat. Res. Soc. Symp. Proc.* **1998**, *497*, 99.
(363) Okumura, K.; Asakura, K.; Iwasawa, Y. *Catal. Today* **1998**, *39*, 343.

(364) Okumura, K.; Ichikuni, N.; Asakura, K.; Iwasawa, Y. *J. Chem. Soc., Faraday Trans.* **1997**, *93*, 3217.
(365) Nariman, K. E.; Lerou, J. J.; Bischoff, K. B.; Foley, H. C. *Ind. Eng. Chem. Res.* **1993**, *32*, 263.
(366) Niwa, M.; Itoh, H.; Kato, S.; Hattori, T.; Murakami, Y. *J. Chem. Soc., Chem. Commun.* **1982**, 819.
(367) Niwa, M.; Kato, M.; Hattori, T.; Murakami, Y. *J. Chem. Soc., Faraday Trans.* **1984**, *80*, 3135.
(368) Niwa, M.; Kawashima, Y.; Hibino, T.; Murakami, Y. *J. Chem. Soc., Faraday Trans.* **1988**, *84*, 4327.
(369) Hibino, T.; Niwa, M.; Hattori, A.; Murakami, Y. *Appl. Catal. A* **1988**, *44*, 95.
(370) Sawa, M.; Kato, K.; Hirota, K.; Niwa, M.; Murakami, Y. *Appl. Catal. A* **1990**, *64*, 297.
(371) Niwa, M.; Kawashima, Y.; Murakami, Y. *J. Chem. Soc., Faraday Trans.* **1985**, *81*, 2757.
(372) Yan, Y.; Vansant, E. F. *J. Phys. Chem B* **1990**, *94*, 2582.
(373) Niwa, M.; Kato, M.; Hattori, T.; Murakami, Y. *J. Phys. Chem.* **1986**, *90*, 6233.
(374) Hibino, T.; Niwa, M.; Murakami, Y. *J. Catal.* **1991**, *128*, 551.
(375) Kim, J.-H.; Ishida, A.; Okajima, M.; Niwa, M. *J. Catal.* **1996**, *161*, 387.
(376) Kim, J.-H.; Ikoma, Y.; Niwa, M. *Microporous Mesoporous Mater.* **1999**, *32*, 37.
(377) Weber, R. W.; Möller, K. P.; Unger, M.; O'Connor, C. T. *Microporous Mater.* **1998**, *23*, 179.
(378) Röger, H. P.; Krämer, M.; Möller, K. P.; O'Connor, C. T. *Microporous Mater.* **1998**, *21*, 607.
(379) Shaikh, R. A.; Hedge, S. G.; Behlekar, A. A.; Rao, B. S. *Catal. Today* **1999**, *49*, 201.
(380) Wang, I.; Ay, C.-L.; Lee, B.-J.; Chen, M.-H. *Appl. Catal. A* **1989**, *54*, 257.
(381) Bhat, Y. S.; Das, J.; Halgeri, A. B. *J. Catal.* **1995**, *155*, 154.
(382) Shimizu, S.; Abe, N.; Iguchi, A.; Dohba, M.; Sato, H.; Hirose, K *Microporous Mater.* **1998**, *21*, 447.
(383) Zheng, J.; Chun, Y.; Dong, J.; Xu, Q. *J. Mol. Catal.* **1998**, 1*30*, 271.
(384) Lin, C. H.; Lee, K. C.; Wan, B.-Z. *Appl. Catal. A* **1997**, *164*, 59.
(385) Baeck, S. H.; Lee, K. M.; Lee, W. H. *Catal. Lett.* **1998**, *52*, 221.
(386) Kuno, H.; Shibagaki, M.; Takahashi, K.; Honda, I.; Matsushita, H. *Bull. Chem. Soc. Jpn.* **1991**, *64*, 2508.
(387) Kuno, H.; Shibagaki, M.; Takahashi, K.; Honda, I.; Matsushita, H. *Bull. Chem. Soc. Jpn.* **1992**, *65*, 1240.
(388) Bhat, Y. S.; Das, J.; Halgeri, A. B. *Bull. Chem. Soc. Jpn.* **1996**, *69*, 469.
(389) Niwa, M.; Kawashima, Y.; Murakami, Y. *J. Chem. Soc., Faraday Trans.* **1985**, *81*, 2757.
(390) Suzuki, M.; Amano, J.; Niwa, M. *Microporous Mater.* **1998**, *21*, 541.
(391) Hibino, T.; Niwa, M.; Murakami, Y.; Sano, M.; Shin-ichi, K.; Hanaichi, T. *J. Phys. Chem.* **1989**, *93*, 7847.
(392) Hibino, T.; Niwa, M.; Murakami, Y.; Sano, M. *J. Chem. Soc., Faraday Trans.* **1989**, *85*, 2327.
(393) Tynjälä, P.; Pakkanen, T. T. *J. Mol. Catal.* **1997**, *122*, 159.
(394) Asakura, K.; Aoki, M.; Iwasawa, Y. *Catal. Lett.* **1988**, *1*, 395.
(395) Pozzo, R. L.; Baltanas, M. A.; Cassano, A. E. *Catal. Today* **1997**, *39*, 219.
(396) Gao, X.; Wachs, I. E. *Catal. Today* **1999**, *51*, 233.
(397) Kinney, J. B.; Staley, R. H. *J. Phys. Chem.* **1983**, *87*, 3735.
(398) Schrijnemakers, K.; van der Voot, P.; Vansant, E. F. *Phys. Chem. Chem. Phys.* **1999**, *1*, 2569.
(399) Schrijnemakers, K.; Impens, N. R. E. N.; Vansant, E. F. *Langmuir* **1999**, *15*, 5807.
(400) Haukka, S.; Lakomaa, E.-L.; Root, A. *J. Phys. Chem B* **1993**, *97*, 5085.
(401) Lakomaa, E.-L.; Haukka, S.; Suntola, T. *Appl. Surf. Sc.* **1992**, *60/61*, 742.
(402) Yang, Q.; Wang, S.; Lu, J.; Xiong, G.; Feng, Z.; Xin, Q.; Li, C. *Appl. Catal. A* **2000**, *194*, 507.
(403) Wang, S.; Yang, Q.; Wu, Z.; Li, M.; Lu, J.; Tan, Z.; Li, C. *J. Mol. Catal.* **2001**, *172*, 219.
(404) Klaas, J.; Schulz-Ekloff, G.; Jaeger, N. I. *J. Phys. Chem. B* **1997**, *101*, 1305.
(405) Anpo, M.; Chiba, K. *J. Mol. Catal.* **1992**, *74*, 207.
(406) Jackson, N. B.; Wang, C. M.; Schwitzgebel, J.; Ekerdt, J. G.; Brock, J. R.; Heller, A. *J. Electrochem. Soc.* **1991**, *138*, 3660.
(407) Anpo, M.; Aikawa, N.; Kubokawa, Y.; Che, M.; Louis, C.; Giamello, E. *J. Phys. Chem.* **1985**, *89*, 5017.
(408) Anpo, M.; Aikawa, N.; Kubokawa, Y.; Che, M.; Louis, C.; Giamello, E. *J. Phys. Chem.* **1985**, *89*, 5689.
(409) Ding, Z.; Hu, X.; Lu, G. Q.; Yue, P.-L.; Greenfield, P. F. *Langmuir* **2000**, *16*, 6216.
(410) Kirkbir, F.; Komiyama, H. *Can. J. Chem. Eng.* **1987**, *65*, 759.
(411) Segawa, K.; Katsuta, M.; Kameda, F. *Catal. Today* **1996**, *29*, 215.
(412) Pophal, C.; Kameda, F.; Hoshino, K.; Yoshinaka, S.; Segawa, K. *Catal. Today* **1997**, *39*, 21.
(413) Yoshinaka, S.; Segawa, K. *Catal. Today* **1998**, *45*, 293.
(414) Segawa, K.; Takahashi, K.; Satoh, S. *Catal. Today* **2000**, *63*, 123.
(415) Foger, K.; Anderson, J. R. *Appl. Catal. A* **1986**, *23*, 139.
(416) Asakura, K.; Inukai, J.; Iwasawa, Y. *J. Phys. Chem*, **1992**, *96*, 829.
(417) Coronas, J.; Santamaria, J. *Catal. Today*, **1999**, *51*, 377.
(418) Tsapatsis, M.; Kim, S.; Nam, S. W.; Gavalas, G. *Ind. Eng. Chem. Res.* **1991**, *30*, 2152.
(419) Megiris, C.; Glezer, J. H. E. *Ind. Eng. Chem. Res.* **1992**, *31*, 1293.
(420) Sea, B. K.; Watanabe, M.; Kusakabe, K.; Morooka, S.; Kim, S. S. *Gas. Sep. Purif.* **1996**, *10*, 187.
(421) Nijmeijer, A.; Bladergroen, B. J.; Verweij, H. *Microporous Mater.* **1998**, *25*, 179.
(422) Cameron, M. A.; Gartland, I. P.; Smith, J. A.; Diaz, S. F.; George, S. M. *Langmuir* **2000**, *16*, 7435.
(423) Yan, S.; Maeda, H.; Kusakabe, K.; Morooka, S. *Ind. Eng. Chem. Res.* **1994**, *33*, 616.
(424) Morooka, S.; Yan, S.; Yokoyama, S.; Kusakabe, K. *Sep. Sci. Technol.* **1995**, *30*, 2877.
(425) Xomeritakis, G.; Lin, Y. S. *J. Membr. Sci.* **1996**, *120*, 261.
(426) Xomeritakis, G.; Lin, Y. S. *AIChE J.* **1998**, *44*, 174.
(427) Uemiya, S.; Kajiwara, M.; Kojima, T. *AIChE J.* **1997**, *43*, 2715.
(428) Uemiya, S.; Kato, W.; Uyama, A.; Kajiwara, M.; Kojima, T.; Kikuchi, E. *Sep. Purif. Technol.* **2001**, *22*−*23*, 309.
(429) Kikuchi, E.; Nemoto, Y.; Kajiwara, M.; Uemiya, S.; Kojima, T. *Catal. Today* **2000**, *56*, 75.
(430) Yano, M.; Ohno, K.; Imanaka, H. *J. Phys. IV Colloque C5* **1995**, *5*, 1069.
(431) Daub, K.; Wunder, V. K.; Dittmeyer, R. *Catal. Today* **2001**, *67*, 257.
(432) Daub, K.; Emig, G.; Chollier, M.-J.; Callant, M.; Dittmeyer, R. *Chem. Eng. Sci.* **1999**, *54*, 1577.
(433) Dittmeyer, R.; Höllein, V.; Daub, K. *J. Mol. Catal.* **2001**, *173*, 135.
(434) Pina, M. P.; Irusta, S.; Menéndez, M.; Santamaria, J.; Hughes, R.; Boag, N. *Ind. Eng. Chem. Res.* **1997**, *36*, 4557.
(435) De Jong, K. P. *Curr. Opin. Solid State Mater. Sci.* **2001**, *4*, 55.

CR9903508